TIME DEPENDENT WEAR AND ITS MECHANISMS IN ENGINE CYLINDERS

FINAL TECHNICAL REPORT

Contract No. DAAE 07-93-C-R088

Prepared by

Naeim A. Henein

Center for Automotive Research
College of Engineering
Wayne State University
Detroit, MI 48202

Submitted to

US Army Tank-Automotive AND Armaments Command
Tank-Automotive Research
Development and Engineering Center
Warren, MI 48397-5000

October, 1997

Time Dependent Wear and Its Mechanisms in Engine Cylinders

FINAL TECHNICAL REPORT

Contract No. DAAE 07-93-C-R088

Prepared by

Naeim A. Henein

Center for Automotive Research
College of Engineering
Wayne State University
Detroit, MI 48202

Submitted to

US Army Tank-Automotive AND Armaments Command
Tank-Automotive Research
Development and Engineering Center
Warren, MI 48397-5000

October, 1997

UNCLASSIFIED
SECURITY CLASSIFICATION OF THIS PAGE

REPORT DOCUMENTATION PAGE

Form Approved OMB No. 0704-0188

1a. REPORT SECURITY CLASSIFICATION: Unclassified	1b. RESTRICTIVE MARKINGS
2a. SECURITY CLASSIFICATION AUTHORITY	3. DISTRIBUTION / AVAILABILITY OF REPORT: UNLIMITED
2b. DECLASSIFICATION / DOWNGRADING SCHEDULE	
4. PERFORMING ORGANIZATION REPORT NUMBER(S): Center for Automotive Research College of Engineering	5. MONITORING ORGANIZATION REPORT NUMBER(S): 13740
6a. NAME OF PERFORMING ORGANIZATION: Wayne State University; 6b. OFFICE SYMBOL (If applicable)	7a. NAME OF MONITORING ORGANIZATION: U.S.Army Tank-Automotive and Armaments Comman
6c. ADDRESS (City, State, and ZIP Code): Detroit, MI 48202	7b. ADDRESS (City, State, and ZIP Code): Warren, MI 48397-5000
8a. NAME OF FUNDING / SPONSORING ORGANIZATION; 8b. OFFICE SYMBOL (If applicable)	9. PROCUREMENT INSTRUMENT IDENTIFICATION NUMBER: DAAE07-93-C-R088
8c. ADDRESS (City, State, and ZIP Code)	10. SOURCE OF FUNDING NUMBERS: PROGRAM ELEMENT NO. / PROJECT NO. / TASK NO. / WORK UNIT ACCESSION NO.

11. TITLE (Include Security Classification)
Time Dependent Wear and its Mechnisms in Engine Cylinders

12. PERSONAL AUTHOR(S)

13a. TYPE OF REPORT	13b. TIME COVERED	14. DATE OF REPORT (Year, Month, Day)	15. PAGE COUNT
Final	FROM 8/9/93 TO 9/30/97	October, 1997	106

16. SUPPLEMENTARY NOTATION

17. COSATI CODES: FIELD	GROUP	SUB-GROUP	18. SUBJECT TERMS (Continue on reverse if necessary and identify by block number)

19. ABSTRACT (Continue on reverse if necessary and identify by block number)

This contract is a joint effort between the Center for Automotive Research at Wayne State University and Ford Motror Company, with a goal of reducing the testing time of wear in the cylinder bore of reciprocating combustion engines. This is accomplished by developing a new probe to determine the in-situ wear in the liner at the top ring reversal point in an engine under actual running conditions without the need to disassemble the engine. The wear probe is then utilised to measure the wear and surface roughness at several intervals during and after the break-in period. A 3-D surface topography of a pre-designated area on the wear probe is obtained before and after a wear test is made. The volume of the topography above a common reference plane is calculated. The decrease in the volume due to wear is measured, and the average nominal wear depth is calculated over the whole area. In addition to wear measurements, the total instantaneous engine frictional torque is measured. Correlations are developed between the rate of change in wear, surface roughness and engine friction. This correlation is used to predict the effect

20. DISTRIBUTION / AVAILABILITY OF ABSTRACT	21. ABSTRACT SECURITY CLASSIFICATION
☒ UNCLASSIFIED/UNLIMITED ☐ SAME AS RPT. ☐ DTIC USERS	Unclassified

22a. NAME OF RESPONSIBLE INDIVIDUAL	22b. TELEPHONE (Include Area Code)	22c. OFFICE SYMBOL
Milad H. Mekari	810-574-5834	AMSTA-TR-R

DD Form 1473, JUN 86 — Previous editions are obsolete. — SECURITY CLASSIFICATION OF THIS PAGE

UNCLASSIFIED

TOTAL P.02

19. of varying the surface properties on wear rate.

Table of Contents

INTRODUCTION

This contract is a joint effort between the Center for Automotive Research at Wayne State University and Ford Motor Co. with a goal of reducing the testing time of the wear in the cylinder bore of reciprocating combustion engines.

One of the most critical tribological areas in an engine is the cylinder-ring interface. Cylinder-ring wear has been known to play a major role in internal combustion engine durability, performance, emissions and fuel economy. Recently, cylinder liner wear in automotive engines has gained attention because of the stringent emission standards needed to be met during 100,000 miles of vehicle usage.

The traditional method for measuring cylinder liner wear in a real engine is the gauge method which measures the increase in the bore diameter as a result of wear. To make such a measurement, the engine needs to be dismantled. Therefore, cylinder-ring wear tests are expensive and time consuming. To cut time and cost, many attempts have been made to estimate cylinder liner wear using test benches under simulated engine conditions[1-9]. Rotary methods include the pin-on disk (ASTM G99) and the block-on-ring (ASTM G77). Other test bench devices include the ring-on-ring, ball-on-flat, four-ball, and thrust washer. Reciprocating methods include the Cameron-Plint High Frequency Friction Machine and the EMA-LS9 machine. The bench tests are useful for the general purpose of screening ring and liner materials or oil and additives. However, test benches could not simulate all of the conditions that exist in a fired engine.

In-situ measurement of cylinder liner wear in engines under actual running conditions was made by using SLA (surface layer radio-activation) techniques [10,11]. The radioactive marker technique can directly measure the activity decrease from a small activated area on the component of interest as wear occurs. The technique can provide accurate wear data within a short time without dismantling the engine[11]. However, this method requires special precautionary preparations and cannot provide any information about surface topography of the cylinder liner.

Material loss in cylinder liners of internal combustion engines is primarily from the upper part of the liner where wear reaches its maximum value at the top ring reversal point (TRRP)[1,12,14,19], as shown in Figure A, when the piston is at top dead center (TDC). The high wear at TRRP is the result of the contact between the asperities caused by the thin oil film between the top ring and the cylinder wall. The oil film thickness is minimum at this location because of a combination of the high contact pressure, a very slow sliding speed approaching zero, and the low oil viscosity. The high contact pressure between the top ring and cylinder wall is caused by the peak cylinder gas pressure acting on the back of the top ring in addition to the initial elastic force of the ring. The sliding speed of the ring relative to the cylinder wall reaches zero at TRRP. The low oil viscosity is caused by the increase in the oil temperature, as it gets in contact with the hot wall surfaces. These surfaces are exposed to the products of combustion at their highest temperature, before they are covered by the piston when it reaches TDC[1]. The lubrication around the dead centers, and in particular TDC, is believed to be of the severe boundary lubrication regime[19].

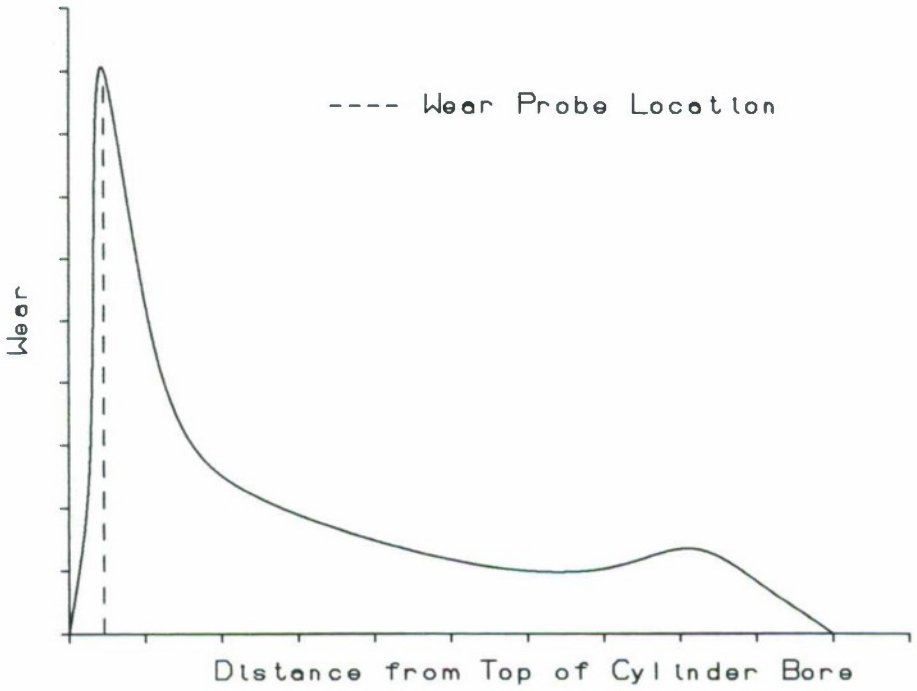

Figure A. Typical cylinder liner wear in major thrust side

The major goal of this project is to develop a new technique to determine the in-situ wear in the liner at the top ring reversal point, as shown in Figure A, in an engine under actual running conditions without the need to disassemble the engine. The wear probe is then utilised to measure the wear and surface roughness at the TRRP of the cylinder liner. A 3-D surface topography of a pre-designated area on the wear probe is obtained before and after a wear test is made. The volume of the topography above a common reference plane is calculated using a numerical integration algorithm. The decrease in the volume after the wear test is measured, and the average nominal wear depth is calculated over the whole area. The wear test is repeated after specified intervals of time during the break-in period. In addition to the wear measurements, the total instantaneous engine frictional torque is measured. A correlation is then made between the rate of changes in wear, surface roughness and engine friction over the break-in period. In addition, a correlation is developed for the power lost in friction over the break-in period.

OBJECTIVES

The following are the objectives of this project:

1- To design and manufacture the wear probe.

2- To determine a wear measuring method with enough accuracy to detect probe wear.

3- To improve the accuracy of measuring the instantaneous engine friction torque and account for the effect of torsional vibration of the crankshaft.

4- To design the instrumentation to measure the piston-ring assembly friction, by measuring the cylinder gas pressure and the axial force in the connecting rod.

5- To develop a cooling system to control the lubricating oil temperature.

6- To run the engine during the break-in period and measure the wear of the probe.

7- To determine the mechanisms of wear during the break-in period.

8- To relate the probe wear and the engine friction level over the break-in period.

1.0 WEAR PROBE DESIGN AND MANUFACTURE

The in-situ wear probe was developed to measure the cylinder liner wear at the top ring reversal point. The design of the probe and its fixture was developed at Wayne State University in collaboration with Ford Motor Company. The probe and cylinder were fabricated using Electric Discharge Machining at Ford Motor Company. Figure 1 shows the assembly drawing of the wear probe. Figure 2 to Figure 4 show the part manufacturing drawings of the wear probe, the probe holder and the modified cylinder liner.

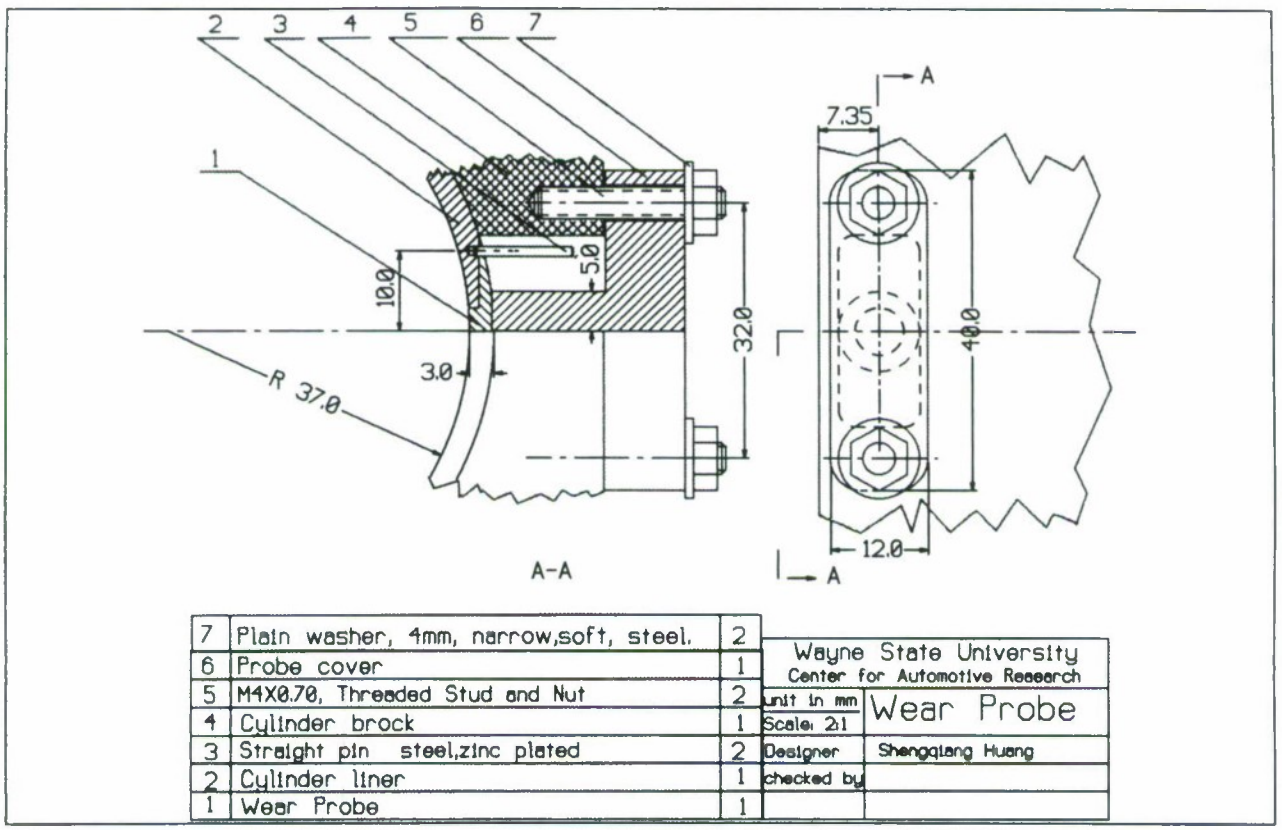

7	Plain washer, 4mm, narrow,soft, steel.	2	Wayne State University Center for Automotive Research	
6	Probe cover	1		
5	M4X0.70, Threaded Stud and Nut	2	unit in mm	Wear Probe
4	Cylinder brock	1	Scale: 2:1	
3	Straight pin steel,zinc plated	2	Designer	Shengqiang Huang
2	Cylinder liner	1	checked by	
1	Wear Probe	1		

Figure 1. Cylinder block - wear probe assembly

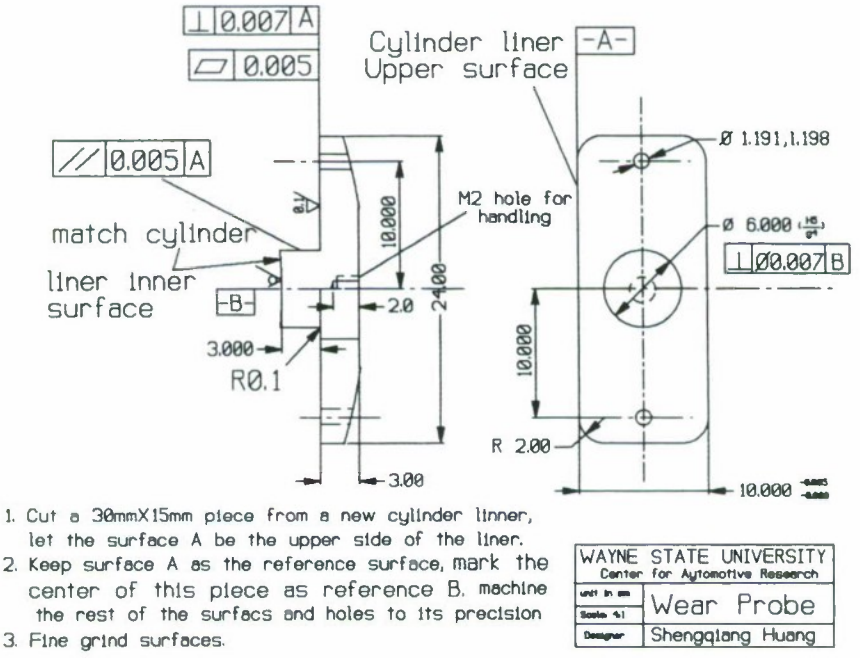

Figure 2. Manufacturing drawing of the wear probe

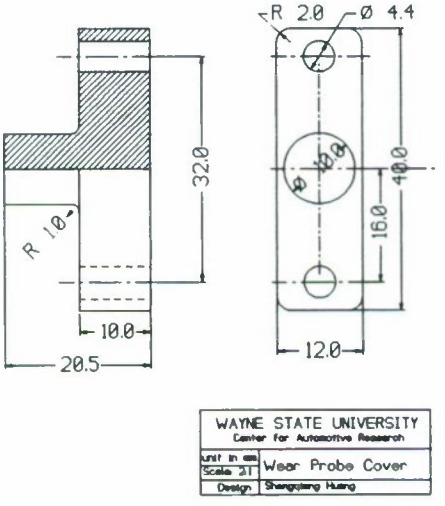

Figure 3. Manufacturing drawing of the probe holder

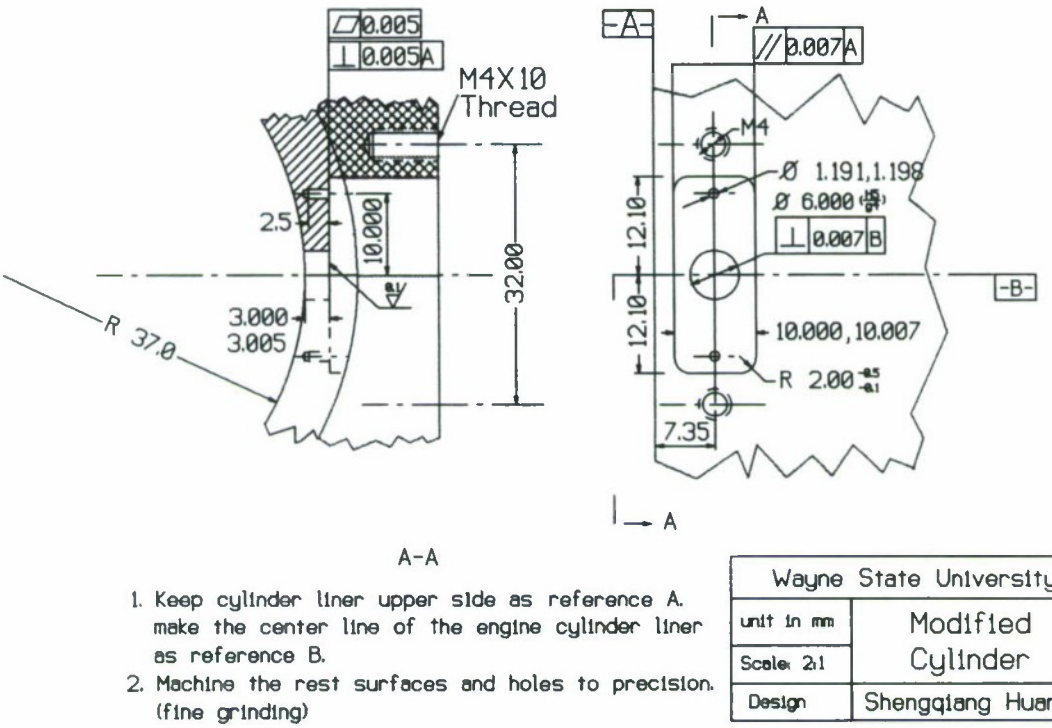

Figure 4. Manufacturing drawing of the modified cylinder liner

The wear probe is 24 mm x 10 mm x 3 mm, shown in Figure 5, and is cut from an unused cylinder identical to the cylinder under test. Accordingly, its surface has the same properties as the surface of the cylinder. The probe is located in the cylinder so that the top ring is approximately centred on it when the piston was at TDC. The top quarter of the surface does not contact the top ring and is used as a reference surface. Upon installation, the wear probe surface is flush with the inside bore surface to form a continuum of the power cylinder surface. The installed probe and the cylinder liner are later honed as a unit as shown in Figure 6. Figure 7 shows the honing marks on the surface of the probe and liner.

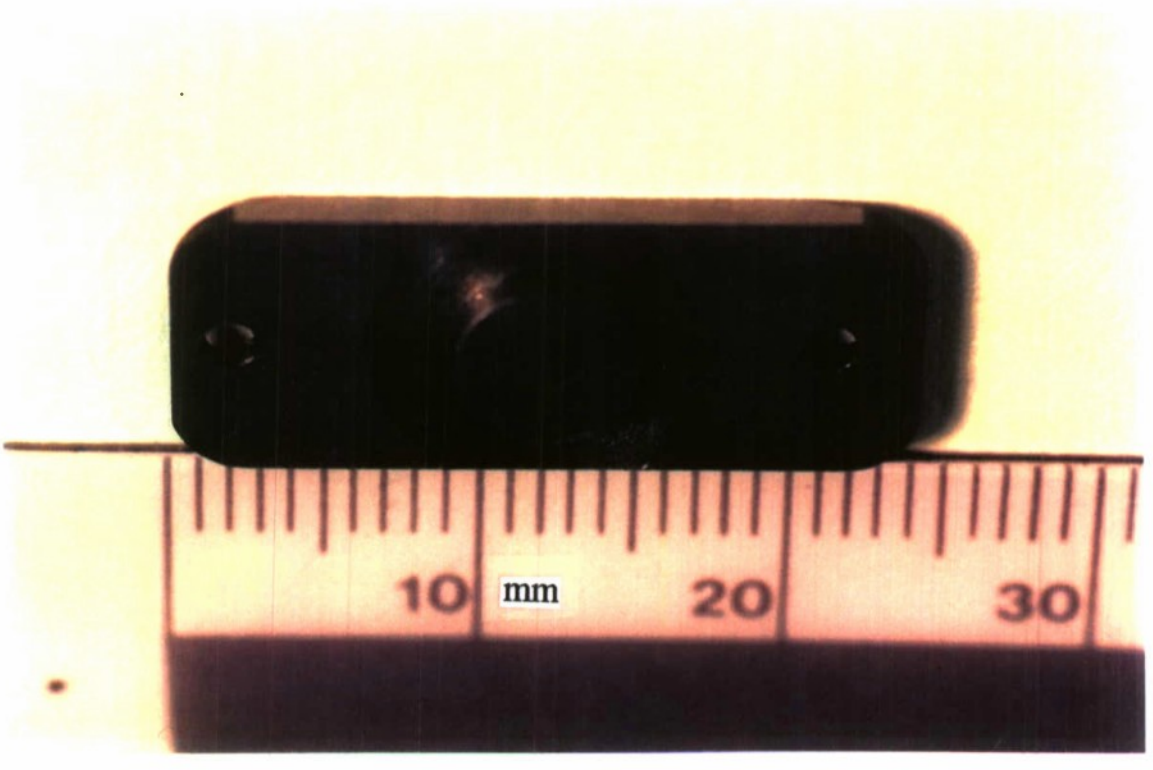

Figure 5. Picture of the wear probe

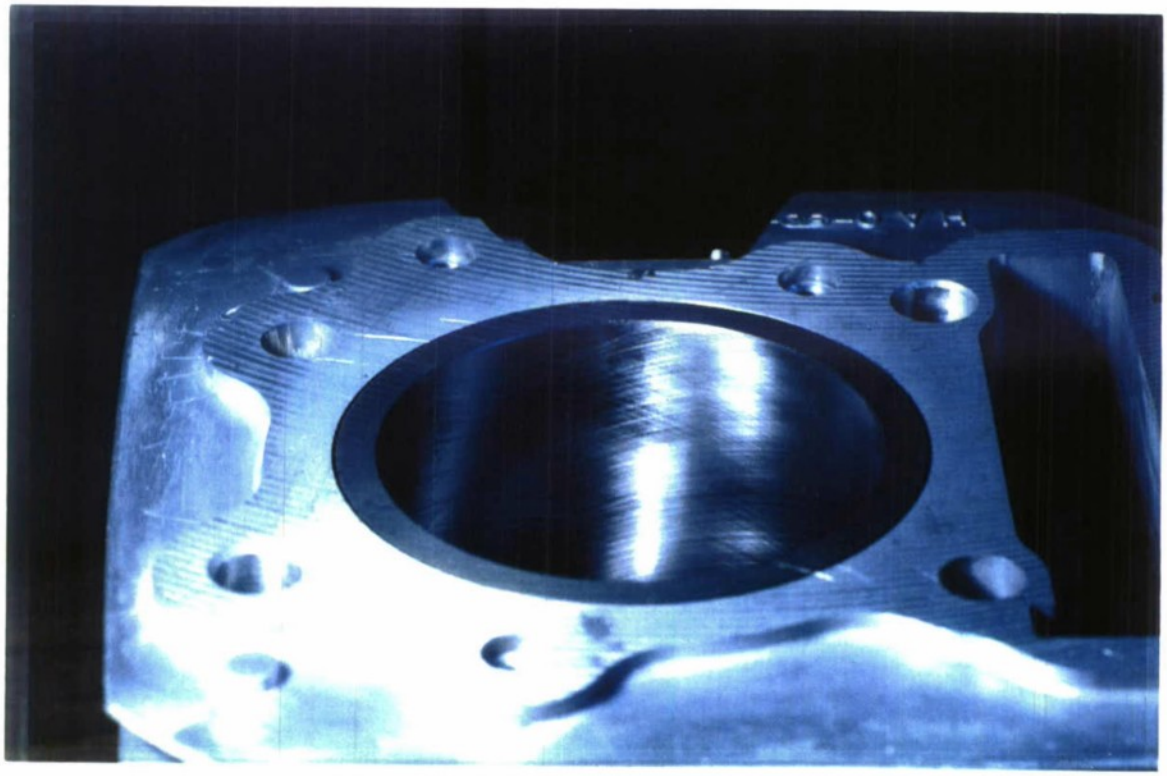

Figure 6. Picture of the cylinder block assembled with the wear probe

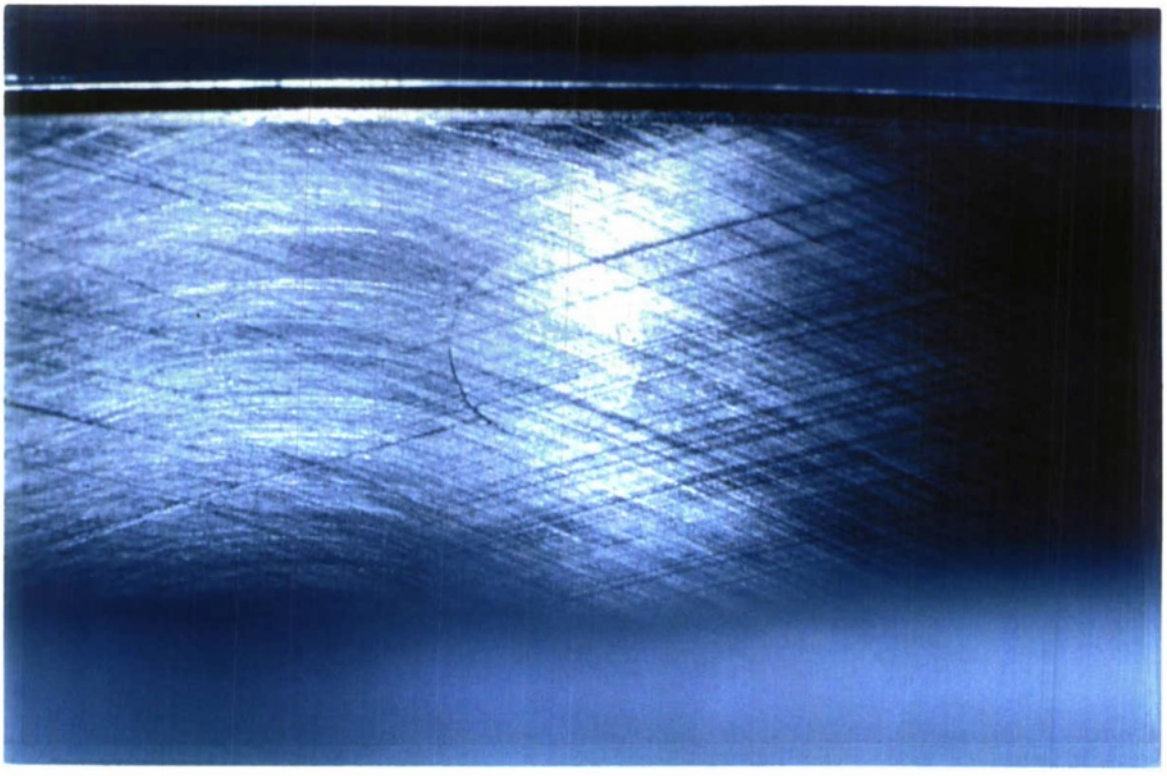

Figure 7. Honing marks on the wear probe and cylinder liner

The probe was designed and manufactured to ensure that its position in the cylinder liner is reproduced axially, radially and circumferentially, as it is installed into the cylinder liner. The flatness and the surface roughness of the shoulder surfaces of the wear probe and cylinder block is of strictly high precision in order to guarantee the continuity between the wear probe surface and the cylinder liner surface and at the same time to seal the combustion chamber. The perpendicularity, between the probe tip axis and the shoulder surface on the

wear probe and between the liner probe hole and the shoulder surface on the liner, is highly required in order to assure that the shoulder surfaces of the liner and the probe can well contact each other. Two dowel pins are used to prevent probe rotation. The probe is pushed against the machined cylinder housing shoulder by a cover. Two threaded studs with double nuts at each side are used to mount the cover on the cylinder block. The tightening torque of the nuts was decided before the cylinder liner with the wear probe was honed. The wear probe was always mounted onto the cylinder liner with that certain tightening torque by using a precise torque rench afterwards in order to keep the surface continuity between the wear probe and cylinder liner surface.

2.0 GUARANTEE AND VERIFICATION OF THE SURFACE CONTINUITY OF THE LINER SURFACE

The surface continuity of the liner surface is primary guaranteed by the design structure of the wear probe. In order to assure the continuity of the probe and cylinder surfaces the following procedure was followed during the whole engine test.

1. Deeply clean the wear probe and probe assembly surfaces on the cylinder liner by using chemical solvent and clean compressed air.
2. Place the wear probe into position and install the two dowel pins.
3. Install and push the cover at its axis while tightening the nuts from left to right until the nuts lightly touch the cover. By doing so, a tilted cover was well avoid.
4. Tighten the left nut using 15% of the total tightening torque then the right nut.
5. Tighten the left nut using 50% of the total tightening torque then the right nut.
6. Tighten the left nut using 100% of the total tightening torque then the right nut.

7. Repeat 4 to 5 for the double nuts.

The surface continuity of the cylinder liner was evaluated by measuring the radial roundness and the axial straightness of the cylinder bore at GM Powertrain Advanced Development Lab. Figure 8 shows the bore liner cylindricity. Figure 9 shows the roundness of the cylinder surface at three different levels passing through the wear probe. The probe is located at angle 0°. Figure 8 and 9 indicate that the surface profile at the wear probe is within the distortion range of other portions of the cylinder.

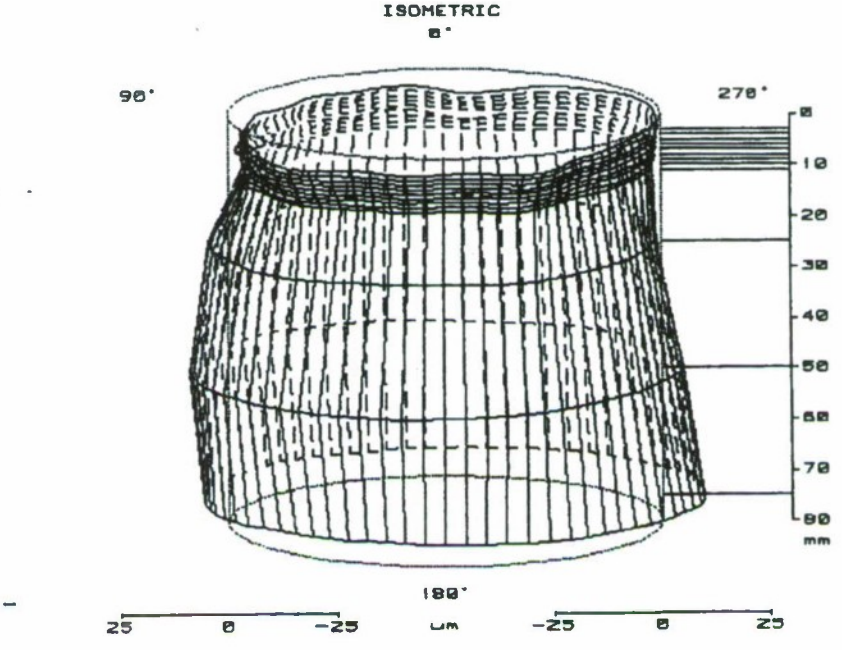

FOURIER SYNTHESIS WITH A0,A1,B1

MINIMUM VALUE	:	-10.4 µm	AT	8.0 mm, 355.0 °
MAXIMUM VALUE	:	9.9 µm	AT	75.0 mm, 265.0 °
MINIMUM DIAMETER	:	-12.1 µm	AT	7.0 mm, 55.0 °
MAXIMUM DIAMETER	:	16.1 µm	AT	75.0 mm, 115.0 °
CYLINDRICITY	:	20.3 µm		

Figure 8. Cylinder liner cylindricity measured under 30 in-lb probe mounting torque

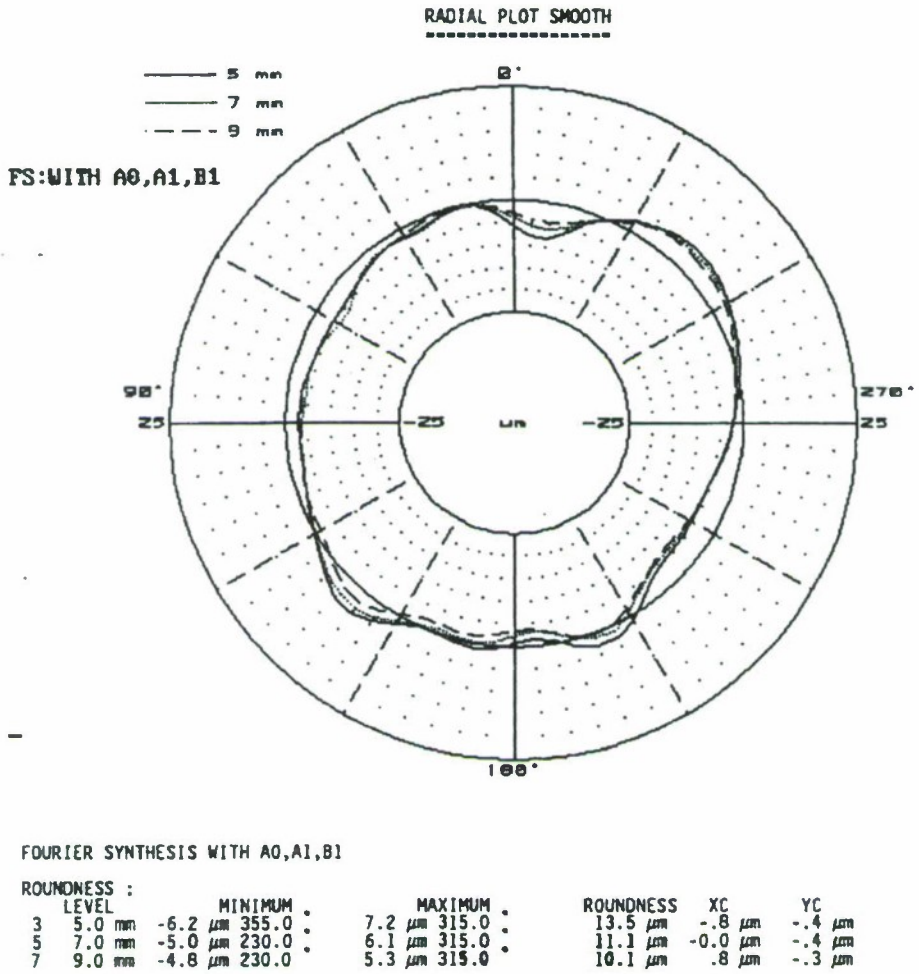

Figure 9. Cylinder liner roundness measured under 30 in-lb probe mounting torque

The interface between the wear probe and the cylinder liner was examined by a 3-D surface profile measurement at GM Powertrain Advanced Development Lab. An area of 0.9 ×

1.2 mm^2 was scanned and the 3-D surface profile was provided. Figure 10 shows a 3-D surface profiles of the interface between the wear probe and the liner surface. Figure 11 is a 2-D profile of the above 3-D profile along the vertical direction. Figure 11 shows that the probe discontinuity with the cylinder liner is about 2 μm.

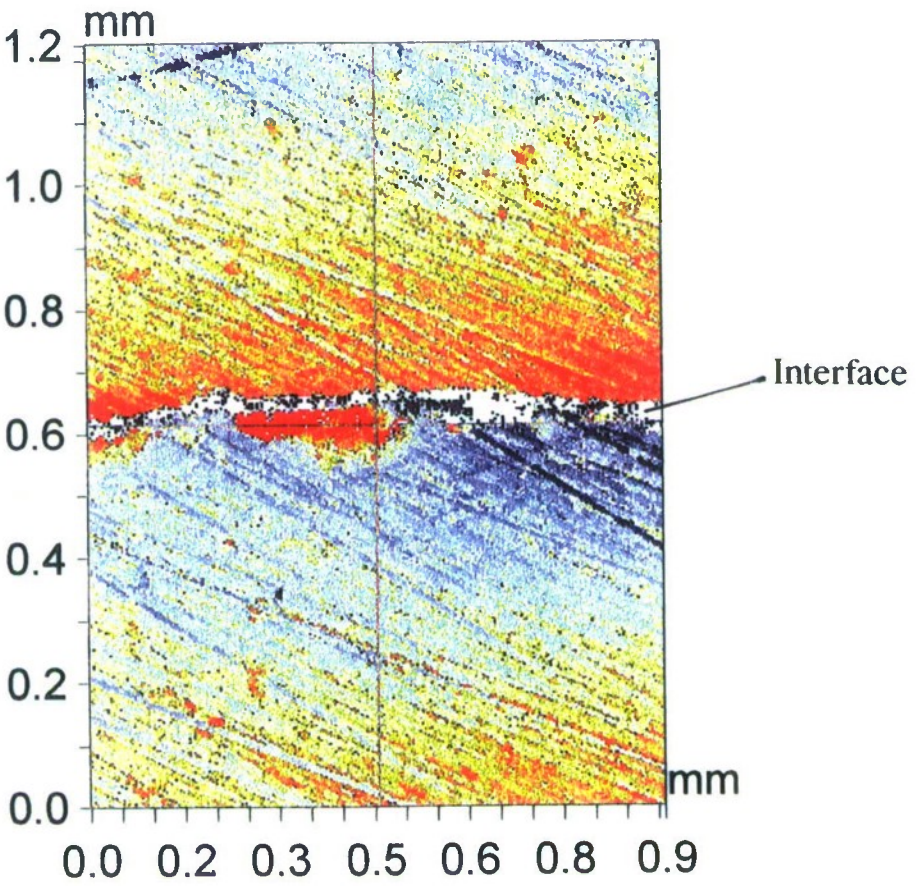

Figure 10. 3D Surface profile of the interface of the liner and the probe

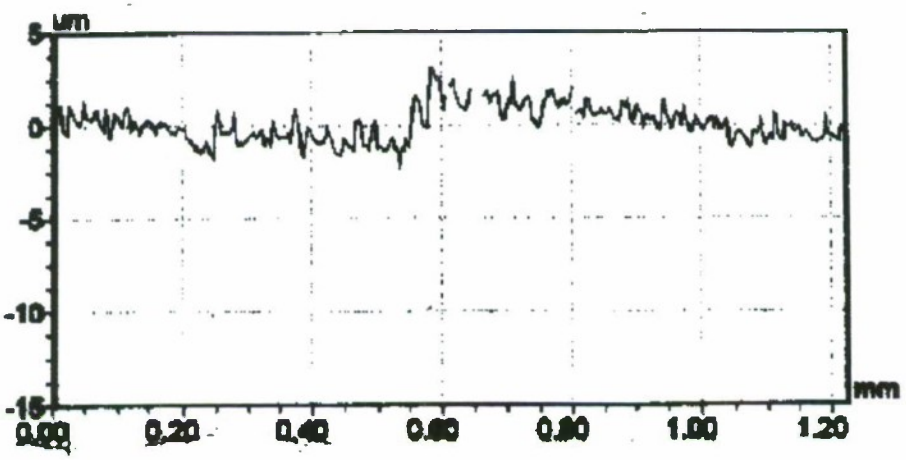

Figure 11. 2D Surface profile of the interface of the liner and the probe

3.0 MEASUREMENT OF SURFACE TOPOGRAPHY AND WEAR OF THE WEAR PROBE

A Rodenstock 3-D Laser Stylus is used to measure the 3D surface topography of the wear probe. The measurement principle of the Laser Stylus is based on a servo-controlled focused laser beam detecting the height deviation of the test sample surface. The motions in X-Y directions are achieved by a precision stepper motor-controlled table to which the test sample is fixtured. The system can provide 3D profile, 2D profile, 2D roughness profile and roughness parameters. A zoom function allows enlargements of a measured section to be analysed.

3.1 THE METHOD OF THE WEAR VOLUME MEASUREMENT OF THE WEAR PROBE

The measurement of the wear volume is achieved by using the Laser Stylus. An integration of the 3-D surface profile in a measured area gives the material volume above a reference plane in the measured area as shown in Figure 12. The difference of the material volumes before and after wear gives the volumetric wear of the wear probe in the measured area. Since the cylinder liner surface is not a flat surface, a small error in the position of the scanned area of the wear probe can result in large errors in measured wear. Special effort was made to ensure that the scanned area was the exact same area for each wear measurement. For this purpose, a fixture attached on the moving table of the laser stylus, shown in Figure 13, was designed, made and modified for improving the accuracy to locate the measured area. The wear probe was forced, in two directions by two springs, to contact the position surfaces on the fixture. Therefore, the wear probe is relocated on the fixture with high accuracy in two directions and the tendency of a tilted wear probe is well eliminated. In order to more accurately identify the position of the measured area, a small shallow hole, diameter 0.25mm, was machined on the surface of the wear probe as a reference hole. The position of the scanned area is identified relative to the centre of the reference hole.

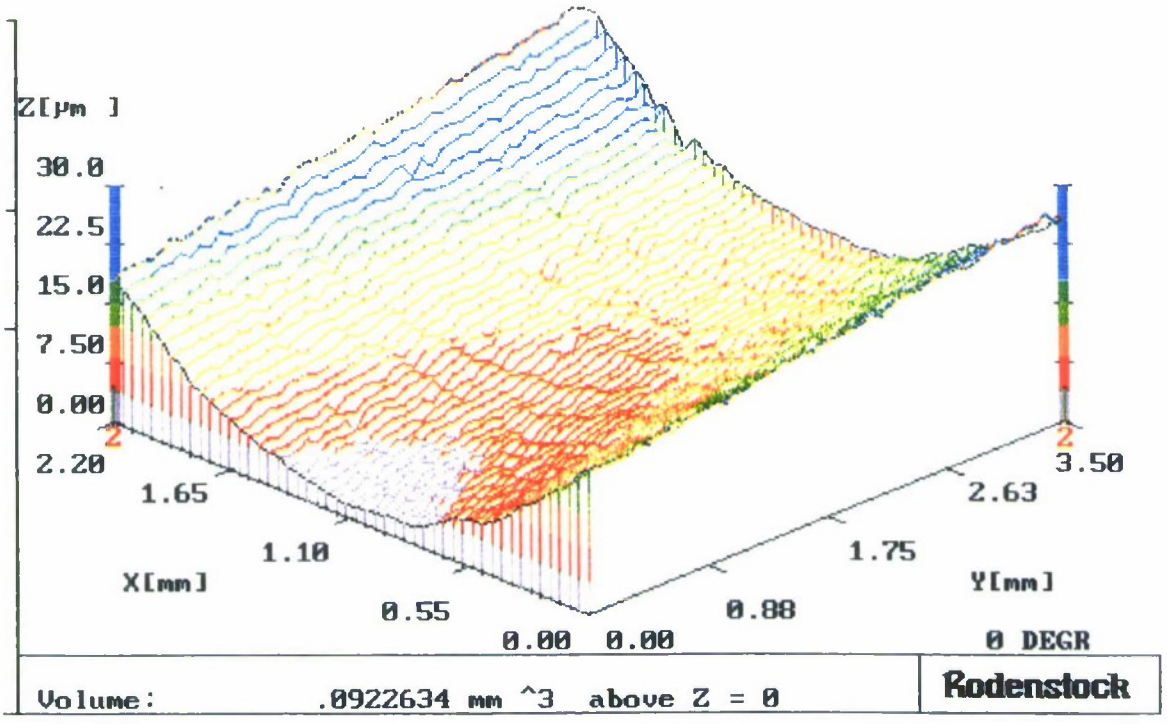

Figure 12. 3D profile display of the surface topography

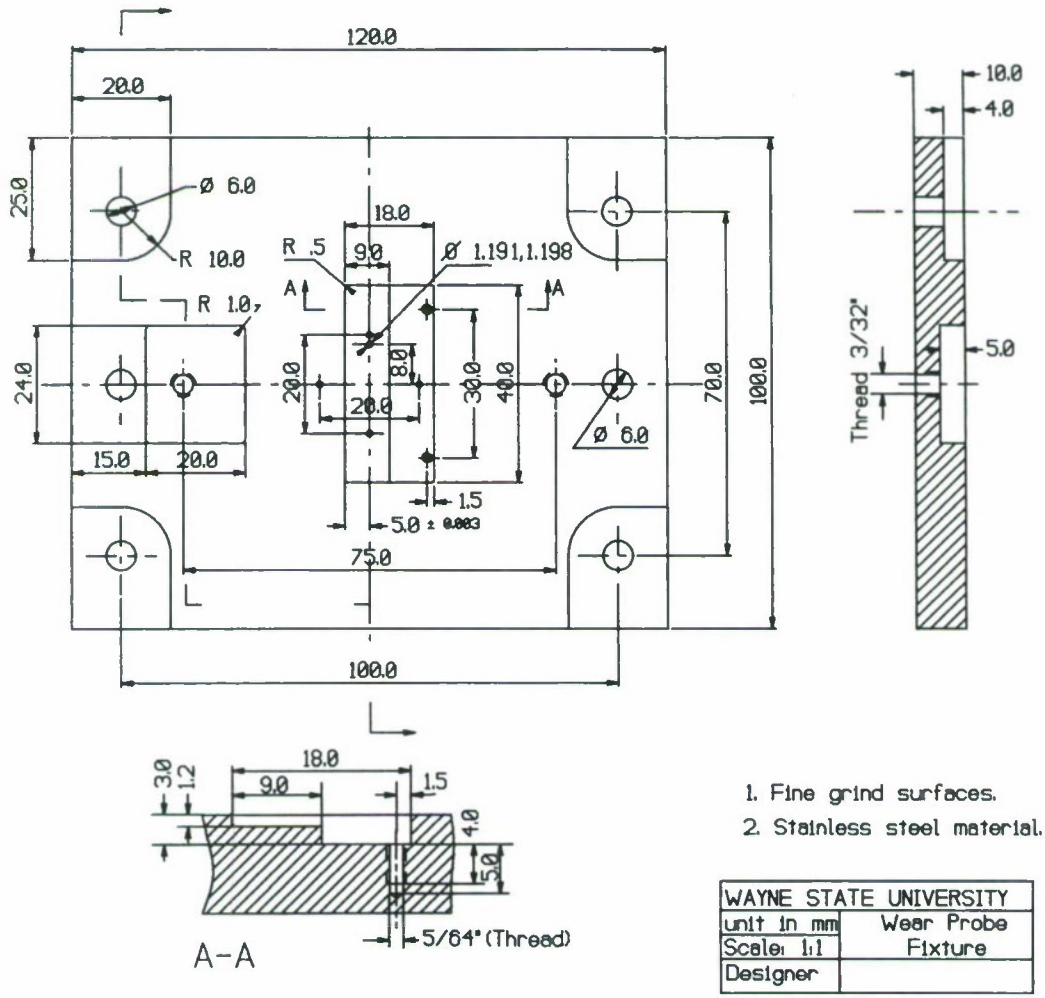

Figure 13. Manufacturing drawing of the fixture on the moving table of Laser Sylus

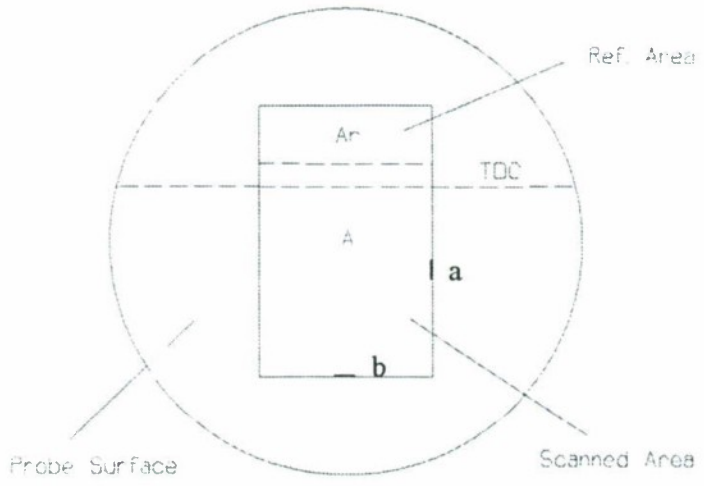

Figure 14. The scanned area on the wear probe

The scanned area (A) of the probe is 2.2 mm × 3.5 mm as shown in Figure 14. The top part (Ar) of the scanned area was used as a reference area. It is located above the TDC line which indicates the position of the top ring when the piston is at TDC. The volume of the material above a reference level z=0 can be calculated by the system software. Therefore, if the reference level z=0 is located at a depth under the unworn part on the probe surface, the wear volume would be the difference between the measured volumes before and after wear as shown in Figure 15.

$$\text{Wear Volume} = V_0 - V_i \qquad (3\text{-}1)$$

However, there is a variation in the Z=0 level from one measurement to another due to the manual calibration of Z=0 level and signal drift caused by temperature changes.

Before Wear

After Wear

Vo: Total Volume Above A

Vr_0: Reference Volume Above Ar

Vi: Total Volume Above A

Vr_i: Reference Volume Above Ar

$$\text{Wear Volume} = V_0 - V_i$$

Figure 15. Wear volume without zero shift

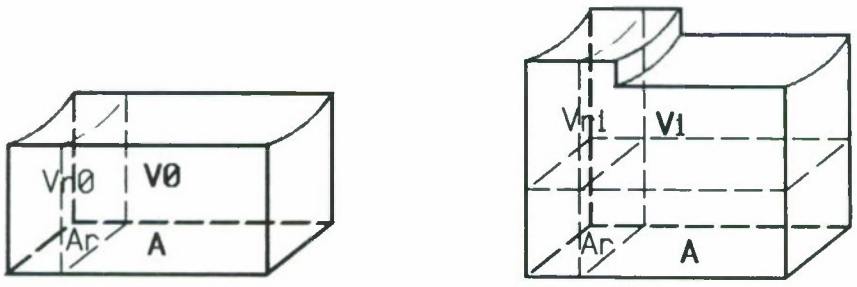

Before Wear

After Wear

Vo: Total Volume Above A

Vr_0: Reference Volume Above Ar

Vi: Total Volume Above A

Vr_i: Reference Volume Above Ar

$$\text{Wear Volume} = (V_0 - V_i) + (Vr_i - Vr_0)(A/Ar)$$

Figure 16. Wear volume with zero shift

In order to eliminate the error due to the variation of the Z=0 level, the volume above the reference area Ar was calculated each time the wear volume was computed. The difference between the volumes before and after wear, above the Z=0 level on the reference area Ar, is caused by variation of the Z=0 level. Figure 16 shows the volume before and after wear. Let Vr_0 and Vr_i be the measured volumes over the reference area Ar before and

after wear and V_0 and V_i the measured volumes over area A before and after wear. The wear volume V_w can be given by the following equation:

$$V_w = (V_0 - V_i) + (Vr_i - Vr_0)*(A/Ar) \qquad (3\text{-}2)$$

The wear is expressed finally by a nominal wear depth h over the area

$$h = V_w / A_w \qquad (3\text{-}3)$$

where

V_w is the wear volume in equation (3-2);

A_w is the part of area A where wear occurs.

3.2 ERROR ANALYSIS OF WEAR VOLUME MEASUREMENTS

There are two main sources of error in the wear volume measurement. The first is related to the probe repositioning and the resulting changes in the position of the scanned area. Although the establishment of the reference point and using springs to clamp the wear probe decreased this error, such an error could not be completely eliminated. The second source of error is the noise and signal drifting of the measurement system. The resolution for the Laser Stylus is 0.02 μm.

To reduce these errors the following procedure was followed:

1. V_{0I} and corresponding Vr_{0I} were measured 10 consecutive times and recorded as shown in Table 1. Subscript i refers to the sequence of the measurement.

Table 1. Raw Measured Volume

Meas.#i	0	1	2	3	4	5	6	7	8	9
V_{0i}	.0793607	.0812210	.0803502	.0805618	.0825916	.0834368	.0866437	.0879136	.0922749	.0981253
Vr_{0i}	.0209523	.0215520	.0212892	.0210924	.0217678	.0219421	.0228539	.0232649	.0245001	.0261575

2. The raw measured volumes were modified to exclude the influence of the variation of z=0 level by

$$V_i = V_{0i} - (Vr_{0i} - Vr_0) * (A/Ar) \qquad (i = 0,9)$$

3. The modified volumes V_i are shown in Table 2 where V is the arithmetic average of V_i. 4. The standard sample deviation σ of V_i was calculated and found to be equal to 0.0003328 (mm^3) or 0.40 % of V. Accordingly, the precision of the wear depth measurement for our wear probe is about ± 0.1 μm.

Table 2. Error of Volume Measurement

Meas. # i	V_i (mm^3)	V_i-V (mm^3)	$(V_i-V)/V$ (%)
0	0.0830277	-.0003400	-0.408
1	0.0827890	-.0005787	-0.694
2	0.0828380	-.0005297	-0.635
3	0.0837384	.0003707	0.445
4	0.0834043	.0000366	0.044
5	0.0836395	.0002718	0.326
6	0.0836551	.0002874	0.345
7	0.0834865	.0001188	0.143
8	0.0835245	.0001568	0.188
9	0.0835740	.0002063	0.247
Average	V = 0.0833677	σ = 0.0003328	

4.0 MEASUREMENT OF ENGINE FRICTION

The engine friction was measured by determining the Instantaneous Frictional Torque (IFT) of the engine. The method used to determine IFT is based on the fact that all the torques acting on the crankshaft should be in equilibrium at any point during the engine cycle as illustrated in Figure 17.

$$M_{IFT} = M_P - M_L - M_I$$

where

M_{IFT} = Instantaneous frictional torque;

M_P = Instantaneous torque due to cylinder and crankcase gas pressures acting on the piston;

M_L = Instantaneous torque due to the load on the engine;

M_I = Instantaneous torque due to the inertia of the moving parts of the engine.

Figure 17. Balanced torques acting on the crankshaft

IFT is computed from the measured cylinder gas pressure, crankcase gas pressure, angular velocity and acceleration of the crankshaft, and the load on the engine[25].

The IFT of an engine varies over the cycle and reaches its maximum amplitude shortly after the piston reaches TDC during the expansion stroke as shown in Figure 18. The average friction torque over the whole cycle is given by

$$\overline{M}_{IFT} = \frac{1}{4\pi} \int_0^{4\pi} M_{IFT} \, d\theta \qquad (4\text{-}1)$$

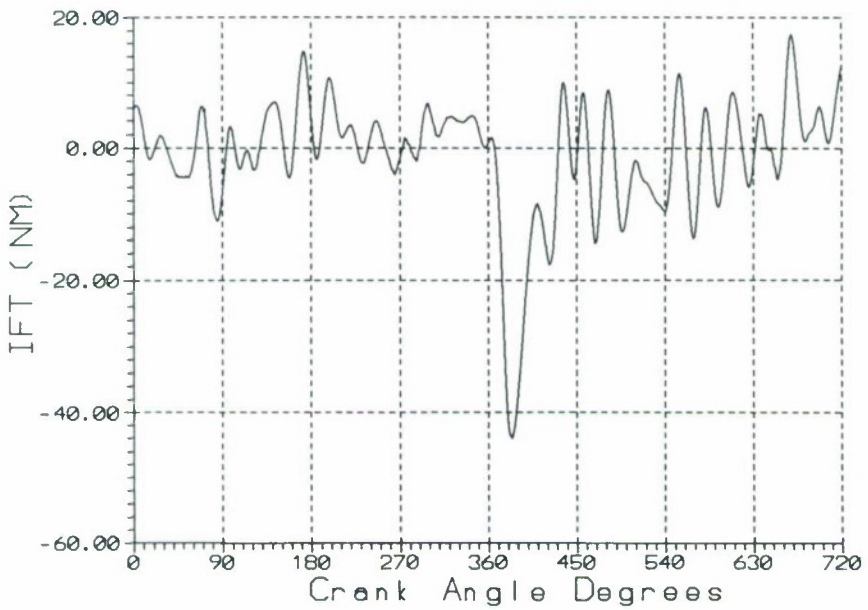

Figure 18. A sample of experimental result of engine IFT

5.0 EXPERIMENTAL SET-UP

5.1 TEST ENGINE

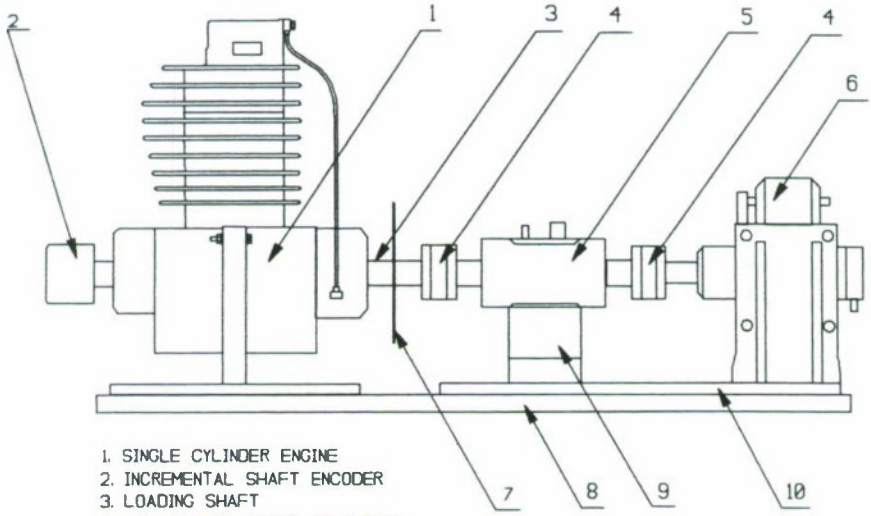

Figure 19. Layout of experimental setup

Figure 19 shows a line sketch of the experimental setup. Figure 20 and Figure 21 are two pictures of the test engine. The engine used in the experiments is a production four-stroke, high-speed, single-cylinder, air-cooled spark-ignition gasoline engine. Engine specifications are given in Table 3. The engine oil temperature was thermostatically controlled at 85 °C by an external heat exchanger. The cylinder gas pressure was measured by a flush mounted, water cooled piezo quartz crystal pressure transducer. A low range pressure

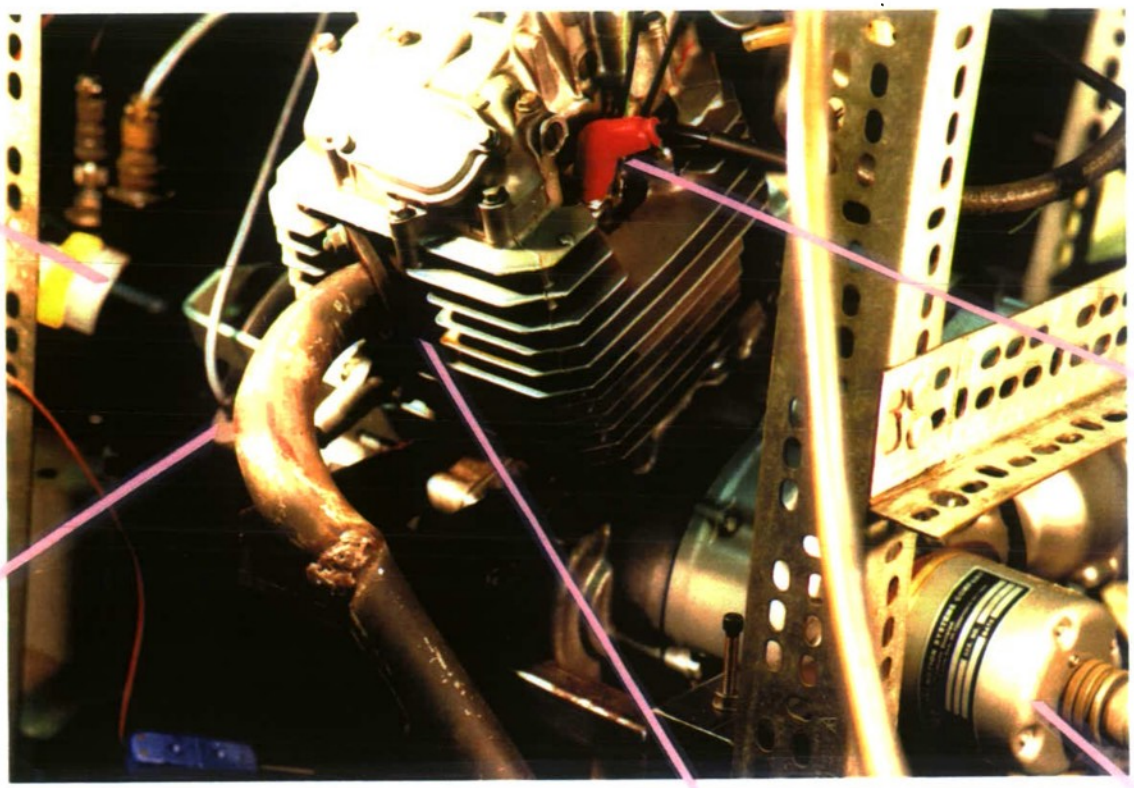

Figure 20. A front view of the test engine

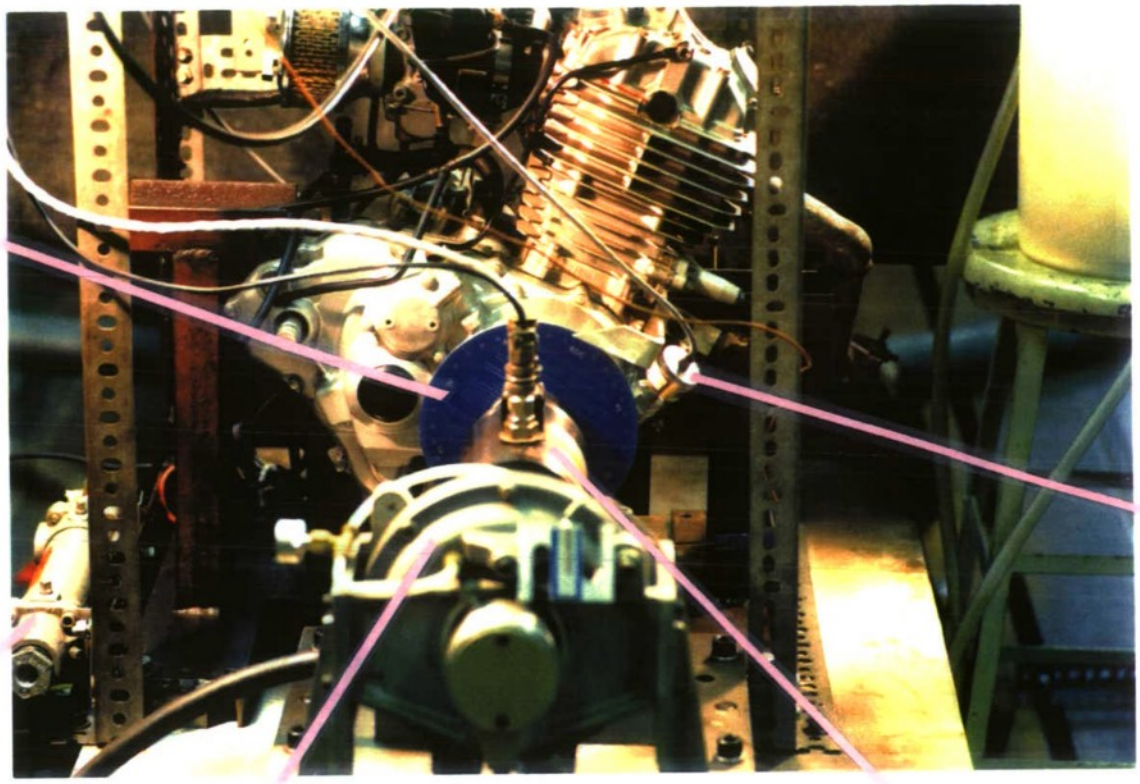

Figure 21. A side view of the test engine

transducer was mounted on the crankcase to measure the instantaneous gas pressure on the bottom of the piston. The pressure transducers were calibrated by using a modified dead weight tester to account for the effect of thermal stresses[25]. The crankshaft instantaneous angular velocity was measured by an optical shaft encoder. The engine load torque was applied by a low inertia water dynamometer and measured by a torque meter.

Table 3. Engine Specifications

Type	Gasoline, air-cooled, 4-stroke
Cylinder arrangement	Single cylinder inclined 20°
Bore X stroke	74.5 X 57.3 mm
Displacement	246 cc
Compression ratio	9:1
Valve train	Overhead camshaft chain drive
Maximum horsepower	17.8 BHP/7000rpm
Maximum torque	1.9 Kg-m/6000rpm
Oil capacity	2.5 liter after disassembly
Lubrication system	Forced pressure and wet sump

5.2 MEASUREMENT OF CONNECTING ROD FORCE

A full bridge strain gages is installed on the engine connecting rod. The strain gage is of resistance type made by Micro Measurements (number WK-06-062TT-350). The gages are applied to the neutral axis of the connecting rod to compensate bending and temperature variations. The orientation of the gages in the full bridge circuit is arranged to give maximum output. Since the gages are located on a point along the connecting rod axis of symmetry, half

of the gage is in tension whereas the other half is in compression when there is a bending moment. Therefore the strain gage bridge only senses the net compression and extension force. Temperature compensation is achieved by locating gages as close together as possible in order to subject all of them to the same temperature. High temperature conductance of the forged steel of the connecting rod is helpful in this point.

The connecting-rod of this engine is one piece which cannot be separated from the engine without disassembling the crankshaft. Accordingly the strain gages had to be installed on the connecting-rod without disassembling the crankshaft.

The strain gages and their bounding adhesives are coated to avoid contamination with fuel and oil. Baking and curing are required for these high temperature adhesives and coatings. To achieve this a heating tape with temperature controller device was assembled and built at WSU, and used to minimise the thermal effect on the bearing surfaces of connecting-rod and crankshaft.

The surface of the connecting-rod where the strain gages are mounted is chemically cleaned. Special gages are designed and machined to make marks on both sides of the connecting-rod for strain gage alignment.

The engine used is a compact motorcycle engine. Its crankcase cannot be extended to accommodate a grass hopper linkage to lead the strain gages wires and excitation power supply wire from the connecting-rod to the outside of the crankcase. Several other methods have been designed and compared. The method chosen is to coil the lead wires as a spring. This allows the reciprocating motion to be transferred to spring compression and extension. One end of the "spring" is attached to the small end of the connecting-rod by a special clamp (for directing and protecting the motion of the wire), and the other end to the inner wall of the crankcase at the bottom of the cylinder block. Then the wire is lead out of the crankcase

through the enlarged vent of the crankcase. The lead wires are fixed and secured on the wall of the crankcase by epoxy resin. The lead wires at the end of the small end of the connecting rod are soldered to the tabs of the strain gage terminal strip. Figure 22 shows a picture of the instrumental connecting-rod and leading wire spring mechanism. Outside the engine, the wires from the strain gage were connected to the measurement group signal conditioning amplifier Model 2310.

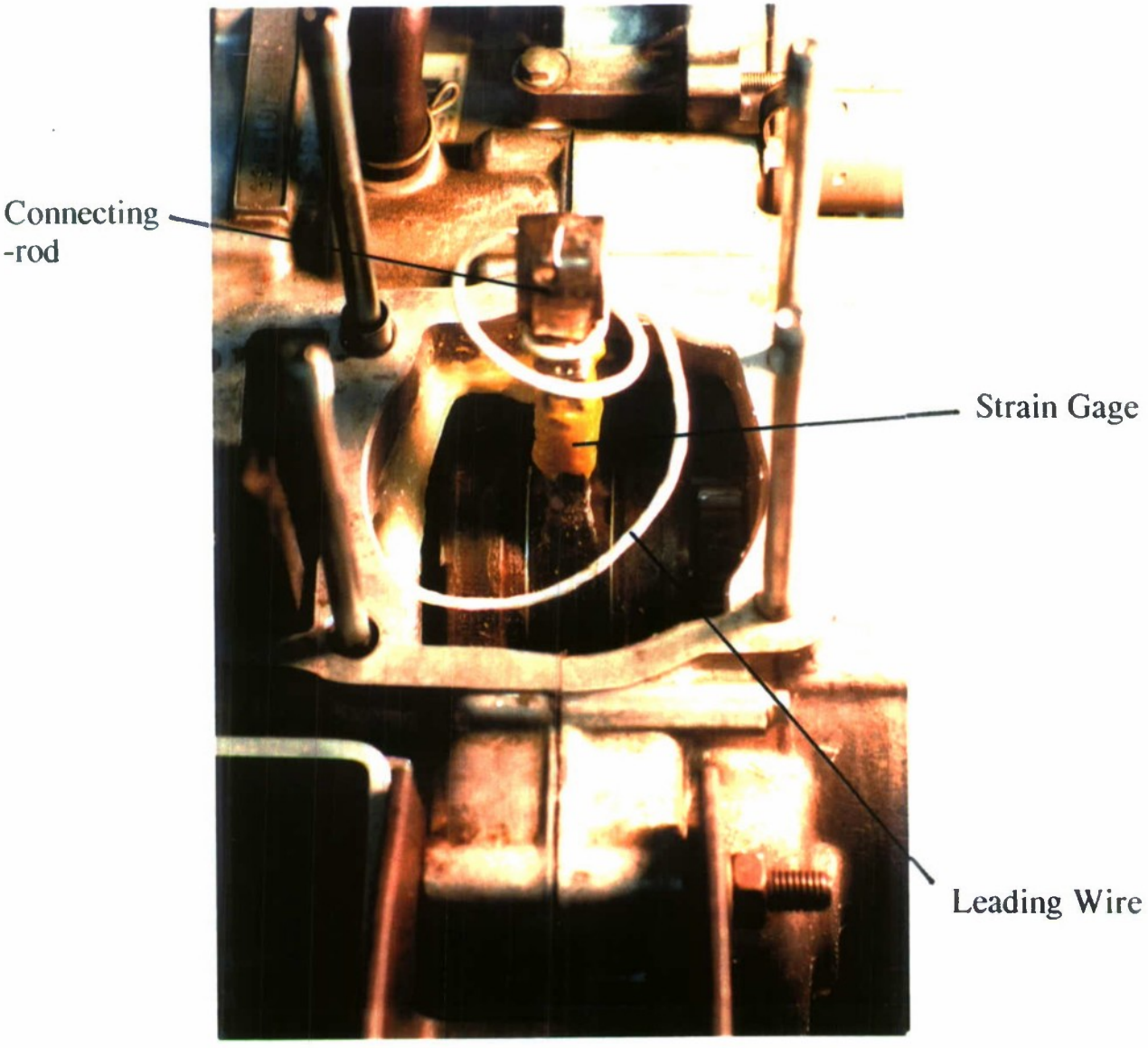

Figure 22. Picture of instrumental connecting-rod and leading wire spring mechanism

Dynamic calibration of the strain gage was performed during every run. At TDC, the frictional forces of the piston assembly changes direction and the PRAFF is close to zero. The only forces acting on the piston are the inertial forces the gas pressure force. This point served for the dynamic calibration of the strain gages. The inertia forces are calculated from the reciprocating masses and acceleration. The gas force acting on the piston are calculated from the measured cylinder gas pressure.

5.3 ENGINE LUBRICATING OIL TEMPERATURE CONTROL SYSTEM

An lubricating oil temperature control system is added to the air cooled engine to control the lubricating oil temperature. Therefore the engine oil temperature becomes one of the controllable engine operating parameters.

The engine oil filter cover is modified to allow all the lubricating oil to flow out of the engine after the oil filter. A fixed tube bundle heat exchanger, made by Young Radiator Company, is used to cool the oil. An RTD (Resistor Temperature Detector) is put on the outlet of the heat exchanger to sense the oil temperature after cooling and to signal the control unit. The controller compare the signal from the RTD to the set point and controls the opening of the cooling water valve. Figure 23 is a schematic of the cooling system.

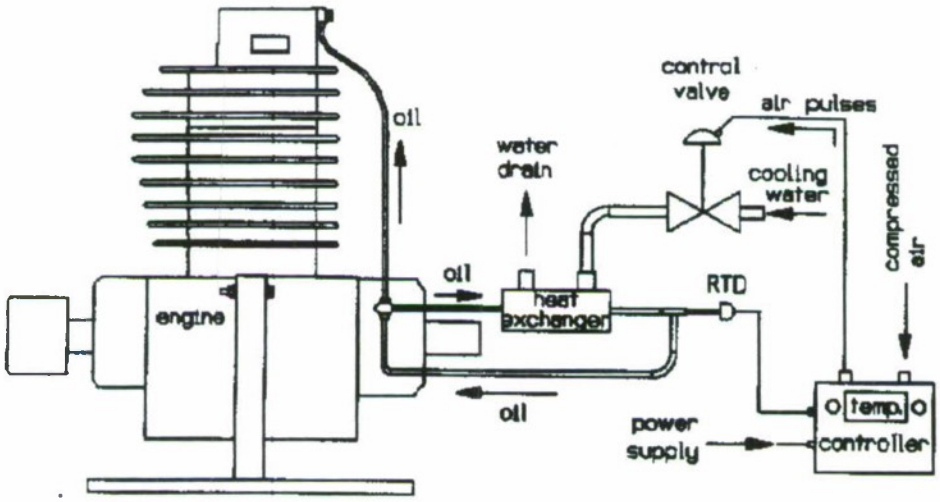

Figure 23. Schematic of cooling system

6.0 ENGINE BREAK-IN TEST

6.1 BREAK-IN SCHEDULE

Two sets of new cylinder liners and piston-rings were used for broken-in tests. The scheduled cumulative break-in time for both break-in tests is 28 hours. Expecting the wear rate to dramatically change at the beginning of the break-in period, the wear probe sampling was done every 10 minutes during the first half hour of the break-in. The break-in schedule for the first break-in test is listed in Table 4. The break-in schedule for the second break-in

test, which is listed in Table 5, is slightly modified according to the test result from the first break-in test. The major modification is to sample the wear probe every 20 minutes during the first hour. For the two break-in schedules, the engine speed was increased from 1600 rpm to 3000 rpm and the load from 10% to 100% of full load (10 NM load torque) in 14 steps.

Table 4. Engine Break-in Schedule for First Wear Probe

Step No.	Step Time(hr)	Cumu. Time(hr)	Speed (rpm)	Load (%)
1	0.1667	0.1667	1600	10
2	0.1667	0.3333	1600	10
3	0.1667	0.5	1600	10
4	0.5	1.0	1600	10
5	1.0	2.0	1600	20
6	1.0	3.0	1800	30
7	1.0	4.0	1800	30
8	2.0	6.0	2000	40
9	2.0	8.0	2200	45
10	2.0	10.0	2400	50
11	4.0	14.0	2700	60
12	4.0	18.0	3000	70
13	2.0		2500	80
	2.0	22.0	3000	90
14	2.0		2000	100
	2.0		2500	100
	2.0	28.0	3000	100

Table 5. Engine Break-in Schedule for Second Wear Probe

Step No.	Step Time(hr)	Cumu. Time(hr)	Speed (rpm)	Load (%)
1	0.3333	0.33	1600	10
2	0.3333	0.67	1600	10
3	0.3333	1.0	1600	10
4	0.5	1.5	1600	20
5	0.5	2.0	1600	20
6	1.0	3.0	1800	30
7	1.0	4.0	1800	30
8	2.0	6.0	2000	40
9	2.0	8.0	2200	45
10	2.0	10.0	2400	50
11	4.0	14.0	2700	60
12	4.0	18.0	3000	70
13	2.0		2500	80
	2.0	22.0	3000	90
14	2.0		2000	100
	2.0		2500	100
	2.0	28.0	3000	100

The entire second break-in test was successfully performed. However the first break-in test lasted for 3 hours only, because abnormal wear was observed. The cause of the abnormal wear was the contamination of the oil with particles brought into the engine during the intake valve repair. The intake valve was damaged after the timing belt broke. The intake valve seat needed to be lapped. Some sanding particles got into the engine and caused abnormal wear.

6.2 TEST DATA FOR PROBE WEAR

The data for the first three hours of the first break-in test, and for the whole break-in period of the second test were given in Figure 24 to 26. Figure 24 and 25 shows the nominal wear depth, w_d, plotted as a function of time for the first and second tests respectively. Both figures show that the wear occurred at a sharp rate during the first hour of engine break-in. After the first hour, wear rate decreased. This means that the early period of the break-in schedule is responsible for most of the wear. After one hour of the break-in schedule the wear particles reach a high concentration in the lubricating oil. Accordingly, an oil change after one hour would remove the wear particles, part of which might circulate with the oil and result in more wear. This result is consistent with Gumblenton's findings, as reviewed by Barber[1], where 75% of the total wear during a two-hour test occurred in the first 6 minutes.

Figures 24 and 25 indicate that the magnitude of wear for the second probe is three times that of the first. The possible reason for this difference is given below.

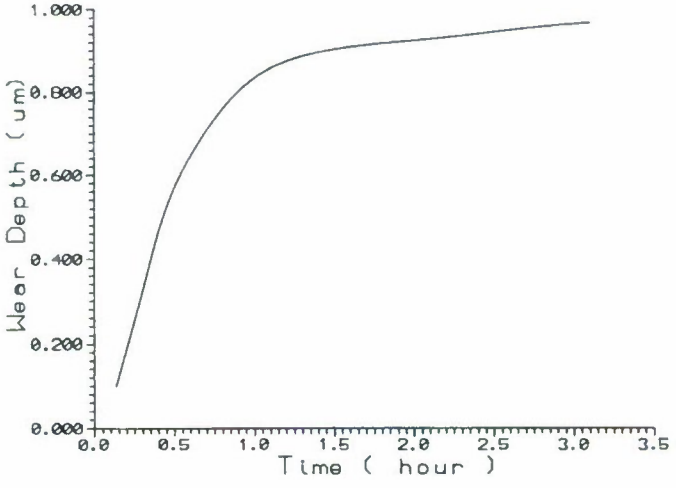

Figure 24. Nominal wear depth as a function of engine break-in time

The torque used for the installing the first probe before honing the liner was set by the machine shop and wasn't well controlled. The wear probe installation torque was later selected by the liner roundness measurement. Also, the torque wrench used during the first break-in test was of much less precision than that used in the second break-in test. The precision in installing the second wear probe is the reason for the difference in the wear data for the two probes.

6.3 WEAR RATE

The high wear rate at the start of the break-in period is due to the high contact pressure between the ring and cylinder, and the very low sliding velocity as the piston reaches its TDC position. These conditions cause the lubricant film to be thin enough to result in metal-to-metal contact at the asperities of the piston ring and the cylinder liner. At the beginning of the break-in period, the bearing area of the asperities is minimal and the unit pressure is the highest. This causes plastic deformation, local cohesion and shear, seen as metal removal, and high wear. As wear proceeds, the contact area increases, contact stress decreases and wear rates decrease. At a certain point, the two mated surfaces reach an equilibrium state and wear stabilises.

Let's take a detail look at wear of the probe over the whole engine break-in period,shown in Figure 25. In order to develop a mathematical expression for the rate of wear, reference is made to a correlation developed by Chung et al [24] for ring wear during the break-in period.

$$dw_d / dt = a\, e^{-bt} + c \qquad (6\text{-}1)$$

where w_d = nominal wear depth of the cylinder liner at TDC , in μm;

t = cumulative engine break-in time, in hour;

a = difference between wear rate at $t=0$ of break-in period and the steady wear rate after completing the break-in, in μm/hour;

b = the time dependence of break-in, in hour^{-1}

c = steady wear rate after the break-in period is completed, in μm/hour

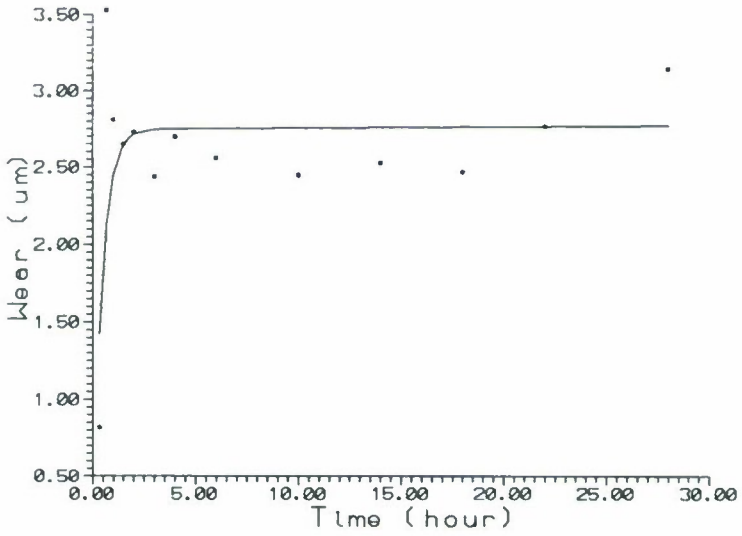

Figure 25. Wear as a function of engine break-in time

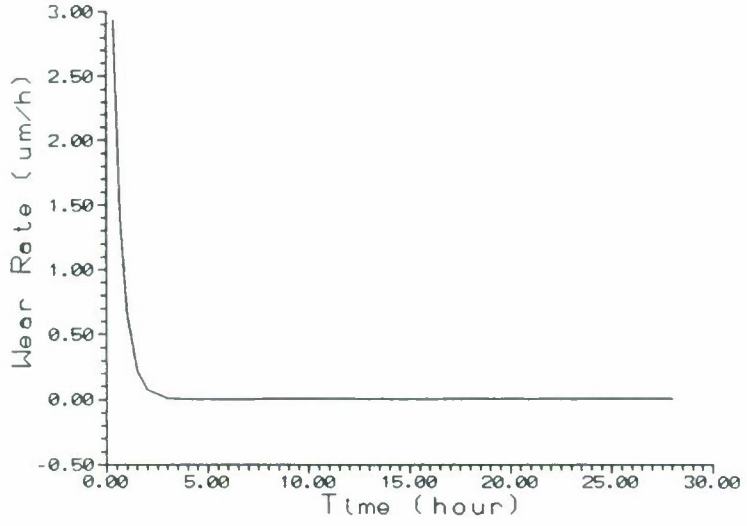

Figure 26. Wear rate as a function of engine break-in time

Integrating Equation (6-1) and since w_d at t=0 equals zero,

$$w_d = (a/b)(1-e^{-bt}) + ct \qquad (6\text{-}2)$$

According to Equation (6-2) the experimental data for the nominal wear depth can be expressed as

$$w_d = 2.75\,(\,1-e^{-2.21t}\,) + 0.001t \qquad (6\text{-}3)$$

Equation (6-3) is shown as a solid line in Figure 25. By diffrenciating Equation (6-3), the rate of change in the nominal wear depth (the wear rate) can be given by

$$w_r = dw_d / dt = 6.08\, e^{-2.21t} + 0.001 \qquad (6\text{-}4)$$

Equation (6-4) is presented in Figure 26.

Equation (6-2) shows that the total break-in wear can be considered to consist of two

parts: a steady state wear (c×t) which will continue at a constant rate after the break-in, and a transient part $(a/b)(1-e^{-bt})$ which occurs only during the break-in period. The experimental data given by Equation (6-3) shows that the contribution of the steady state wear (c×t) is very small compared to the break-in wear. Therefore, the cumulative wear during break-in is almost equal to (a/b).

6.4 TEST DATA OF SURFACE ROUGHNESS

The parameters used to determine the surface roughness include Ra, Rq, Rp, Rt, Rsk, HSC, Δa and Δq. These are illustrated in Appendix.

Figure 27 shows the roughness parameters Ra and Rq plotted against engine break-in time for the first wear probe. Similar to wear, the major change in roughness occurs during the first hour of the break-in.

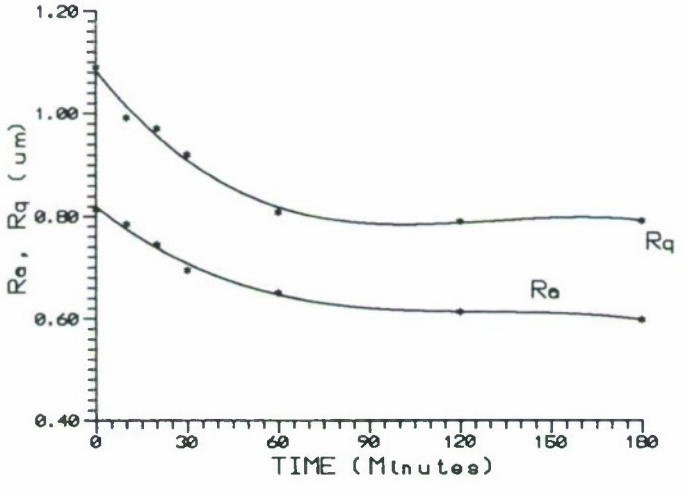

Figure 27. Ra and Rq during the first three hours of engine break-in period

Figure 28 shows several roughness parameters: Ra, Rq, Rp, Rt, Rsk, HSC, Δ_a and Δ_q before and after three hours of break-in for the first wear probe. Ra and Rq decrease due to the surface becoming smoother after wear. Rt and Rp decrease significantly because of the highest peaks of the asperities are removed. However, the decrease of Rp is not as significant as Rt since the new center line of the worn surface profile is lower than that of the original surface.

Rsk, HSC, Δ_a and Δ_q provide more details about the changes in the surface topography. The increase of HSC shows more asperity peaks, both original and newly created by wear, are crossed by the new centre line. The increase of Δ_a and Δ_q after wear indicates that the wear process creates a profile length longer than the original[15]. This can be explained by equation (6-5).

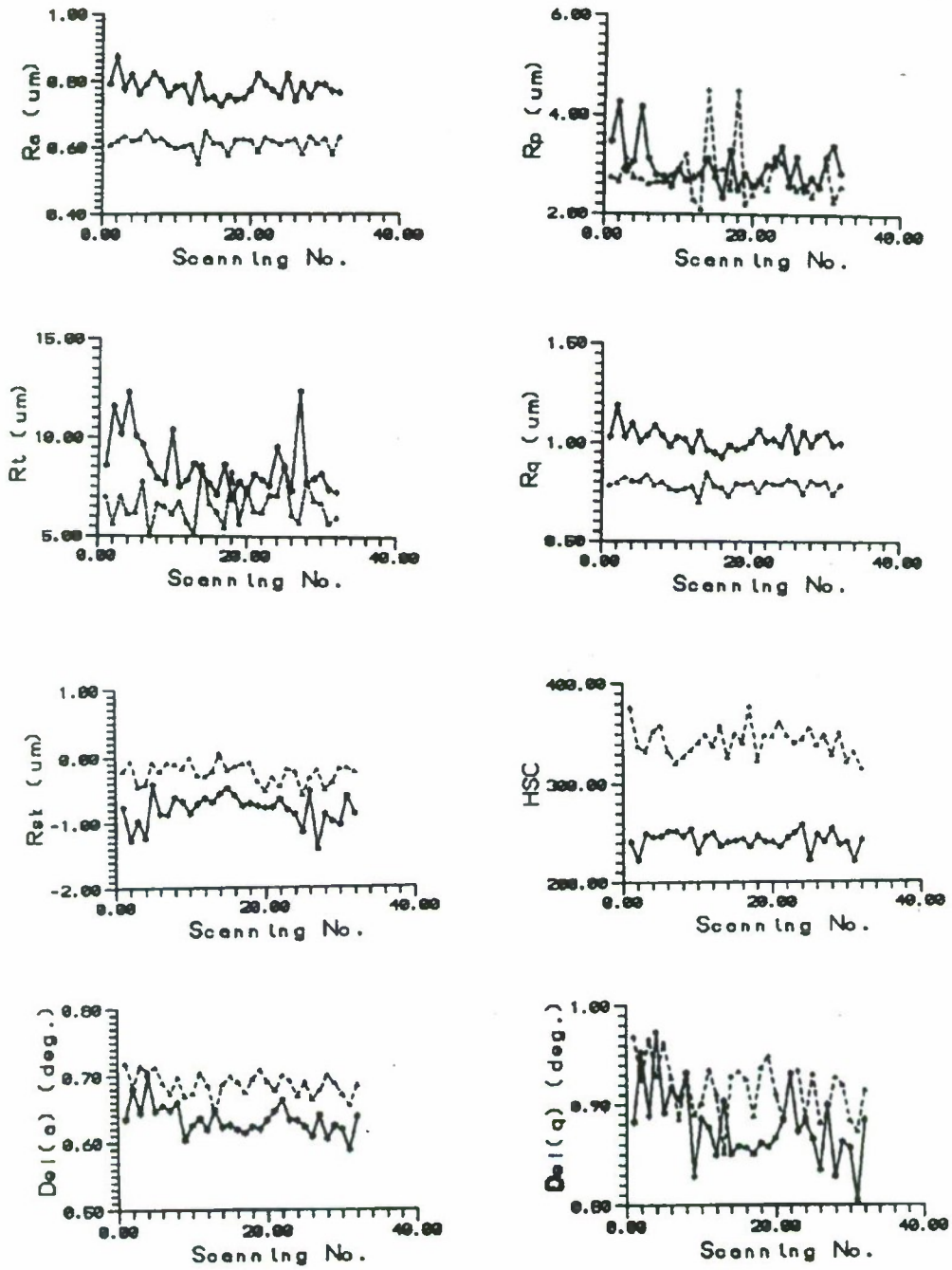

_____ before wear ; - - - - after wear

Figure 28. Roughness parameters before and after 3 hours of break-in

$$1+\frac{1}{2}(\Delta_a)^2 = 1+\frac{1}{2}(\Delta_q)^2 = \frac{\textit{actual profile length}}{\textit{nominal profile length}} \qquad (6-5)$$

As wear occurs, some material is removed from the old peaks and new peaks and valleys are created. If the newly exposed surface after wear is larger than the original surface, both Δ_a and Δ_q increase.

The skewness Rsk is a measure of profile symmetry about the center line. A perfectly symmetrical profile has Rsk=0. A negative Rsk indicates that the profile is dominated by valleys and vice versa.

The original Rsk, shown in Figure 28, is negative. This is a characteristic of plateau honed surfaces. After wear, Rsk increases and approaches zero. This would imply that the surface profile has become more symmetrical about the new centre line after break-in. To explain this, reference is made to the surface profiles before and after wear as shown in Figure 29. These profiles indicate that wear occurs and result in the removal of a thin layer of the surface. This layer includes peaks as well as some valleys, as illustrated in Figure 30(b). This type of wear is different from that observed by Stout[17,18] where the top part of the asperities is removed as illustrated in Figure 30(a). It is obvious that the worn surface profile, illustrated in Figure 30(b), is more symmetric around its new centre line than the original profile.

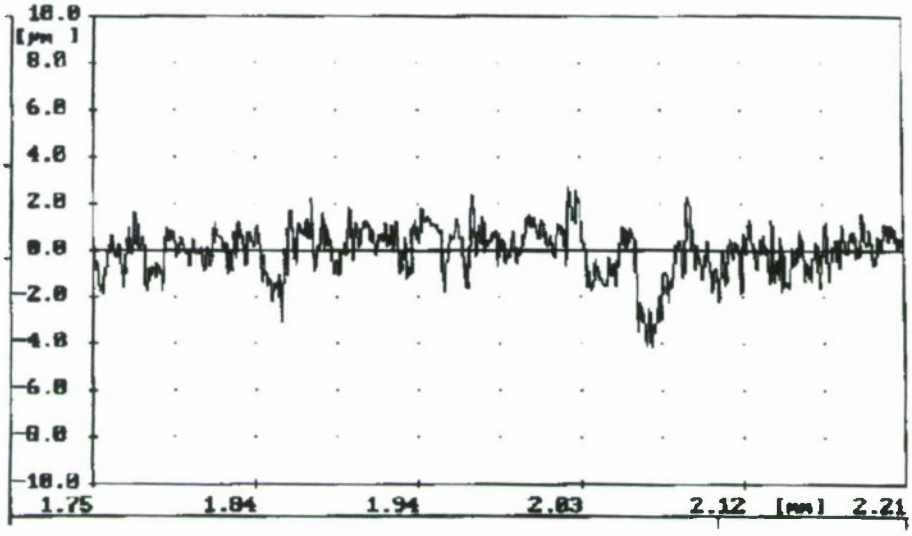

(a) Before Wear

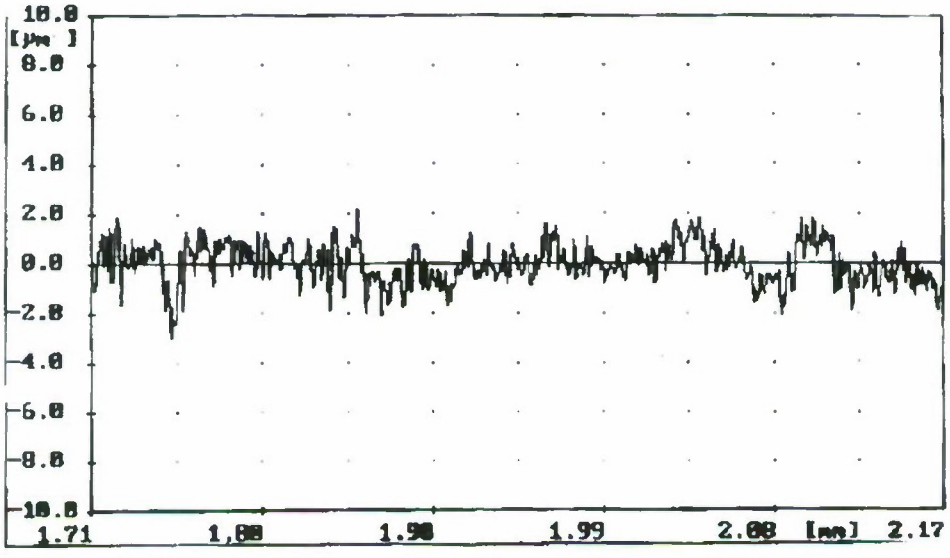

(b) After Wear

Figure 29. 2D roughness profile of the probe before and after wear

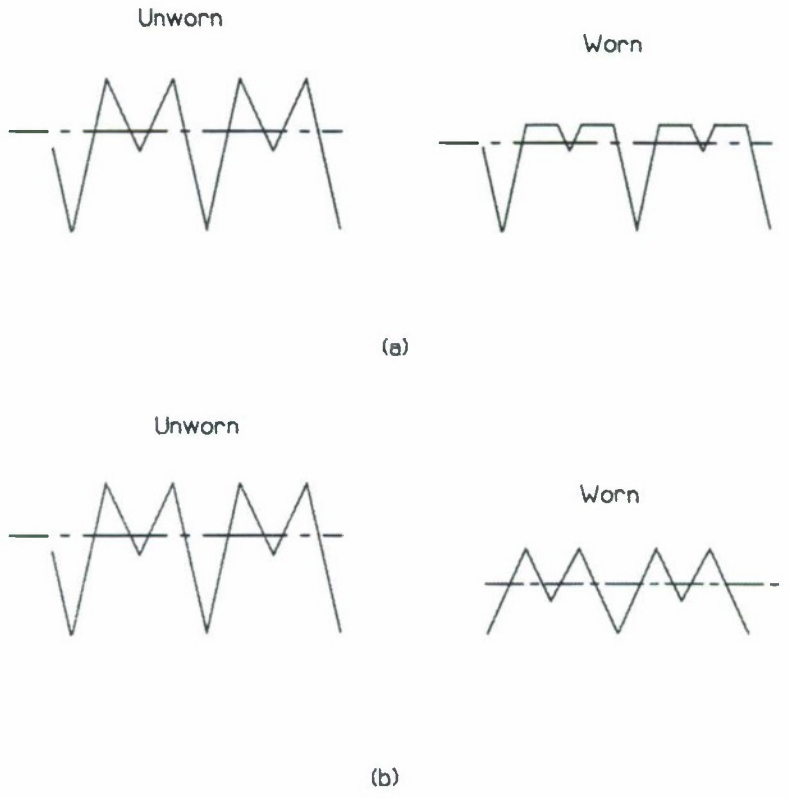

Figure 30. Two wear behaviours of an ideal surface roughness profile

The variation of the surface roughness Ra during the break-in period for the second wear probe is shown in Figure 31. The best fitting curve for this data can be given by

$$Ra = 0.06\, e^{-0.2t} + 0.54 \qquad (6\text{-}6)$$

By comparing Figure 26 and Figure 31, it is clear that most of the wear occurred within the first hour, while the surface roughness took longer time (about 24 hours) to reach its steady state. This indicates that the surface texture characteristics were significantly changing even

after the material wear reached a steady state. Therefore, the completion of the break-in process cannot be considered to be achieved when the wear reaches its steady rate.

6.5 TEST DATA OF INSTANTANEOUS FRICTIONAL TORQUE

The experimental data of the cycle-averaged instantaneous frictional torque $\bar{M}_{IFT}$ for the second wear probe is given in Figure 32. It shows that $\bar{M}_{IFT}$ decreased sharply at the beginning of the break-in procedure, after which it decreased at a much lower rate. This type of change is similar to that of the surface roughness, shown in Figure 31. The best fitting curve for $\bar{M}_{IFT}$ is

$$\bar{M}_{IFT} = \alpha e^{-\beta t} + \gamma \qquad (6\text{-}7)$$

where $\bar{M}_{IFT}$ = average instantaneous frictional torque over engine cycle, in NM

t = cumulative engine break-in time, in hour

α = (average IFT at t=0 of break-in) - (steady average IFT when break-in is completed), in NM

β = the time dependence of break-in, in hour^{-1}

γ = steady average IFT when the break-in procedure is completed, in NM

According to Equation (6-7) the experimental IFT data can be given by

$$\bar{M}_{IFT} = 1.76\, e^{-0.2\, t} + 0.88 \qquad (6\text{-}8)$$

Equation (6-8) is shown by the solid line in Figure 32.

Similar to surface roughness, about half of the total change in the mean IFT happened during the first 3.5 hours of the engine break-in time. Also, the mean IFT took longer time, about 24 hours, to reach its steady state as compared to 3.5 hour for the wear rate. This indicates that wear rate is not a good indicator of friction.

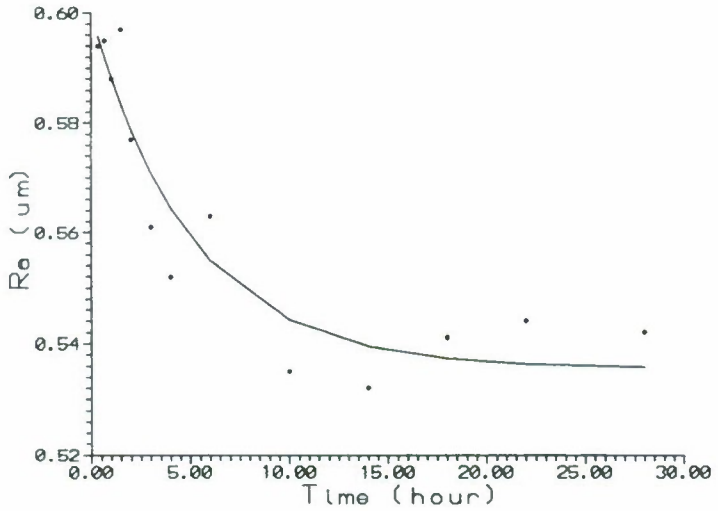

Figure 31. Surface roughness as a function of engine break-in time

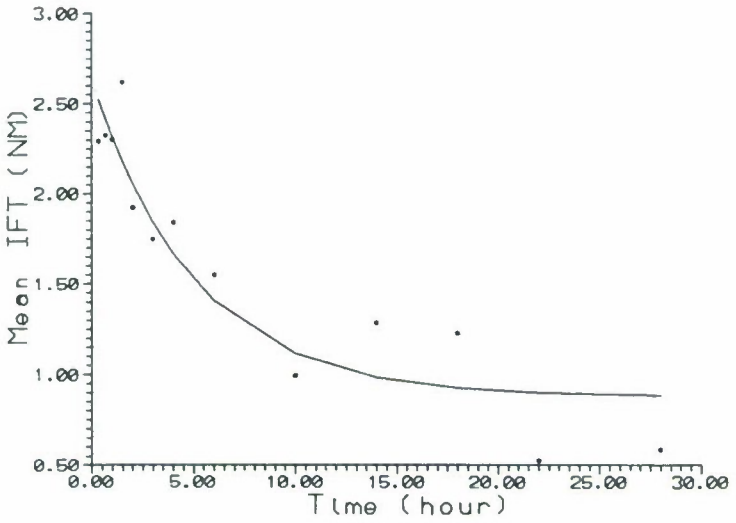

Figure 32. Mean IFT as a function of engine break-in time

6.6 CORRELATION BETWEEN SURFACE ROUGHNESS AND ENGINE FRICTION

The engine used in this investigation has been tested in our laboratories for many years. For the current investigation, the only new components which needed to be broken-in are the cylinder liner, piston and piston rings. Therefore, the change in the total engine friction can be considered to be due to changes in the surface roughness of the piston, piston-rings and cylinder liner. Accordingly, a relationship between the liner surface roughness and the mean IFT can be developed, as given by the Equation (6-9).

$$\bar{M}_{IFT} = 29.33\ Ra - 14.96 \qquad (6\text{-}9)$$

Equation (6-9) is plotted in Figure 33 which shows that engine friction during the whole break-in period is linearly dependent on the surface roughness Ra. A possible explanation is given below:

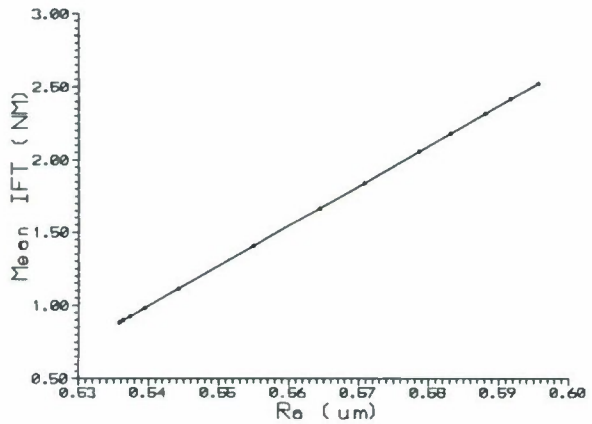

Figure 33. Mean IFT as a function of surface roughness Ra

The piston-ring assembly friction can be considered to consist of two modes. The first is the friction caused by the direct contact of the surfaces of the moving pairs. This can be in the dry, boundary or mixed lubrication regimes. This mode is referred to as surface contacting friction. The other mode is the viscous drag force of the lubricant film in the hydrodynamic lubrication regime where the surfaces are well separated. This mode is referred to as lubricating film friction. By comparing these two modes, it is clear that the friction coefficient for the surface contacting mode is much larger than that for the lubricating film mode. At the beginning of the break-in period, since the surface roughness is high and the engine speed is low, as shown in Table 5, the surface contacting mode is the major contributor in total engine friction. As the engine break-in procedure goes on, the roughness of the frictional surfaces becomes smaller and smaller due to wear as shown in Figure 31, meanwhile the engine speed is increased. As a result, more and more of the frictional

surfaces, originally in surface contacting mode, change to the lubricating film mode. This change in the friction mode decreases the PRA friction.

6.7 RELATIONSHIP OF ENGINE FRICTION AND WEAR

Comparing the exponents in Equation (6-4) and (6-8) indicates that the friction break-in takes longer time to stabilize than the wear break-in. This is similar to Blau's[21] finding for unlubricated materials. In general, the relationship between friction coefficient and wear rate for steady state or for break-in cannot be generalized[21]. Wear and friction are not necessarily correlated especially when lubrication and tribochemistry reactions are present at the contact interfaces[22].

The average IFT may be expressed as function of wear-rate, by combining Equation (6-4) and (6-8) as given by equation (6-10)

$$\bar{M}_{IFT} = 1.49\ (w_r - 0.001)^{0.091} + 0.88 \qquad (6\text{-}10)$$

The change in the PRA frictional torque during the break-in period can be considered to occur in three regimes as shown in Figure 34:

Regime I. Material Removal Regime (MRR)

Regime II. Transient Regime

Regime III. Surface Roughness Smoothing Regime (SRSR)

The characteristics of each regime are discussed in the following sections.

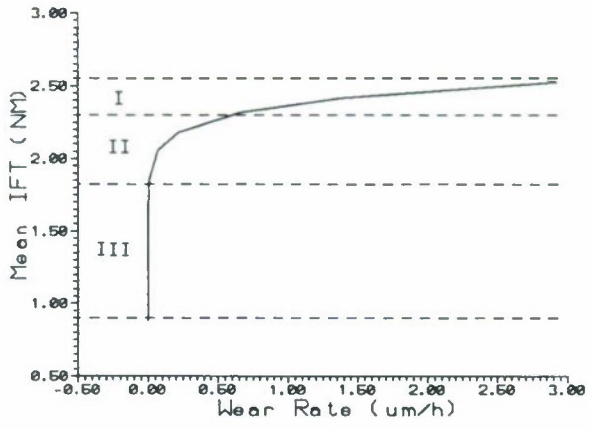

Figure 34. Mean IFT as a function of wear rate

Regime I: Material Removal Regime (MRR)

This regime occured over the first hour of the break-in period. During this regime there was a sharp drop in wear rate, and a relatively small change in PRA friction. Figure 31 indicates that there was a small change in surface roughness. A possible explanation of the small change in friction, in spite of the large drop in wear rate can be made by referring to the adhesion theory of friction[21] , with the following assumptions:

1. The friction force in this regime is mainly contributed to the direct contact between the wearing surfaces.
2. The friction force F is equal to the product of the real area contact A_r and the shear strength of bond in that region. According to the adhesion theory of friction[23]

$$F = A_r \sigma_s \qquad (6\text{-}11)$$

where, σ_s is the shear strength of the softer material.

3. The normal load N, carried by the tips of asperities which are under plastic deformation

when the surfaces contact each other, can be given by

$$N = A_r \sigma_y \qquad (6\text{-}12)$$

where σ_y is the hardness of the softer material.

4. The wear is mainly based on the cutting mechanism. The softer material which is plastically deformed by the harder surface will be removed as wear debris.

At the beginning of the break-in period (Regime I), the engine load was kept constant, according to the break-in schedule given in Table 5. Thus we can assume that N was constant as long as the load was kept constant. According to Equation (6-12) A_r would not change (as wear goes on) as long as σ_y remains constant. This may be justified if we neglect the effect of work hardening of the material on σ_y. Therefore, with an almost constant A_r the friction force, given by Equation (6-11), should not change much as long as σ_s is a constant.

The reason for the sharp drop in the wear rate can be explained as follows. At the beginning of the break-in period the two surface are poorly conformed. In order to have enough contacting surface area to support the normal load, the tips of the asperities must undergo a large plastic deformation according to the assumption 3. According to the assumption 4, those plastic deformed material will be removed as wear debris. As break-in continues, the wearing surfaces become more and more conformed. Therefore, there will be less and less plastic deformed asperities and the wear rate will become smaller and smaller.

Regime II: Transient Regime

This regime is between the high wear-rate (MRR) and the Surface Roughness Smoothing Regime (SRSR) when low wear-rate occurs. In this regime, changes in wear rate and in PRA friction were obvious. Unlike MRR regime, friction in this regime was no more dominated by

shearing the asperities. Meanwhile, wear was not as intensive as in MRR regime due to the better conformity of the surfaces. Wear-rate and PRA friction are both under transient status in this regime.

Regime III: Surface Roughness Smoothing Regime (SRSR)

This regime began when the wear reached its steady low rate after 3.5 hours, ended after 24 hours. This regime is characterised by a large drop in friction associated with a relatively small drop in wear-rate. The drop in friction may be contributed to the change in the surface roughness. Figure 33, shows the linear relationship between friction and surface roughness, over the whole running period. Figures 31 and 32 show that about half of the change in friction and surface roughness occurred during this regime, after wear reached its steady rate. It should be mentioned that although the change in the value of IFT is large, its rate of change in regime III is smaller than that in the first two regimes.

By considering the change in PRA friction, it is hard to say there is a direct relationship between wear-rate and friction. A large change in wear-rate in Regime I was not accompanied by a corresponding change in friction. In regime III a small drop in wear-rate was associated with a large drop in friction. Therefore we conclude that during the break-in period, the PRA friction is poorly related to wear-rate, but is directly proportional to surface roughness.

6.8 ENERGY LOSS DUE TO FRICTION DURING BREAK-IN PERIOD

The work done δW_f by the engine to overcome the PRA friction in a small increment

of time δt can be calculated as

$$\delta W_f = \bar{M}_{IFT}\, \omega\, \delta t \qquad (6\text{-}13)$$

where

ω = the angular velocity of the engine

and from Equation 10

$$\delta W_f = (1.76\, e^{-0.2t} + 0.88)\, \omega\, \delta t \qquad (6\text{-}14)$$

The power lost to overcome friction, given by Equation (6-14), is plotted in Figure 35. It can be divided into two terms. The first term on the right hand side of Equation (6-14) is a transient which has its highest value at the beginning, and diminishes at the end of the break-in period.

The second is a steady term which continues during and after the break-in period.

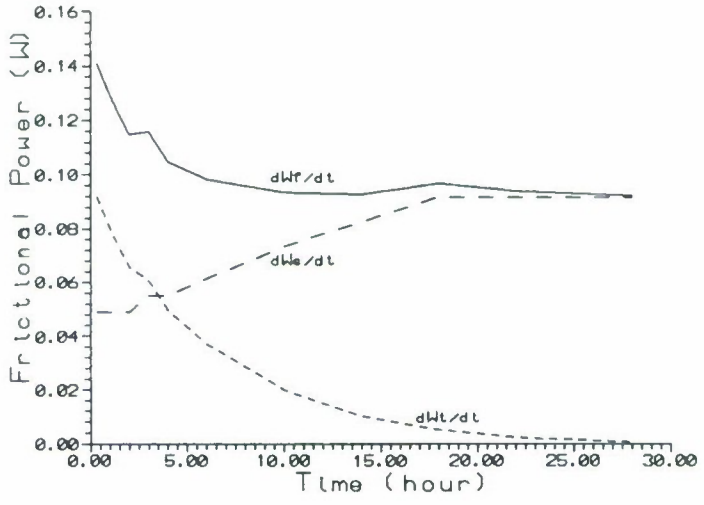

Figure 35. Power lost in friction as a function of engine break-in time

It should be noted that, in the engine used in this investigation, the only parts that were not broken-in are the liner and PRA. Therefore the second term in Equation (6-14) includes the friction in other parts of the engine such as bearings, valve train and auxiliaries.

6.9 SURFACE TEXTURE OBSERVATION —— A DISCUSSION ABOUT WEAR MACHANISM

6.9.1 Methods for Detecting Wear Mechanisms

The methods for detecting wear mechanisms includes wear particle morphology, surface texture observation and chemical component analysis of the wear debris.

The classification of wear particles in terms of their morphological attributes such as shape, size and surface texture represents an essential aspect of understanding the mechanisms which control particle processes and which determine the responses to changes in the operating cycle[27]. Particle morphology is defined comprehensively in terms of six attributes, i.e., profile, edge detail, surface texture, size, colour and thickness[27]. To perform particle analysis, two primary approaches are used, i.e., behavioural techniques and image analysis. In the former, particles are scanned visually and then categorised in terms of a specific qualitative description. With the latter, quantitative techniques are utilised which can provide an abundance of shape descriptors. A computer image processing and analysis system has been developed to help the analysis of the size distribution, profile, outline shape through Fourier analysis and the use of Fractals, edge detail and surface texture[22].

Wear mechanism detection can also be achieved by observing the changes of the surface

texture of rubbing surfaces. The components of the products formed due to corrosive wear can be revealed by spectroscopy techniques. Therefore, stylus roughness tracers, microscopy, SEM (Scanning Electron Microscopy), XPS (X-Ray Photoelectron Spectroscopy), EDIX, Auger Electron Spectroscopy etc. are useful in wear mechanism research.

6.9.2 A Review of Wear Mechanisms of Cylinder Liners

Wear mechanisms of the cylinder liner and piston rings are not well understood. Different engine operating stages, i.e. the break-in stage, the progressive wear stage and the catastrophic wear stage, have different wear mechanisms. Different locations on a cylinder liner surface have different wear mechanisms due to the cyclical variations of the cylinder chamber gas pressure, the gas temperature and the sliding speed of the piston rings against the cylinder liner.

Observation of the wear mechanisms of the cylinder liner and piston rings is difficult. If SEM is used, the cylinder liner surface need to be dismantled during the operation period and the sample needed to be made small enough. If ferrography is used, the particles coming from the liner and rings are difficult to be separated from the particles coming from other engine parts such as the crank shaft, gears and bearings.

Wear mechanisms of the cylinder liner include abrasion, corrosion, adhesion and plastic deformation. Cylinder wear is believed to be mostly by abrasion and corrosion [1,12]. The mechanism which governs wear in the top portion of the cylinder liner is primarily adhesion at the beginning and is accentuated with time by corrosive and abrasive processes. When metal-to-metal contact occurs under boundary lubrication condition during the early stages of running-in, the area of contact between the two surfaces is limited to the contacting peaks of the asperities. The high temperatures generated by friction accompanied by the pressure exerted by the piston rings are

sufficient to cause plastic flow and micro-welding of the contacting asperities. Therefore, adhesive wear happens. As the roughness profiles of the two surfaces become more conformed after the initial critical moment of the running-in, abrasion and corrosion become the dominate wear mechanisms. Abrasive wear of the cylinder liner happens in the mixed and boundary lubrication regimes at TDC and BDC and is caused by the rubbing by the hard piston-ring surface or the hard particles in the lub oil. Those hard particles can be core sand, metal swarf, dust and accumulated wear particles in the lub oil. As a chemical film begins to form on the surfaces of the asperities in contact, wear becomes more corrosive in two stages. The first stage is rapid formation of the protective coherent film on the surface. The second stage is removal of the protective film by wear and re-exposure of the surface to more corrosive attack.

Typical wear particles were observed by Jin[28] in the crankcase lubricating oil at different distinctive periods of operation of a diesel engine by using ferrography. It was found that the typical particles during the running-in process were comparatively large rubbing wear particles in considerable quantities, cutting wear particles, a few metallic spherical particles, non-ferrous wear particles and particles of iron oxide. After the running-in, the particles in the lubricating oil were mainly platelet-type normal rubbing wear particles. Near the overhaul time of the diesel engine, the particles in the lubricating oil were large wear particles from the unstable shear-mixed layer, severe sliding wear particles, which had surface striations as a result of sliding as well as approximately straight edges, having sizes varying from 150 to 70 μm. The particles are iron and silicon, derived probably from the cylinder liner, and reappearing as cutting wear particles.

Jin etc.[29] found that the spherical metallic particles which appear in the lubricating oil during running-in, originate mainly from steel in the molten state. The formation of microspheres is considered to be due to local high flash temperatures exceeding the melting point of the steel. X-ray microanalysis indicated that rough-surfaced microspheres originated mainly from the cylinder

liner. Jin developed a special method to examine the interior structure of microsphere particles. He that the cast ledeburite structure, produced by solidification from the molten state at a high cooling rate, was present on cross-sections of the solid sphere particles. Another evidence of solidification of molten state was that some of microspheres were hollow spheres with dendrite arms. When hollow microspheres solidify from molten state, the outer shell contracts during crystallisation so that the internal pressure is greater than the external pressure. Therefore, the internal molten metal or the vapours wrapped in the sphere can break through the shell and result in some branches, or dendrite arms, on the spherical surface.

Corrosion wear was found by Williams[30] to be important. It predominated wear at low cylinder wall temperature, i.e. when the products of combustion condensed on the cylinder walls. Below certain cylinder-wall temperatures, there was a very rapid increase in wear. Such corrosion appears to mainly result from the formation of combustion products of fuel, such as carbon dioxide and sulphur oxide, and additives in the lubrication oil[19]. The water[31] and acidic[19] condensate causes high wear rates by corrosion. By using X-ray diffraction technique, Yahagi[19] found that the reaction products detected were $CaSO_4.2H_2O$, $FeSO_4.H_2O$,Fe_3O_4 and $Fe_2O_3.2SO_3.nH_2O$. Consequently, sulphuric acid in oil, was found to highly promote the corrosion of the lubricated reciprocating surfaces around TDC and BDC[19]. Like sulphuric acid, carbon soot in oil was found to degrade the lubricating state of the oil[19] therefore promote wear of the cylinder liner. The mass of wear particles in the oil filter was found [32] to be only a small portion of the total wear masses. This indicated that the wear particles are extremely small and mostly pass through the pores in the filter.

The worn surface of the cylinder was found to be covered with a surface layer which Montgomery[1] believed to be composed of graphite and Fe_3O_4. Kang and Ludema[1] reported the results of scuffing tests using cylindrical bearings sliding on flat steel specimens. They found that,

at the beginning of sliding, metallic debris was formed, apparently due to low cycle fatigue. Simultaneously, a soft and ductile film, composed of Fe_3O_4, was formed on the steel surface and it functioned as a "solid lubricant". They described early sliding as competition between the rate of oxide formation and the rate of oxide removal by the metallic debris particles. If the oxide prevails, break-in is considered to be successful. Therefore, the oxides could be a significant mechanism in the slow wear of cylinder walls[1].

6.9.3 Surface Texture Observation by Using Laser Stylus

To observe more clearly the change in the surface texture, the surface topography was obtained during this project by using the Laser Stylus. This is shown for a zoomed area before break-in and after three hours in Figure 36 and Figure 37 respectively. The surface at $y \leq 1.0$ mm is above the TDC position of the top ring and does not experience wear. The surface of $y > 1.0$ mm is contacted by the top ring and experience wear. This is evident from the above two figures, as the surface below TDC is obviously worn, while the surface above TDC is similar in the two figures. A careful examination of the topography indicates that the honed valleys remained unchanged while the peaks were mostly removed. In addition, a small pit was formed just below the TDC line which running at approximately $x = 1.2$ mm and $y = 1.1$ mm. It appears that a small bore segment (190 μm x 150 μm x 0.75 μm) peeled off the surface. The wear mechanism producing this surface peeling is fatigue, caused by under-surface shear stresses, and probably enhanced by surface defects or micro-cracks produced in the surface during manufacturing or honing[16].

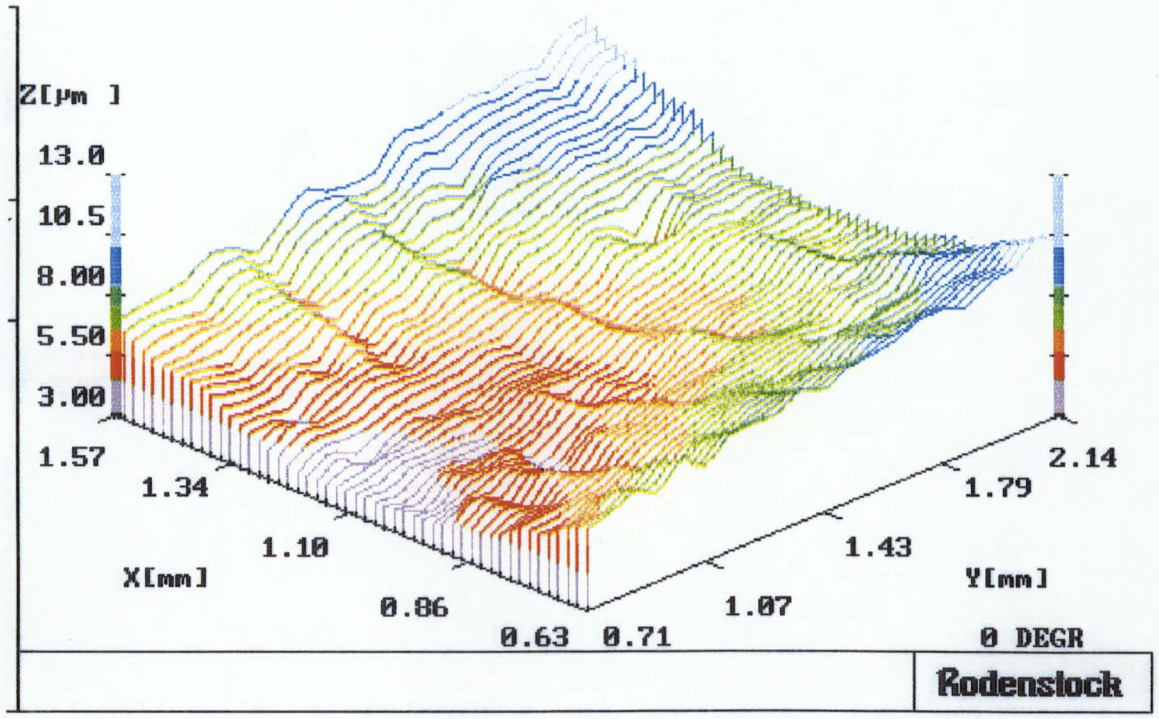

Figure 36. Zoomed surface topography before break-in

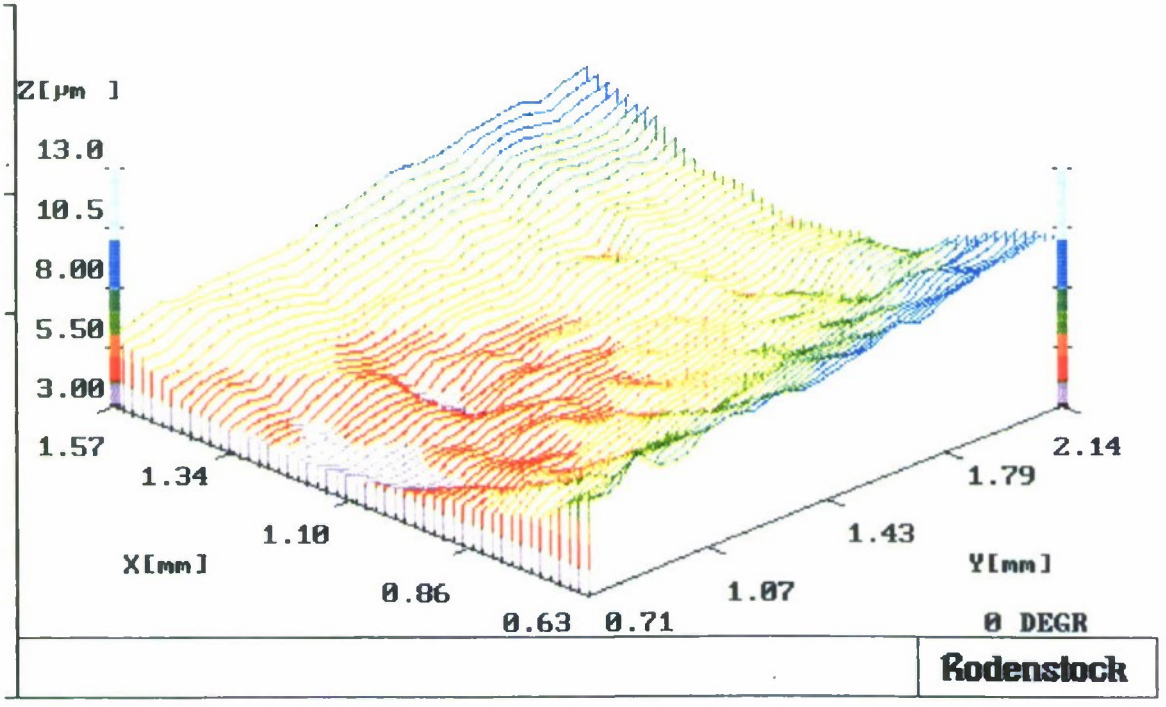

Figure 37. Zoomed surface topography after 3h of break-in

6.9.4 Surface Texture Observed by Using Scanning Electron Microscopy (SEM)

Figure 38 shows a original unworn surface texture of the wear probe examined by a Scanning Electron Microscope (SEM). The magnification is ×500. Cross-hatch feature of the surface is a result of the cylinder honing operation. The grooves created by honing are believed to be able to "store" oil to prevent scuffing and other dire consequences[1]. The grooves are also believed to be able to act as a repository for wear particles, thereby removing them from the contact region between the rings and cylinder wall[31]. A more likely explanation is that the roughness is needed only in the early stages of engine operation to enhance the removal or wearing off of cylinder wall and ring material in places of high interference between these components. They are not made accurately enough to effect good conformity to each other. The reason for the honed roughness is to allow a high wear rate, without catastrophic scuffing, in locations of high stress between poorly conforming parts[1].

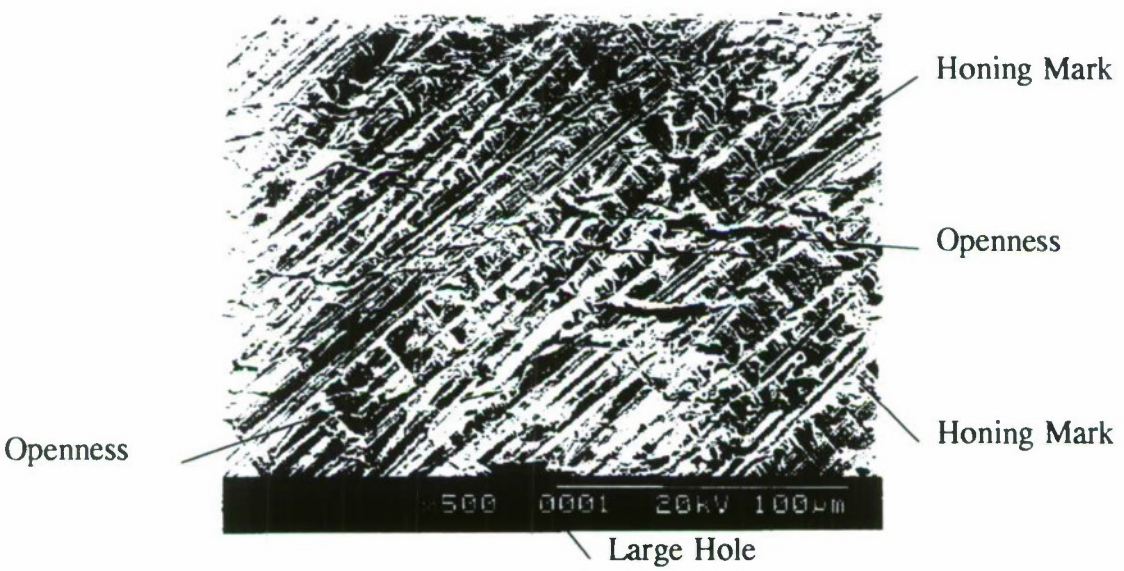

Figure 38. SEM picture of the unworn probe surface

The torn or folded metal is apparent in Figure 38. This folded metal would naturally break off during the initial running-in of the engine and cause wear of the cylinder liner and further cause wear of the piston and rings and the engine bearings where the same oil ultimately came into contact.

Figure 38 also revealed some openness of material and one large hole. By increasing the magnification on the electron scanning microscope to 1000×, crushed and crazed material, shown in Figure 39, was revealed. It was believed to be created by the honing process. Some of the openness of material might have been caused by some graphite flakes, which cropped out to the surface, breaking away from the surface during the honing process.

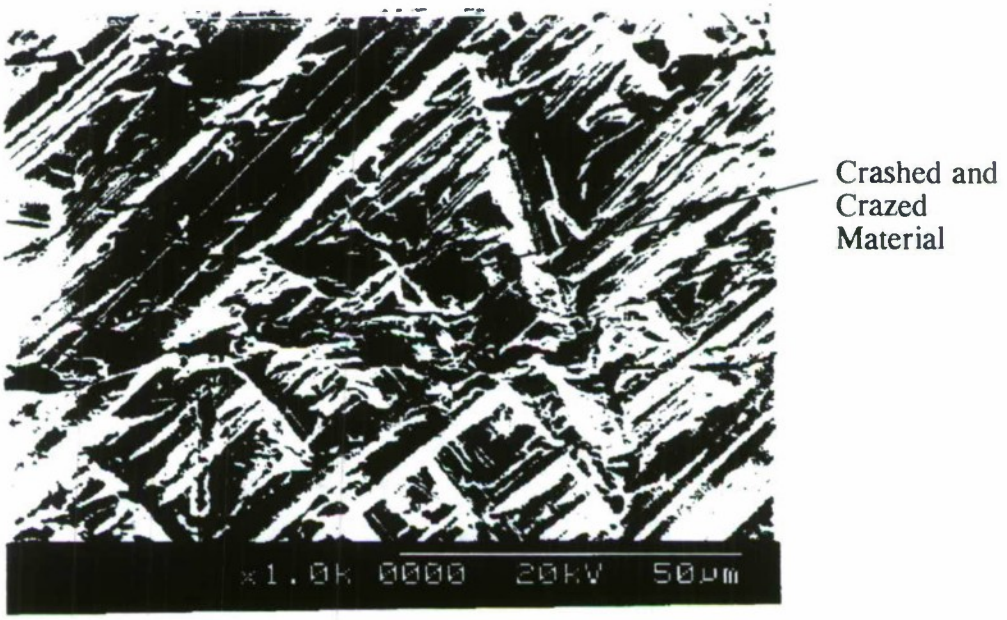

Figure 39. Crushed and crazed material on the unworn probe surface

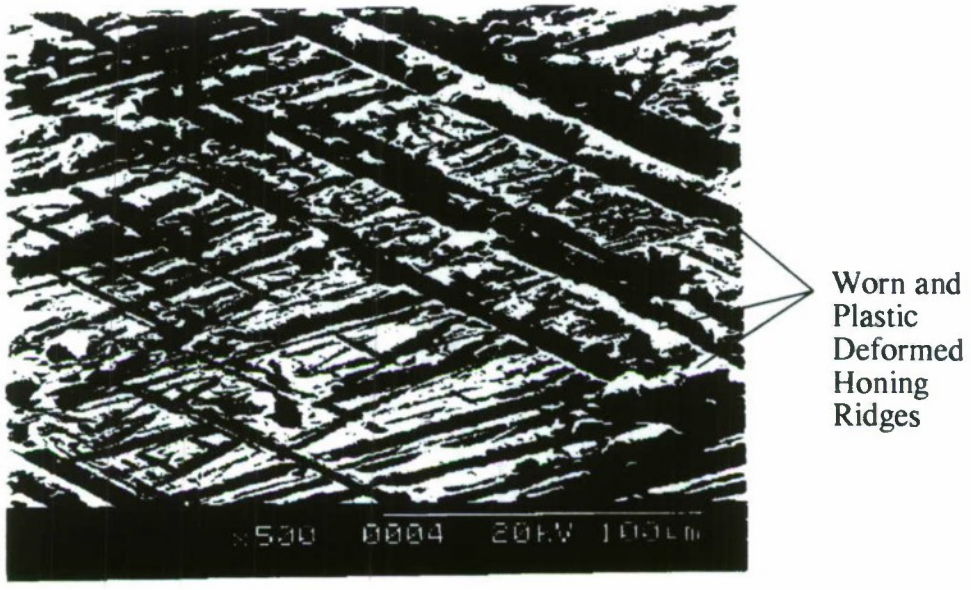

Figure 40. Worn surface of the wear probe

Figure 40 shows the surface texture of the wear probe after 8 hours of the engine break-in. It was noticed that the large amount of ploughed-aside ridges along the honing grooves produced during the honing process were partially worn and partially plastic deformed on their summits. It proves that the folded material created by the honing process was the first one to be worn off during the beginning of the break-in. A more detail examination of the surface revealed a lot of scratches along the sliding direction as shown in Figure 41 to Figure 46. The scratches were mainly caused by metallic and oxide particles that developed by accumulation of fine wear debris as shown in Figure 41, 42 and 43. The particles accumulated at the piston ring cylinder wall interface, and they ploughed grooves in the surface of the cylinder wall. Some of the scratches were caused by breaking-off folded material along the

honing grooves as shown in Figure 42. Some of the scratches were caused by some graphite flakes cropped out to the surface and acted as abrasive particles as shown in Figure 44 and 45.

Figure 46 shows a scratch which was caused by abrasion combined with plastic deformation. The metal seemed to be once molten during the forming of the scratch. Another molten spot on the surface is shown in Figure 47.

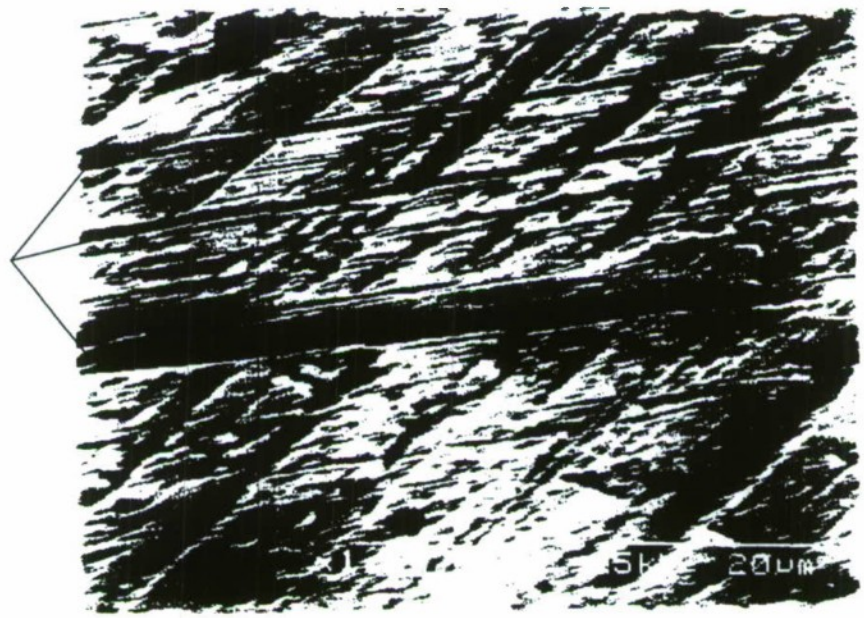

Figure 41. Abrasive scratches on the worn wear probe surface

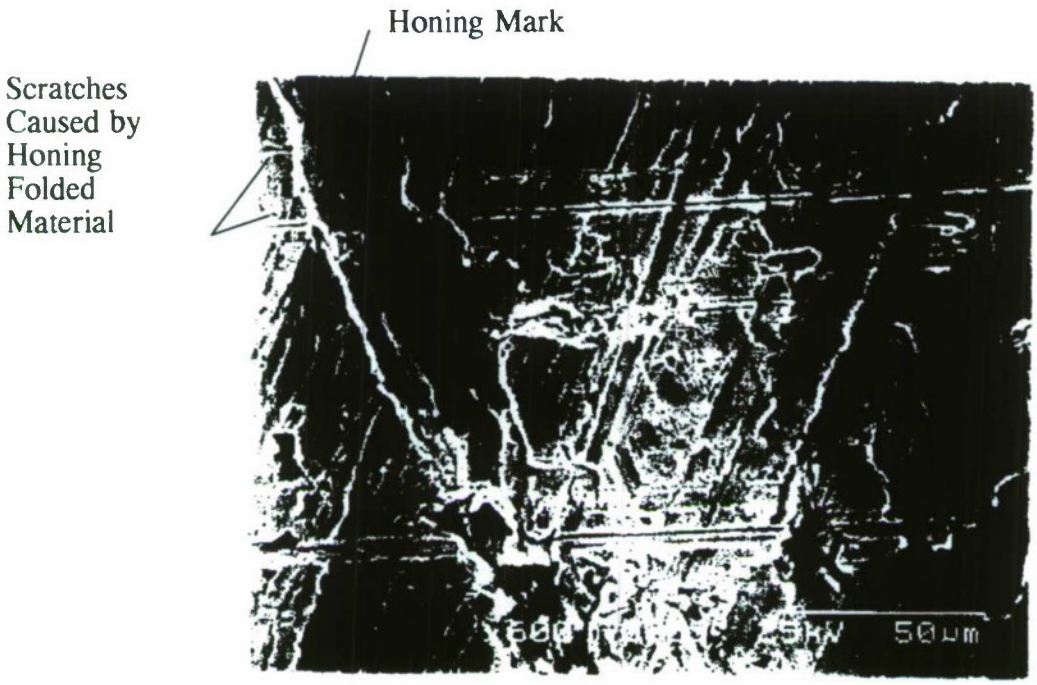

Figure 42. Scratches caused by folded material along the honing grooves

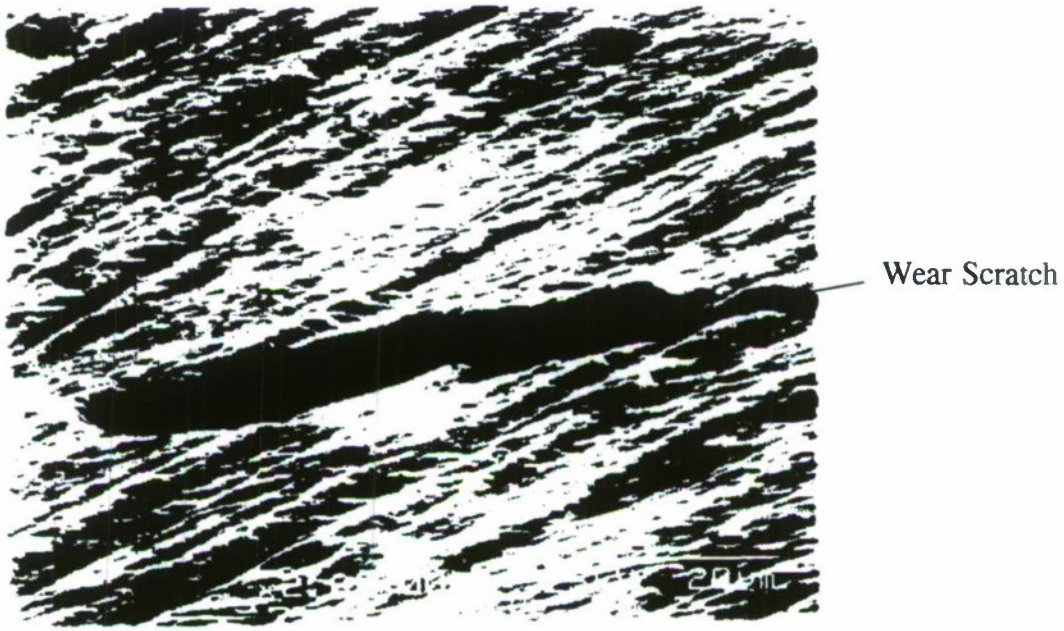

Figure 43. A deep abrasive scratch on the probe surface

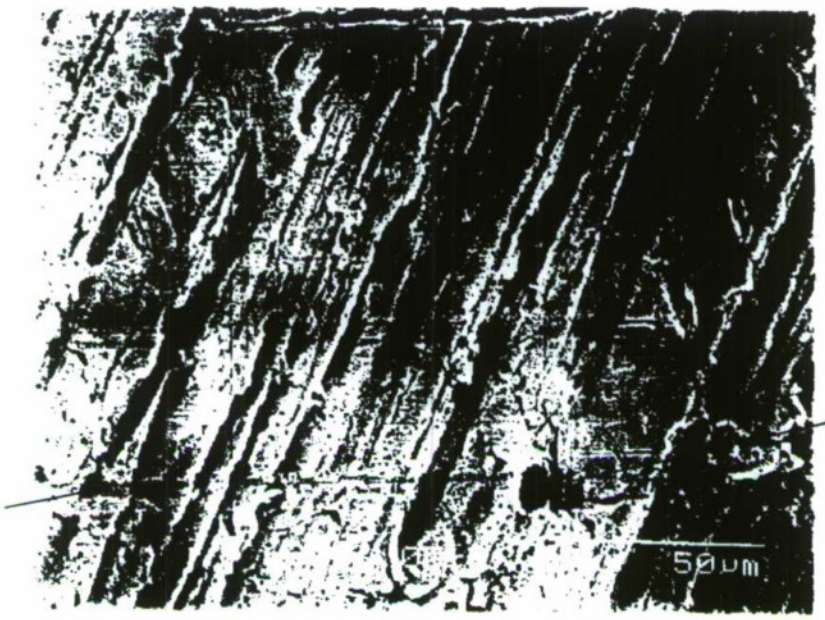

Figure 44. A fine scratch starting from a small pit

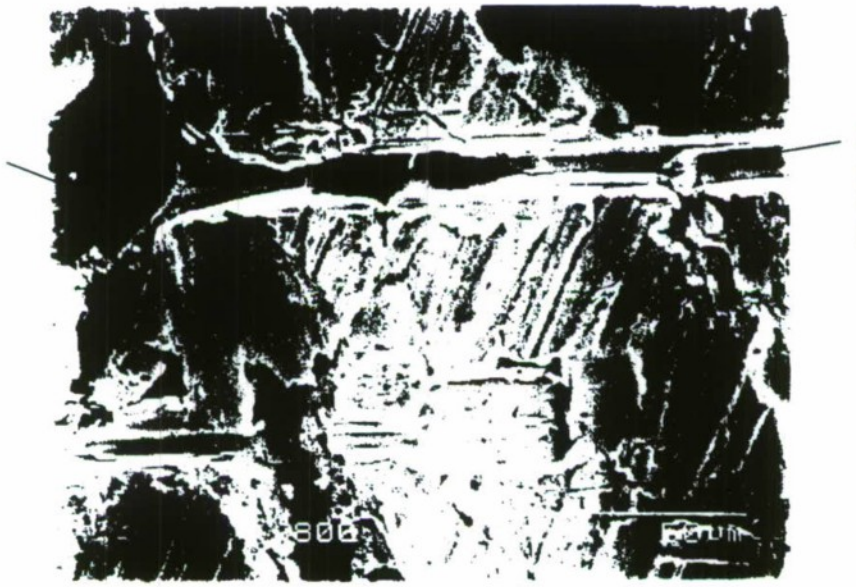

Figure 45. Scratches caused by graphite flakes cropped out to the surface

Figure 46. Scratch caused by abrasion combined with plastic deformation

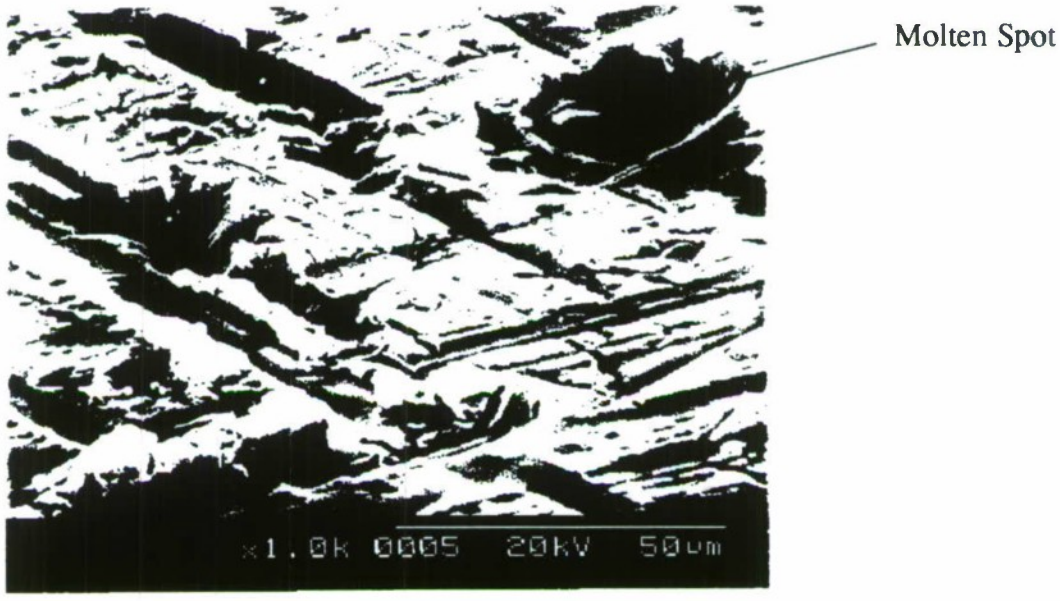

Figure 47. A molten spot on the probe surface

Particles were found embedded in the surface as shown in Figure 48 and 49. They might be the graphite particles which cropped out to the surface by the honing process. Many cracks were found on the surface as shown in Figure 50 and 51. A shallow pit was found as shown in Figure 51. The pit was likely to be formed by surface fatigue. Unlike simple sliding, reciprocating motion of the piston ring/cylinder base system has a changing velocity with the crank angle and a zero value at both reverse points. And since the peak gas pressure is reached at the top reverse point, the contact pressure is much larger and the friction force is much higher at this point than at others. This loading situation has a changing stress field which results in fatigue wear in the contact area of both the ring and liner. Cracking leads to further spalling and particle pull-out.

Figure 48. Embedded particles in the probe surface

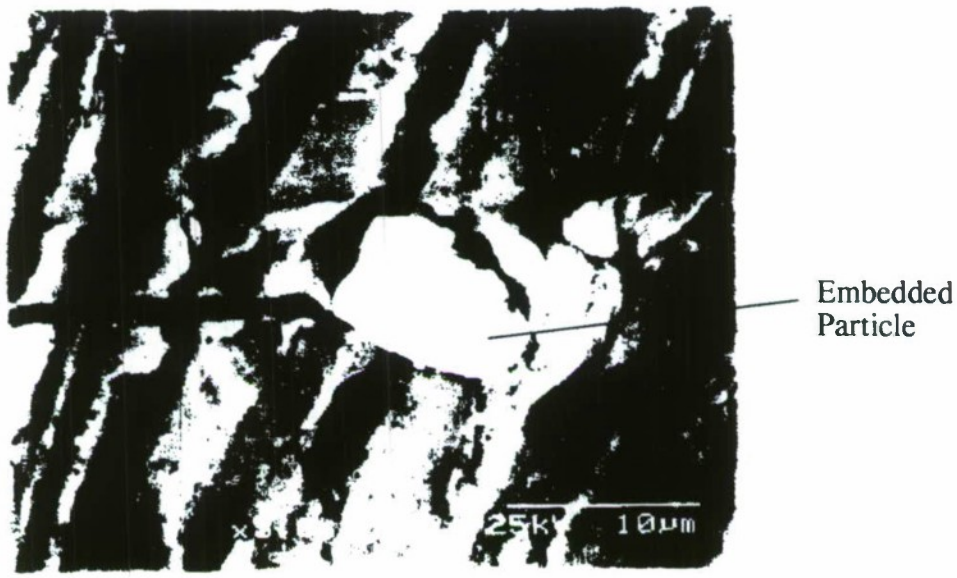

Figure 49. Flat surface particle embedded in the probe surface

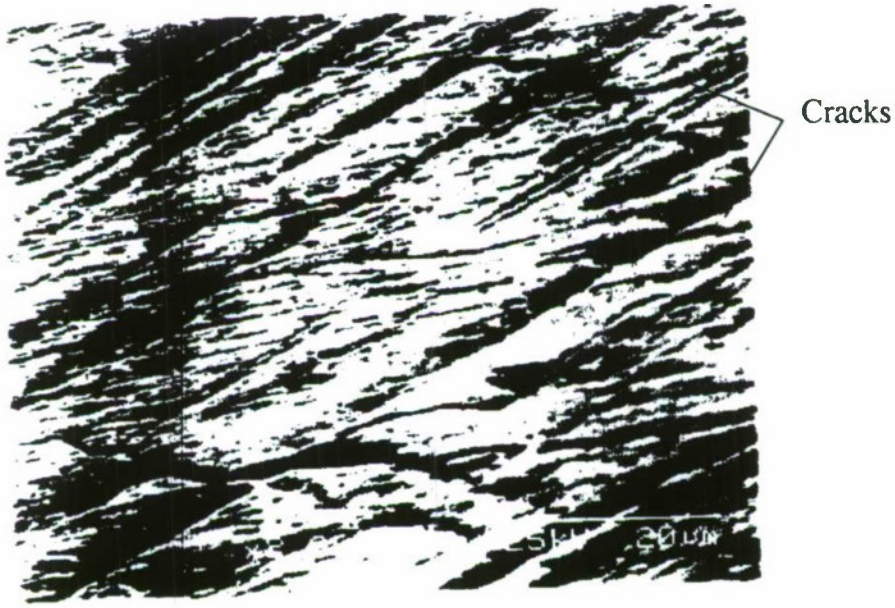

Figure 50. Cracks on the probe surface

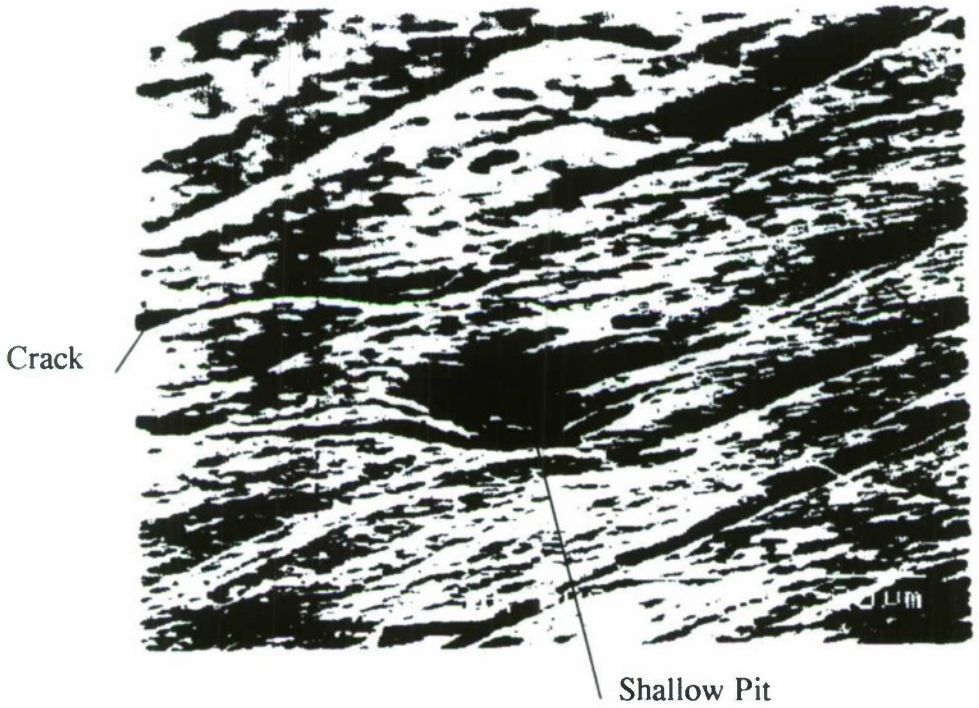

Figure 51. A shallow pit caused by surface fatigue

According to the above observation of the surfaces, the primary wear mechanisms of the cylinder liner on the position where the wear probe located were abrasion, plastic deformation and fatigue. Adhesive wear is not found.

6.9.5 Surface Texture Observed by Using Optical Microscopy

Fine scratches were also found to begin from the honing marks when the probe surface

was examined by using optical microscope. Figure 52 is a picture of the wear probe surface after four hours of engine break-in. The deep dark groove is a honing mark. A much shallow and narrow scratch along the sliding direction of the piston and beginning from the honing mark is an indicator that some folded material along the honing grooves created abrasive wear. Figure 53 is a picture of the same spot of the wear probe as in Figure 52 after 14 hours of engine break-in. The abrasive scratch looks a little bit narrower than that in Figure 52 due to the uniform wear (or "polishing" wear called by some people) of the surface of the wear probe during 10 hours of break-in.

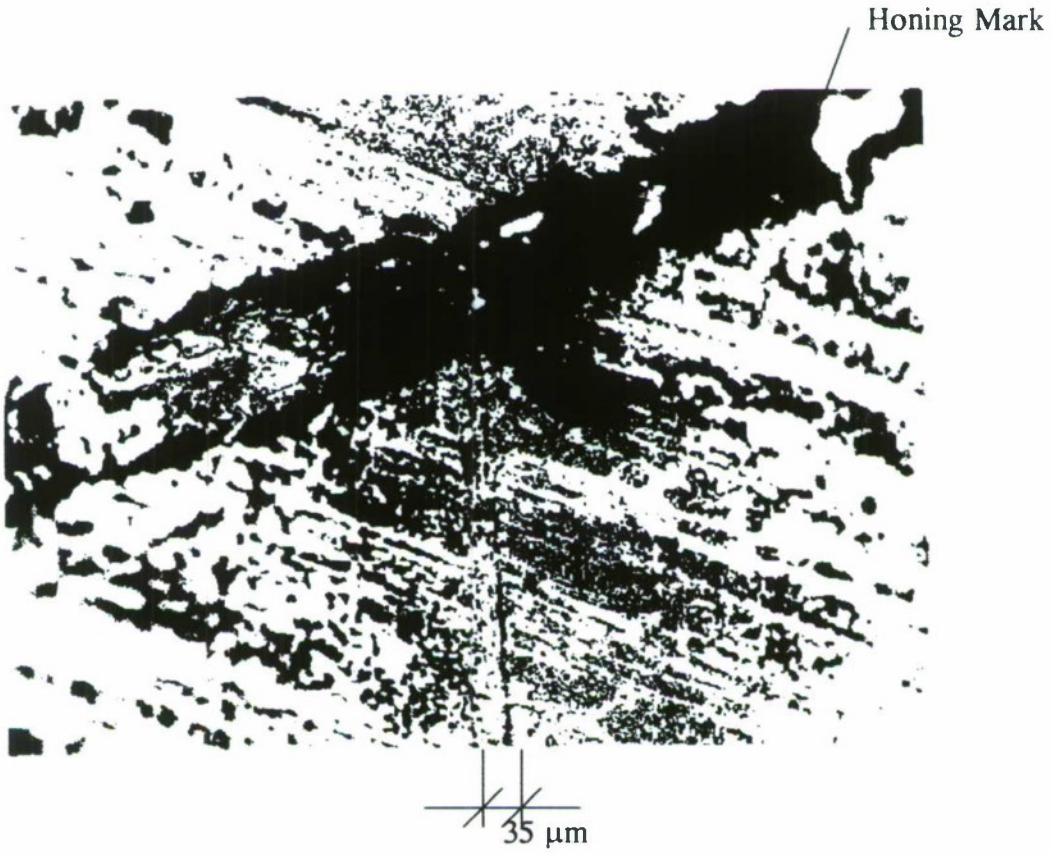

Figure 52. A scratch beginning from honing mark after 4 hours of break-in

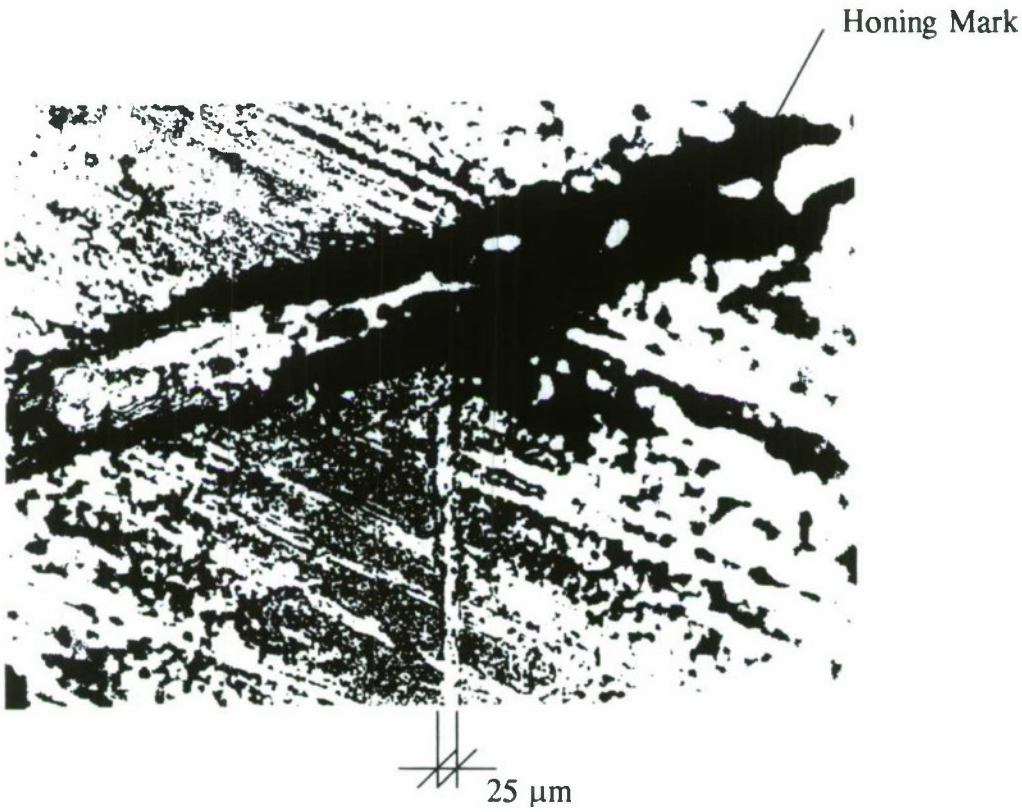

Figure 53. The same scratch as in Figure 52 after 14 hours of break-in

Abrasive scratches were found beginning at TDC position as shown in Figure 54 after 4 hours of engine break-in. The shinning part of the picture is the TDC line. Figure 55 is a picture of the wear probe surface in the same location as in Figure 54 after 14 hours of engine break-in. The surface is obviously uniformly worn or "polished" if compared to Figure 54. The wear mechanism for "polishing" wear process might be a kind of abrasive wear which caused by some very fine abrasive particles and the smooth and hard top ring surface.

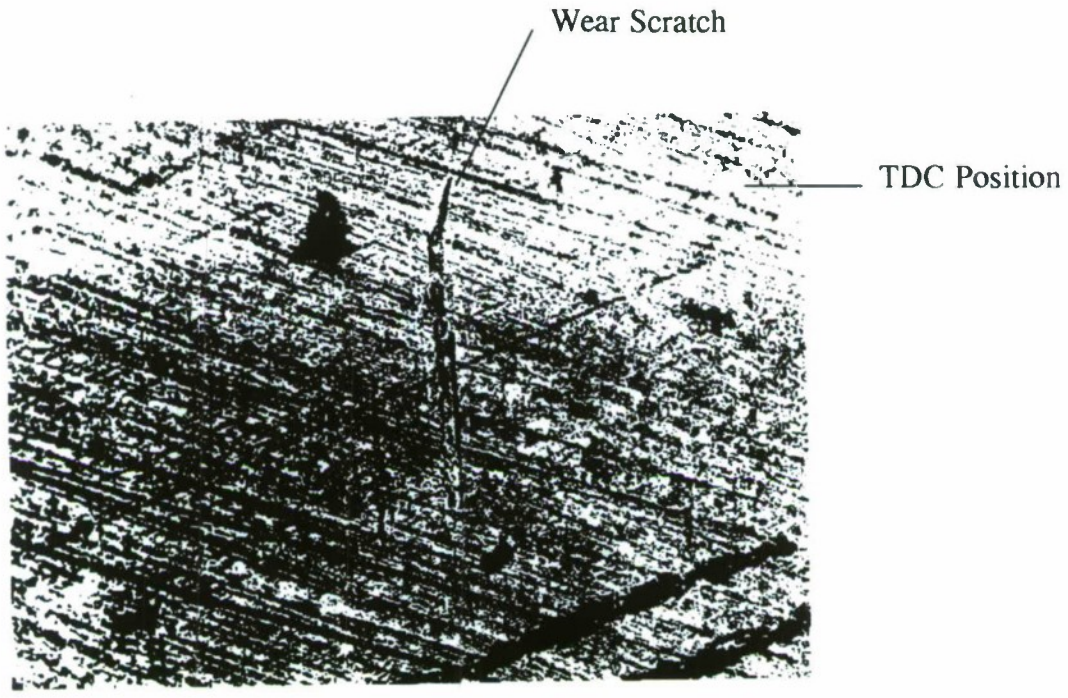

Figure 54. A wear scratch beginning at TDC after 4 hours of break-in

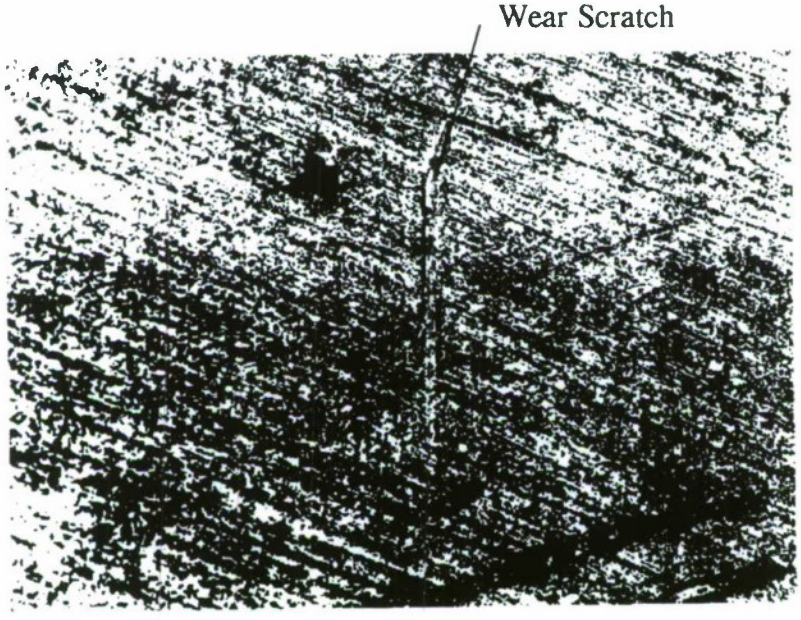

Figure 55. The same wear scratch as shown in Figure 54 after 14 hours of break-in

6.10 EXAMINATION OF WEAR PARTICLES IN LUBRICATION OIL

The examination of wear particles in lubrication oil was made by Emission Spectroscopy. Emission Spectroscopy is based on the study of wavelengths of a substance that is emitted as the substance returns to a normal state after excitation by an external source. When the atoms or molecules are excited by energy input from a spark, they respond in a characteristic manner. Their identity and composition are signalled by the wavelengths of the light they emit. The spectra of elements are in the form of lines of distinctive color; those of molecules are groups of lines called bands. The number of lines present in a spectrum depends on the number and position of the outermost electrons and the degree of excitation of the atoms.

The equipment used to examine our lubrication oil is called the Spectroil M Oil Analysis Spectrometer. It was designed specifically to analyze wear metals, contaminants and additives in lubricants. A group of four oil samples was analyzed. Concentrations of chemical elements of Cr, Cu, Al and Fe in the oil samples were listed in Table 6. Figure 56 shows a plot of the data.

Table 6. Concentration of Chemical Elements in Lubrication Oil

Sample No.	Break-in Time (hour)	Cr (ppm)	Cu (ppm)	Al (ppm)	Fe (ppm)
1	0	0.1	3.1	0.6	2.2
3	0.3333	0.4	9.8	2.6	13.4
5	1.0	0.5	19.2	2.9	19.0
7	3.0	0.8	28.2	7.8	41.1

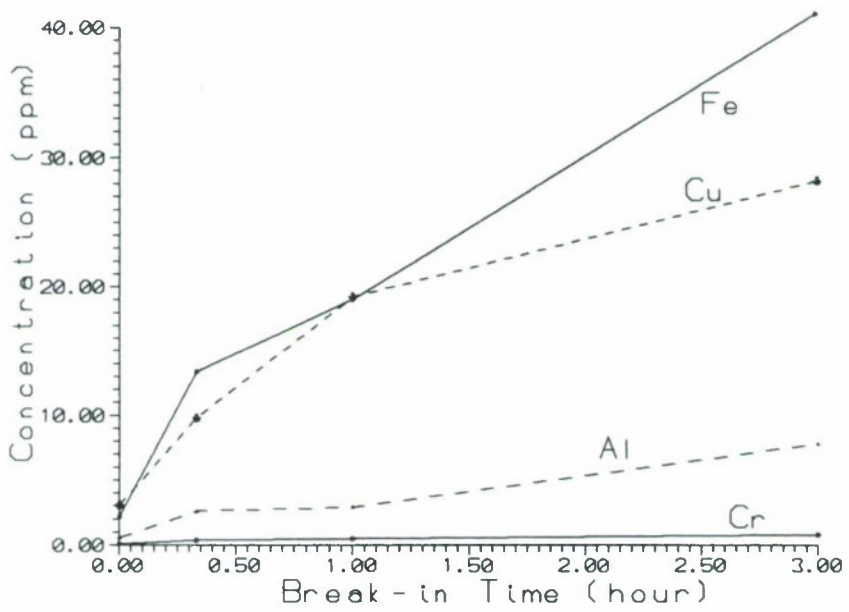

Figure 56. Concentration of elements in lub oil as a function of break-in time

Fe in lubrication oil was mainly due to wear particles worn from cylinder liner which was made of cast iron. Cr in lubrication oil was due to the wear of top piston ring which was coated by Cr. Al mainly came from the wear of the piston. Cu was mainly due to the wear of the bearings. From Figure 56, it is clear that all the above engine parts had increase in wear during the first 3 hours of engine break-in. The wear of cylinder liner (Fe) was the heaviest one among the four parts. The bearing wear was in the second place. The lubrication oil contained less Cr wear particles from the top ring. However, considering that the top ring consisted of a much smaller wear surface compared to the other parts, the wear of the top ring was considerably high.

7.0 POTENTIAL USE OF WEAR PROBE FOR ENGINE RESEARCH AND DEVELOPMENT

The use of the probe for wear and roughness measurements can be very effective in reducing the cost of design, development and manufacturing of new engine-cylinders and piston ring assemblies. The time needed to determine the effect of the different variables on wear can be shortened. The variables include, and are not limited to clearances, surface finish (roughness and honing), material pairs, coatings, lubricating oil and additives. Also, the length of the break-in period of mass produced engines may be shortened if the wear rate of the probe is measured, and the interval of high wear rates determined. This would reduce the cost and time consumed in running-in mass produced engines before delivery. Furthermore, this would assure the manufacturer that the engine passed through the initial running-in period which will reduce the chances of catastrophic failure due to scuffing.

8.0 MODEL SIMULATION OF CYLINDER LINER WEAR

8.1 FORCES ACTING ON THE LINER BY THE PISTON-RING

The forces which act on the cylinder liner by the piston-ring and cause wear include (1) gas pressure force, (2) elastic tension force of the piston ring and (3) piston side thrust force.

(1) The internal gas back pressure p_i of the piston ring

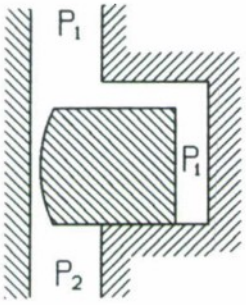

(a) $p_i = p_1$, When $F_{rg}<0$ or when $F_{rg}=0$ & $V_p<0$.

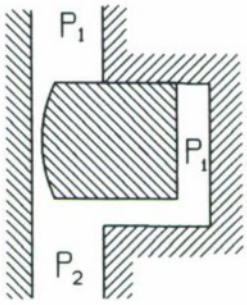

(b) $p_i=p_2$, When $F_{rg}>0$ or when $F_{rg}=0$ & $V_p>0$

Figure 57. The internal gas pressure of the piston ring

The internal gas back pressure p_i depends on the location of the piston ring on the piston ring-grove as shown in Figure 57. If the ring is at the bottom of the grove as illustrated in Figure 57 (a), the internal gas back pressure of the ring is assumed to be the same as the gas pressure above the ring p_1. If the ring is at the top of the house as illustrated in Figure 57 (b), the internal gas back pressure of the ring is assumed to be the same as the gas pressure below the ring p_2. The location of the ring is judged by the direction of the force (F_{rg}) acting on the ring by the grove. If the direction of F_{rg} is upward, the ring is sitting at the bottom of the grove. If the direction of F_{rg} is downward, the ring is sitting at the top of the grove. By neglecting the ring gravity force and the friction force between the ring and the liner surface, and assuming the directions of all the positive forces and velocity are downward, we have:

$$F_{rg} = -F_{ir} - F_{pres}$$

and $$F_{ir} = -m_{ring} a_p \qquad (8\text{-}1)$$

$$F_{pres} = (p_1 - p_2)(\pi D^2 - \pi(D - 2h)^2) / 4$$

where F_{ir} is the inertial force of the piston-ring;

F_{pres} is the total gas force acting on the piston-ring along the sliding direction of the piston;

m_{ring} is the mass of the piston-ring;

a_p is the moving acceleration of the piston;

p_1 is the gas pressure on the top of the ring;

p_2 is the gas pressure on the bottom of the ring;

D is the diameter of the cylinder liner;

h is the width of the ring.

and

If $F_{rg} < 0$, then $p_i = p_1$;

If $F_{rg} > 0$, then $p_i = p_2$;

If $F_{rg} = 0$, then $p_i = p_1$ when $V_p < 0$ and $p_i = p_2$ when $V_p > 0$ (where V_p is velocity of the piston).

At present, since we don't consider the engine blow-by, it is assumed that the gas pressure above the piston-ring p_1 is the cylinder pressure p_{gas} or $p_1 = p_{gas}$, and the gas pressure below the piston-ring is the crankcase pressure p_{case} or $p_2 = p_{case}$.

(2) Piston Ring Elastic Tension Force

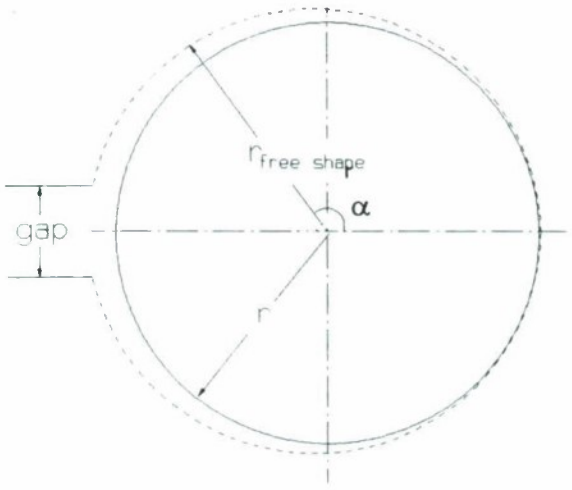

Figure 58. Geometry of the piston-ring

An ideal piston-ring of constant cross section must satisfy the following conditions: (a) It should conform to the cylinder bore, and (b) It should exert a uniform pressure all around on the cylinder wall. If these two conditions are met, the piston ring shape, when free of stress, can be expressed by the following equation[33] (see Figure 58):

$$(r_{\,free\ shape})_{at\ \alpha} = r + \frac{p_0 r^4}{EI}(1 - \cos\alpha + \frac{1}{2}\alpha\sin\alpha) + \frac{r}{2}(\frac{p_0 r^3}{EI})^2(\alpha - \frac{1}{2}\alpha\cos\alpha - \frac{1}{2}\sin\alpha)(3\sin\alpha + \alpha\cos\alpha) \qquad (8\text{-}2)$$

where r is the main radius of the ring in constraint which is approximately equal to cylinder bore radius D/2, p_0 is the uniform constraint force in circumference, EI is the flexural rigidity of the ring and α the angle measured from the back of the ring.

If the piston ring is assumed to be ideal, i.e., the ring is truly circular when confined and it exerts uniform pressure all around the cylinder wall, and also that the ring only moves radially as a unit under loading, the piston ring behaviour is seen to be similar to that of a thin-walled cylinder[33]. With the piston ring treated as a thin-walled cylinder, the radial deflection c, which equals the oil film thickness, is[33]

$$c = \frac{(p_m - p_n)r^2}{Et_r} \qquad (8\text{-}3)$$
$$p_n = p_o + p_i$$

where p_m is the mean pressure which the cylinder liner and lubrication oil film acts on the ring surface, p_n is a combined pressure of the uniform ring's elastic force p_0 and the internal gas back pressure p_i of the piston ring, E is the Yong's modulus of the ring and t_r is the ring thickness.

Oil film temperature and thickness were measured by Wing and Saunders[34] on the piston rings of a diesel engine. They found that the lubricant near the uppermost ring is cyclically subjected to large temperature transients during the power stroke and the film thickness is reduced momentarily to almost zero at the beginning of the power stroke. At present, since the oil film thickness is not calculated, we temporary assume that the oil thickness is zero in the wear measuring region of the wear probe.

(3). Piston-ring reciprocating mechanism and piston side thrust force

The reciprocating mechanism of the Honda single cylinder gasoline engine used in this investigation is shown in Figure 59. The angle β is related to the crank angle θ by

$$\sin\beta = \lambda.\sin\theta$$
$$\lambda = \frac{R}{l} \qquad (8\text{-}4)$$

where R is the radius of the crank and l is the length of the connecting rod.

Figure 59. Piston reciprocating mechanism

Equations of piston displacement y_p, velocity V_p and acceleration a_p of the piston are

$$y_p = R(1 - \cos\theta) + \frac{1}{2}\lambda R\sin^2\theta$$
$$V_p = R\omega(\sin\theta + \frac{1}{2}\lambda\sin 2\theta) \qquad (8\text{-}5)$$
$$a_p = R\omega^2(\cos\theta + \lambda\cos 2\theta)$$

where ω is the crank angular velocity.

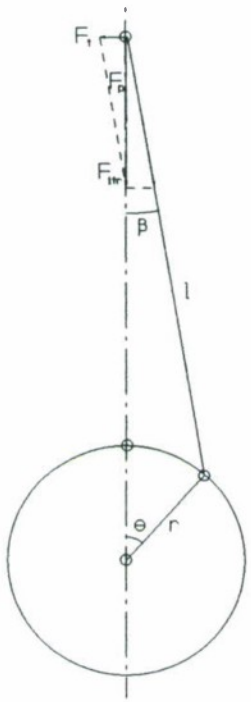

Figure 60. thrust force of the piston

The thrust force F_t as illustrated in Figure 60, by neglecting the gravity force of the piston, rings and piston pin, can be calculated by

$$F_t = (F_p + F_{itr})\tan\beta \tag{8-6}$$

where F_p is the force acting on the piston by gas pressure and F_{itr} is the inertial force of piston ring assembly, and

$$\begin{aligned} F_p &= (p_{gas} - p_{case})(\pi D^2 / 4) \\ F_{itr} &= -(m_{pra} + m_{ctr})a_p \end{aligned} \tag{8-7}$$

At DCs where $\theta=0$ or π, the inertial force of piston assembly $F_{itr} = \mp R\omega^2(m_{pra}+m_{ctr})(1\pm\lambda)$.

where

p_{gas} is the cylinder gas pressure acting on the top of the piston and p_{case} is the crankcase pressure acting on the bottom of the piston respectively. D is the bore diameter. m_{pra} is the mass of the piston ring assembly:

$$m_{pra} = m_{piston} + m_{piston\text{-}pin} + m_{pinton\text{-}rings} \qquad (8\text{-}8)$$

m_{ctr} is the part of the connecting-rod mass m_c which is translate together with the piston shown in Figure 61.

$$m_{ctr} = m_c \frac{l_g}{l} \qquad (8\text{-}9)$$

where l_g is the length from the big end of the connecting-rod to the center of mass of the connecting-rod. l is the length of the connecting-rod.

For simplification m_{ctr} is considered equal $m_c/3$, but in this investigation Equation (8-9) is used.

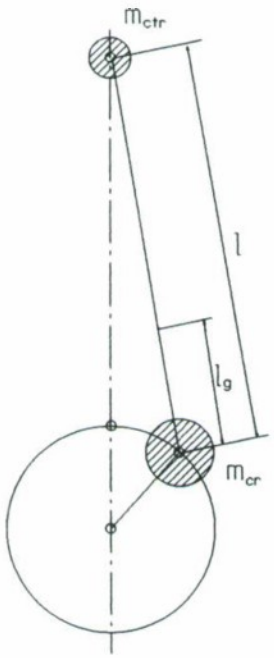

Figure 61. Equivalent masses m_{ctr} and m_{cr} of the connecting rod

The purposes for calculating the piston side thrust force F_t are (a) to determine which side of the cylinder is contacted with the piston-rings, and (b) to determine the wear contributed by the side thrust force.

- **Total Force Resulting in Wear of the Cylinder Liner**

The total pressure p_w which really acts on the cylinder liner by the ring to cause the bore wear is a combination of the ring face pressure p_m in Equation (8-3) and the thrust force F_t in Equation (8-6). Here, the average load pressure between each ring and the cylinder wall caused by piston side thrust is assumed to be equal to the total piston side thrust load divided by the sum of the ring lateral bearing areas. The true load pressure on the rings is highly indeterminate. In principle, less than half of piston side thrust force is carried by the piston skirt, but this force produces very low unit pressure and has been shown to be insignificant in producing bore wear[33].

When $F_t \geq 0$, the thrust force is acting on the major thrust side of the cylinder liner, we assume that p_w at the minor thrust side p_{wmn} at the moment equals p_m. When $F_t < 0$, the thrust force is acting on the minor thrust side of the liner, we assumed that p_w at the major thrust side p_{wmj} at the moment equals p_m. Therefore,

$$p_{wmj} = p_m + \frac{|F_t|}{\Sigma D t_{r_i}}$$
$$p_{wmn} = p_m \qquad When\ F_t \geq 0$$

and (8-10)

$$p_{wmn} = p_m + \frac{|F_t|}{\Sigma D t_{r_i}}$$
$$p_{wmj} = p_m \qquad When\ F_t < 0$$

where tr_i is the thickness of the ith ring.

8.2 CYLINDER LINER WEAR MODEL

The wear along the cylinder wall is calculated by using Archard wear model since the wear of the cylinder liner is sliding wear pattern and its main wear mechanism during the break-in is abrasion. The law states that, generally, the amount of wear is directly proportional to the normal load F and the sliding distance S, but inversely to the hardness H of the surface being worn away. The wear volume can be expressed by

$$W = K_w \frac{FS}{H} \qquad (8\text{-}11)$$

where K_w is the wear coefficient.

In an engine, the force acting on the cylinder liner by a ring in the wear measuring area is

$$F(\theta) = p_w(\theta)A \qquad (8\text{-}12)$$

where A is the nominal contacting area between the liner and the ring within the wear measuring area. Here, the wear measuring area of the wear probe is b × a where b is the width of the measuring area and a is the measuring length along the axis of the cylinder liner. For the piston-ring of thickness t_r, the nominal area A in Equation (8-12) should be b × t_r . Therefore, at crank angle θ Equation (8-11) becomes

$$dW = K_W \frac{p_w(\theta) \cdot b \cdot t_r \cdot ds}{H} \qquad (8\text{-}13)$$

The wear rate with the respect of the crank angle degree at crank angle θ is

$$\frac{dW}{d\theta} = K_w \frac{p_w(\theta) \cdot b \cdot t_r \cdot |V_p(\theta)|}{\omega(\theta) \cdot H} \qquad (8\text{-}14)$$

The crank angle degree which covers the measuring area of the wear probe is from θ_1 to θ_2. Therefore, the wear volume in the measured area of the wear probe, due to piston moving from θ_1 to θ_2 is

$$w_\theta = \frac{K_w}{H} b t_r \int_{\theta 1}^{\theta 2} \frac{p_w(\theta)|V_p(\theta)|}{\omega(\theta)} d\theta = \frac{K_w \quad b \quad t_r}{H} \quad \Theta \qquad (8\text{-}15)$$

The cumulative wear volume of the wear probe on the measured area for the engine operating period time δt under engine speed N for a four stroke (intake, compression, expansion and exhaust) engine should be

$$\begin{aligned} \delta W_t &= \frac{N \cdot \delta t}{2} \left(w_\theta|_{intake} + w_\theta|_{comp.} + w_\theta|_{exp.} + w_\theta|_{exh.} \right) \\ &= \frac{N \quad K_w \quad b \quad t_r \delta \quad t}{2 \cdot H} \left(\Theta_{int\,ake} + \Theta_{comp.} + \Theta_{exp.} + \Theta_{exh} \right) \end{aligned} \qquad (8\text{-}16)$$

The average wear rate (in terms of wear depth) within the measured area (b × a) of the wear probe, shown in Figure 14 during time interval δt is

$$W_r = \frac{\delta W_t}{b \times a \cdot \delta t} = \frac{N K_w t_r}{2 a \cdot H}\left(\Theta_{\text{int ake}} + \Theta_{comp.} + \Theta_{\text{exp.}} + \Theta_{exh.} \right) \quad (8\text{-}17)$$

From experimental data, a correlation of the wear rate (in terms of wear depth) with respect to the break-in time has been developed in Section 5.2. Use the wear model of the probe in Equation (8-17), the wear coefficient K_w as a function of engine break-in time can be computed.

8.3 COMPUTER PROGRAM OF THE WEAR MODEL

The computer program in FORTRAN is listed below.

```
C     ================================
C       PROGRAM PROBE WEAR MODEL
C     ================================
C +++
C +++ MAIN PROGRAM FOR MODELLING THE WEAR OF THE WEAR PROBE
C +++ IN ENINGE CYLINDER. C.A.R. 9-19-97 BY  ZHENG MA
C +++
C
      COMMON PI,NUMRNG
      DIMENSION CAD(721),PRSCYL(721),PRSCRK(721),ANGVEL(721),
     *MSRNG(5),DMRNG(5),EMRNG(5),IMRNG(5),THKRNG(5),WDRNG(5)
      DIMENSION DSTPST(721),SPDPST(721),ACLPST(721),TGBATA(721)
      DIMENSION FCTHRST(721),PRSRNG(721),PRSRNGELS1(721),
     *PRSMJWR1(721),PRSMNWR1(721)
      DIMENSION CARAD(721)
      REAL MSRNG,MSPST,MSCRD,LENCRD,LENGRV,LENSTRK,KOWEAR,IMRNG
```

```
      CHARACTER *12 DATANAME1,DATANAME2,DATANAME3
      CHARACTER *1  OPT
      CHARACTER *82 CH
C
      PRINT *,'INPUT THE NAME OF THE ENGINE PARAMETER FILE:'
      READ (*,'(A)')DATANAME1
      OPEN (UNIT=11,FILE=DATANAME1)
c --- INPUT PARAMETERS OF THE PISTON RINGS ---
      READ (11,*) NUMRNG
      DO 1 I=1,NUMRNG
 1    READ (11,*) MSRNG(I),DMRNG(I),EMRNG(I),IMRNG(I),THKRNG(I),
     *WDRNG(I)
c --- INPUT PISTON PARAMETERS  ---
      READ (11,*) MSPST
c --- INPUT CONNECTING-ROD PARAMETERS  ---
      READ (11,*) MSCRD,LENCRD,LENGRV
c --- INPUT CYLINDER LINER PARAMETERS  ---
      READ (11,*) DIMCYL,LENSTRK,HDNSCYL
c --- INPUT WEAR PROBE PARAMETERS  ---
      READ (11,*) WDAREA,DEGAREA,AREAWR
      CLOSE (11)
      PRINT *,'INPUT THE NAME OF THE TEST DATA FILE FOR THE MODEL:'
      READ (*,'(A)')DATANAME3
      OPEN (UNIT=9,FILE=DATANAME3)
      OPEN (UNIT=12,FILE='COEFWEAR.OUT')
      WRITE (12,101)
 101  FORMAT('    DATAFILE          WEAR COEFICIENT Kw'/'  ')
 2    READ (9,'(A)')OPT
      IF (OPT.EQ.'N'.OR.OPT.EQ.'n') GO TO 5
      IF (OPT.NE.'Y'.AND.OPT.NE.'y') GO TO 2
c --- INPUT THE NAME OF THE PRESSURE DATA FILE OF THE STEP ---
      READ (9,'(A)')DATANAME2
      OPEN (UNIT=10,FILE=DATANAME2)
      READ (10,'(A)') CH
      DO 3 I=1,721
      READ (10,*)CAD(I),A,PRSCYL(I),PRSCRK(I),A,A,ANGVEL(I)
 3    CONTINUE
      CLOSE (10)
c --- INPUT ENGINE OPERATING PARAMETERS ---
c --- INPUT STEP WEAR(um),STEP TIME(hr) AND THE ENGINE RPM ---
      READ (9,*) WEARSTEP,TIMESTEP,RPM
      PI=3.141592654
      FLMTHK1=0.0
      DO 4 I=1,721
 4    CARAD(I)=CAD(I)*PI/180.0
c --- CALCULATE PISTON DYNAMIC VARIABLES  ---
      CALL DYNAMIC(721,CARAD,LENCRD,LENSTRK,ANGVEL,DSTPST,SPDPST,
     *ACLPST,TGBATA)
```

```
c --- CALCULATE PISTON SIDE THRUST FORCE ---
      CALL THRUST(721,PRSCYL,PRSCRK,DIMCYL,MSRNG,MSPST,MSCRD,
     *LENCRD,LENGRV,ACLPST,TGBATA,FCTHRST)
c --- CALCULATE INTERNAL GAS PRESSURE OF THE PISTON RING
      CALL RINGPRS(721,PRSCYL,PRSCRK,MSRNG,WDRNG,DIMCYL,ACLPST,
     *SPDPST,PRSRNG)
c --- CALCULATE PISTON RING ELASTIC FORCE ---
      CALL RINGELS(721,PRSRNG,DMRNG,EMRNG,IMRNG,THKRNG,DIMCYL,
     *FLMTHK1,PRSRNGELS1)
c --- CALCULATE THE TOTAL FORCE ACTING ON THE TOP RING TO CAUSE
c --- CYLINDER WEAR ---
      CALL RNGWRFC(721,PRSRNGELS1,FCTHRST,THKRNG,DIMCYL,PRSMJWR1,
     *PRSMNWR1)
c --- CALCULATE THE WEAR COEFICIENT OF THE WEAR PROBE IN THE
c --- MEASURED AREA OF THE LASER STYLUS ---
      CALL CFWEAR(DEGAREA,PRSMJWR1,SPDPST,ANGVEL,HDNSCYL,WDAREA,
     *THKRNG,AREAWR,TIMESTEP,RPM,WEARSTEP,KOWEAR)
      WRITE(12,'(3X,A12,5X,E16.8)')DATANAME2,KOWEAR
      GO TO 2
 5    CONTINUE
      CLOSE(12)
      CLOSE(9)
      STOP
      END

C     ----------------------------------------------------------------
      SUBROUTINE DYNAMIC(N,CARAD,LENCRD,LENSTRK,ANGVEL,DSTPST,
     *SPDPST,ACLPST,TGBATA)
C     ----------------------------------------------------------------
C
      DIMENSION ANGVEL(721),DSTPST(721),SPDPST(721),ACLPST(721),
     *TGBATA(721),CARAD(721),SINBATA(721)
      REAL LENCRD,LENSTRK
C
      CALL INTG(721,ANGVEL,AVSUM,OMGA)
      GAMA=LENSTRK/(2.0*LENCRD)
      R=LENSTRK/2.0
      DO 10 I=1,N
      SITA=CARAD(I)
      DSTPST(I)=R*((1.0-COS(SITA))+(GAMA/4.0)*(1.0-COS(2.0*SITA)))
      SPDPST(I)=R*OMGA*(SIN(SITA)+(GAMA/2.0)*SIN(2.0*SITA))
      ACLPST(I)=R*OMGA**2*(COS(SITA)+GAMA*COS(2.0*SITA))
      SINBATA(I)=R*SIN(SITA)/LENCRD
      TGBATA(I)=SINBATA(I)/SQRT(1.0-SINBATA(I)**2)
 10   CONTINUE
      RETURN
      END
```

```
C     ------------------------------------------------------------
      SUBROUTINE THRUST(N,PRSCYL,PRSCRK,DIMCYL,MSRNG,MSPST,MSCRD,
     *LENCRD,LENGRV,ACLPST,TGBATA,FCTHRST)
C     ------------------------------------------------------------
C
      COMMON PI,NUMRNG
      DIMENSION PRSCYL(721),PRSCRK(721),MSRNG(5),ACLPST(721),
     *TGBATA(721),FCTHRST(721),FCPRS(721),FCDYN(721)
      REAL MSRNG,MSPST,MSCRD,MSPRA,MSCTR,LENCRD,LENGRV
C
      MSPRA=0.0
      DO 20 I=1,NUMRNG
   20  MSPRA=MSPRA+MSRNG(I)
      MSPRA=MSPRA+MSPST
      MSCTR=MSCRD*LENGRV/LENCRD
      DO 21 I=1,N
      FCPRS(I)=(PRSCYL(I)-PRSCRK(I))*PI*DIMCYL**2/4.0
      FCDYN(I)=-(MSPRA+MSCTR)*ACLPST(I)
   21  CONTINUE
      DO 22 I=1,N
      FCTHRST(I)=(FCPRS(I)+FCDYN(I))*TGBATA(I)
   22  CONTINUE
      RETURN
      END

C     ------------------------------------------------------------
      SUBROUTINE RINGPRS (N,PRSUP,PRSLW,MSRNG,WDRNG,DIMCYL,ACLPST,
     *SPDPST,PRSRNG)
C     ------------------------------------------------------------
C
      COMMON PI,NUMRNG
      DIMENSION PRSUP(721),PRSLW(721),MSRNG(5),WDRNG(5),ACLPST(721),
     *SPDPST(721),PRSRNG(721)
      REAL MSRNG
C
      DO 30 I=1,N
      PRSRNG(I)=PRSUP(I)
      FRCRNG=-(PRSUP(I)-PRSLW(I))*PI*(DIMCYL**2-(DIMCYL
     *-2.0*WDRNG(1))**2)/4.0+ACLPST(I)*MSRNG(1)
      IF (FRCRNG.GT.0.0) PRSRNG(I)=PRSLW(I)
      IF (FRCRNG.EQ.0.0) THEN
        IF(SPDPST(I).GT.0.0) PRSRNG(I)=PRSLW(I)
      ENDIF
   30  CONTINUE
      RETURN
      END

C     ------------------------------------------------------------
```

```
      SUBROUTINE RINGELS (N,PRSRNG,DMRNG,EMRNG,IMRNG,THKRNG,
     *DIMCYL,FLMTHK1,PRSRNGELS1)
C     ------------------------------------------------------------
C
      COMMON PI,NUMRNG
      DIMENSION PRSRNG(721),DMRNG(5),EMRNG(5),IMRNG(5),THKRNG(5),
     *PRSRNGELS1(721),PRSINRG1(721)
      REAL IMRNG
C
      A1=(DIMCYL/2.0)**7*(PI-1.0)*3.0/(4.0*EMRNG(1)**2*IMRNG(1)**2)
      B1=(DIMCYL/2.0)**4*(1.0+PI/4.0)/(EMRNG(1)*IMRNG(1))
      C1=DIMCYL/2.0-DMRNG(1)/2.0
      PRSELS1=(-B1+SQRT(B1**2-4.0*A1*C1))/(2.0*A1)
      PRSELS1=PRSELS1/THKRNG(1)
      DO 30 I=1,N
      PRSINRG1(I)=PRSRNG(I)+PRSELS1
 30   CONTINUE
      DO 31 I=1,N
      PRSRNGELS1(I)=FLMTHK1*EMRNG(1)*THKRNG(1)/(DIMCYL/2.0)**2+
     *PRSINRG1(I)
 31   CONTINUE
      RETURN
      END

C     ------------------------------------------------------------
      SUBROUTINE RNGWRFC(N,PRSRNGELS1,FCTHRST,THKRNG,DIMCYL,
     *PRSMJWR1,PRSMNWR1)
C     ------------------------------------------------------------
C
      COMMON PI,NUMRNG
      DIMENSION THKRNG(5),FCTHRST(721),PRSRNGELS1(721),
     *PRSMJWR1(721),PRSMNWR1(721),AREARNG(5),PRSTHRSTRNG(721)
C
      THKRNGS=0.0
      AREARINGS=0.0
      DO 40 I=1,NUMRNG
      AREARNG(I)=THKRNG(I)*DIMCYL
      AREARINGS=AREARINGS+AREARNG(I)
 40   THKRNGS=THKRNGS+THKRNG(I)
      DO 41 I=1,N
      PRSTHRSTRNG(I)=FCTHRST(I)/AREARINGS
 41   CONTINUE
      DO 42 I=1,N
      IF (PRSTHRSTRNG(I).GE.0.0) THEN
        PRSMJWR1(I)=PRSRNGELS1(I)+PRSTHRSTRNG(I)
        PRSMNWR1(I)=PRSRNGELS1(I)
      ELSE
        PRSMJWR1(I)=PRSRNGELS1(I)
```

```
        PRSMNWR1(I)=PRSRNGELS1(I)-PRSTHRSTRNG(I)
      ENDIF
42    CONTINUE
      RETURN
      END

C     ------------------------------------------------------------
      SUBROUTINE CFWEAR(DEGAREA,PRSMJWR1,SPDPST,ANGVEL,HDNSCYL,
     *WDAREA,THKRNG,AREAWR,TIMESTEP,RPM,WEARSTEP,KOWEAR)
C     ------------------------------------------------------------
C
      DIMENSION ANGVEL(721),THKRNG(5),SPDPST(721),PRSMJWR1(721),
     *PVFCTN(181)
      REAL KOWEAR
C
      COFWR=WDAREA*THKRNG(1)*RPM/(2.0*AREAWR*HDNSCYL)
      INTANG=INT(DEGAREA)+1
c --- PROBE WEAR IN MEASURED AREA DURING THE INTAKE STROKE ---
      DO 50 I=1,INTANG
50    PVFCTN(I)=PRSMJWR1(I)*ABS(SPDPST(I))/ANGVEL(I)
      CALL INTG(INTANG,PVFCTN,WRSTK1,A)
c --- PROBE WEAR IN MEASURED AREA DURING THE COMP. STROKE ---
      DO 51 I=1,INTANG
51    PVFCTN(I)=PRSMJWR1(361-INTANG+I)*ABS(SPDPST(361-INTANG+I))
     */ANGVEL(361-INTANG+I)
      CALL INTG(INTANG,PVFCTN,WRSTK2,A)
c --- PROBE WEAR IN MEASURED AREA DURING THE EXPAN. STROKE ---
      DO 52 I=1,INTANG
52    PVFCTN(I)=PRSMJWR1(360+I)*ABS(SPDPST(360+I))/ANGVEL(360+I)
      CALL INTG(INTANG,PVFCTN,WRSTK3,A)
c --- PROBE WEAR IN MEASURED AREA DURING THE EXHAUS. STROKE ---
      DO 53 I=1,INTANG
53    PVFCTN(I)=PRSMJWR1(721-INTANG+I)*ABS(SPDPST(721-INTANG+I))
     */ANGVEL(721-INTANG+I)
      CALL INTG(INTANG,PVFCTN,WRSTK4,A)
      WRCYC=WRSTK1+WRSTK2+WRSTK3+WRSTK4
      KOWEAR=WEARSTEP/(6.0*(10**7)*TIMESTEP*COFWR*WRCYC)
      RETURN
      END

C     ----------------------------------
      SUBROUTINE INTG(N,FUNC,SUM,AVE)
C     ----------------------------------
C
      DIMENSION FUNC(721)
      SUM=0.0
      DO 10 I=1,N
      A=FUNC(I)
```

```
   IF(I.EQ.1.OR.I.EQ.N)A=FUNC(I)*0.5
10  SUM=A+SUM
   AVE=SUM/FLOAT(N-1)
   RETURN
   END
```

8.4 RESULT OF THE MODELING

The simulation wear of the wear probe can be computed by the above simulation program inputting the test data of the engine cylinder pressure, crankcase pressure, crankshaft angular velocity, engine operation time etc., if the wear coefficient K_w is known. However, we cannot use a wear coefficient of the cylinder liner material under normal wear condition because it is obvious that during the break-in period the wear coefficient K_w is not a constant. It should be large at the beginning of the break-in period and decrease as the break-in goes on. Since we measured the probe wear during the break-in, we can compute the simulated wear, according to the actual probe wear data presented by Equation (4) in Section 6.2, by using the program to compute the wear coefficient K_w. The result is shown in Figure 62.

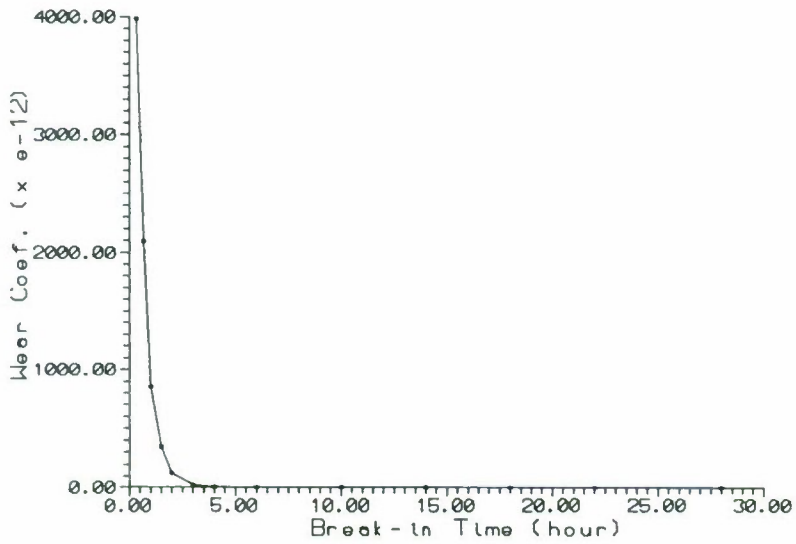

Figure 62. Wear coefficient K_w as a function of engine break-in time

Figure 62 shows that the wear coefficient K_w changed in a very large scale during the break-in time. The wear coefficient K_w was about 4.0×10^{-9} at the beginning and decreased to 0.25×10^{-12} at the end of the break-in period. It decreased about 16,000 times. Since the wear coefficient is a parameter which indicates the seriousness of wear, Figure 62 illustrates the transient wear during the break-in time. And the most serious change happened only during the first one or two hours during the break-in period.

Wear coefficient K_w is a parameter which presents the probability of each asperity of the surface to become a wear particle. Assume that for other materials of different hardness, such as aluminium alloy or steel, the wear coefficients K_w is the same as liner material (cast iron) tested in this program. The wear under the same engine operating conditions and break-in schedule can be computed by the wear model. The results are as shown in Figure 63. This figure shows that three materials follow a similar wear pattern during the break-in, and the material of the lowest hardness (aluminium alloy) has the highest wear level.

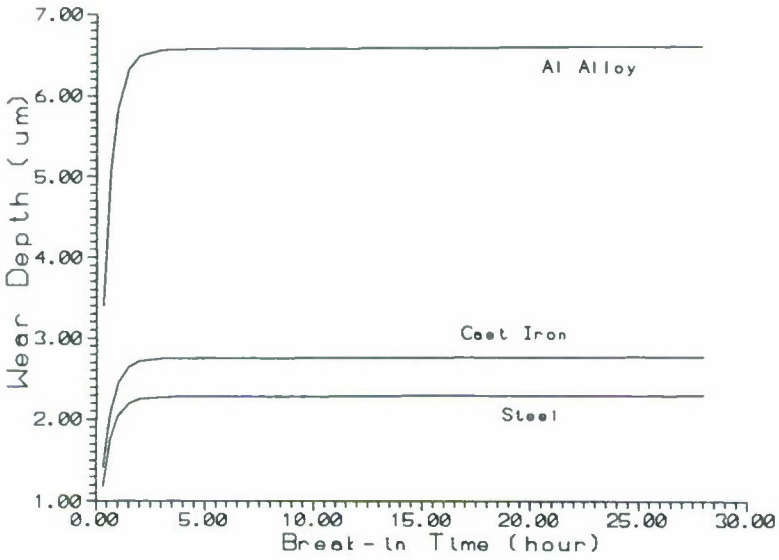

Figure 63. Simulated wear of different liner materials during engine break-in

9.0 CONCLUSIONS

An in-situ wear probe was developed and successfully used to measure wear and surface roughness and to examine surface texture of the cylinder liner at the top ring reversal point of a single-cylinder, air-cooled, gasoline engine, during and after the break-in period. In addition the different wear mechanisms at this location were identified. The cylinder liner, piston-ring assembly were the only parts of the engine being broken-in. The measurements included the cylinder gas pressure, instantaneous engine speed and load torque, needed to determine the instantaneous frictional torque of the engine. Data was obtained at different

intervals during and after break-in period for a total of 28 hours. The following conclusions are based on these tests:

1. The highest rate of wear occurred at the beginning of the break-in period, and decreased sharply during the first hour. The wear reached its low steady rate after three and half hours of engine break-in. Accordingly, the wear particles reached a high concentration in the oil after the first hour. Changing the oil after one hour would reduce the wear in an engine.
2. The instantaneous engine frictional torque and surface roughness Ra had their highest values at the beginning of the break-in period, and decreased at a lower rate than the wear-rate. The engine friction and Ra took about 24 hours to reach their steady rate. About half of the total change in mean IFT and Ra during the break-in period occured after the wear reached its low steady rate.
3. The Piston Ring Assembly (PRA) friction during break-in was found to be linearly correlated to surface roughness. The reason is that the decrease in surface roughness changes the lubrication from mixed to hydrodynamic regime and results in a drop in friction.
4. The data showed that a large change in wear-rate was not associated with a large drop in friction. Meanwhile a small change in wear-rate was associated with a large drop in friction. This indicates that PRA friction and wear are not well correlated during the break-in period.
5. Correlations have been developed for wear-rate, surface roughness, engine frictional torque, and energy lost to overcome friction during and after the break-in period.

6. By examining the probe surface using Scanning Electron Microscope and Optical Microscope, the primary wear mechanisms of the cylinder liner on TDC were found to be abrasion, plastic deformation and fatigue.
7. Abrasion was found to be the main wear mechanism to cause the liner wear during engine break-in. Folded material along the honing marks and graphite flakes on surface, produced during the honing process, broke off the surface and became wear debris to cause further abrasive wear.
8. A simulating model of cylinder liner wear was developed. The model can predict liner break-in wear of different materials.

ACKNOWLEDGEMENTS

The author would like to acknowledge the sponsorship of this project by the US Army National Automotive Center and the technical support of the Engineers and Scientists at US Army Tank-Automotive and Armament Command, Tank-Automotive Research, Development and Engineering Center.

The author acknowledges the effort of Ms. Zheng Ma, a graduate student at Wayne State University for running this project and developing this report.

The help and generosity of the Powertrain Research Lab and Experimental Machine Shop at Ford Motor Company are acknowledged and gratefully appreciated. The machining of the wear probe and cylinder block were all completed at Ford Motor Company. Special thanks are due to Mr. John Glidewell, for his technical discussions, advice, help and encouragement.

APPENDIX —— Definitions of Roughness Parameters

R_a, R_q, W_a, W_q

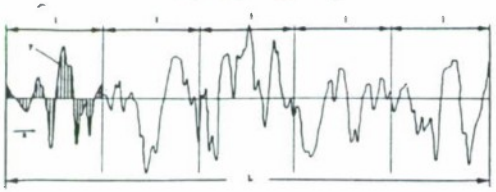

l_1 ... l_5 are consecutive and equal sampling lengths (1 the sampling length corresponds to filter cut-off length).

The assessment length L* is defined as the length of profile used for the measurement of surface roughness parameters (usually containing several sampling lengths; five consecutive sampling lengths are taken as standard).

R_a R_a is the universally recognised, and most used, international parameter of roughness. It is the arithmetic mean of the departures of the roughness profile from the mean line.

$$R_a = \frac{1}{L}\int_0^L |y(x)|\,dx$$

R_q R_q is the rms parameter corresponding to R_a

$$R_q = \sqrt{\frac{1}{L}\int_0^L y^2(x)\,dx}$$

W_a and W_q are the corresponding parameters from the waviness profile.

*The 'assessment length' is called 'traverse measuring length' or 'evaluation length' in ISO terminology.

R_z (ISO)

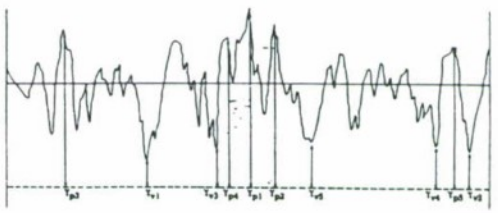

R_z Also known as the ISO 10 point height parameter, is measured on the unfiltered profile only and is numerically the average height difference between the five highest peaks and the five lowest valleys within the traverse length.

HSC, P_c

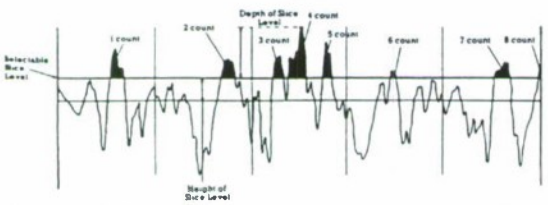

HSC The high spot count is the number of complete profile peaks (within assessment length) projecting above the mean line, or a line parallel with the mean line. This line can be set at a selected depth below the highest peak or a selected distance above or below the mean line.

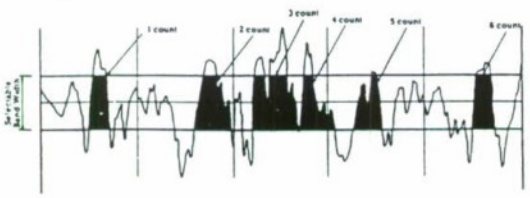

P_c The peak count is the number of local peaks which project through a selectable band centred about the mean line. The count is determined only over the assessment length though the results are given in peaks per cm (or per inch). The peak count obtained from assessment lengths of less than 1 cm (or 1 inch) is obtained by using a multiplication factor. The parameter should therefore be measured over the greatest assessment length possible.

S, S_m

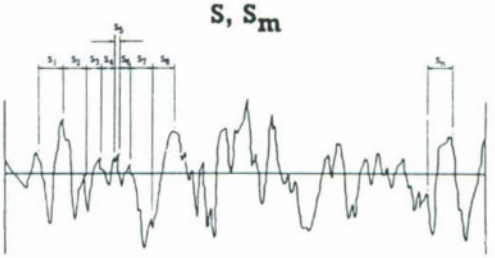

S S is the mean spacing of adjacent local peaks, measured over the assessment length. (A local peak is the highest part of the profile measured between two adjacent minima, and is only included if the distance between the peak and its preceding minima is at least 1% of the P + V of the profile.)

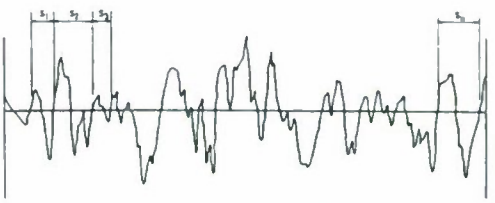

S_m S_m is the mean spacing between profile peaks at the mean line, measured over the assessment length. (A profile peak is the highest point of the profile between an upwards and downwards crossing of the mean line.)

R_{3y}, R_{3z}

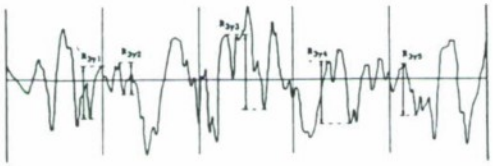

R_{3y} The deviation from the third highest peak to the third lowest valley in each sample length is found. R_{3y} is then the largest of these values.

R_{3z} R_{3z} is the vertical mean from the third highest peak to the third lowest valley in a sample length over the assessment length.

R_{ti}, R_y, R_{tm} (R_zDIN)

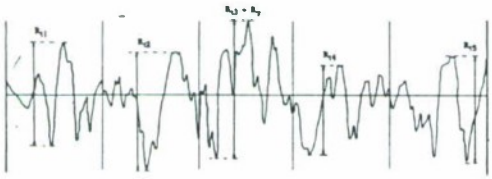

R_{ti} R_{ti} is the maximum peak-to-valley height of the profile in one sampling length.

R_y R_y is the largest R_{ti} value within the assessment length.

R_{tm} R_{tm} is the mean of all the R_{ti} values obtained within the assessment length. It is the equivalent of R_zDIN

Bearing Ratio t_p

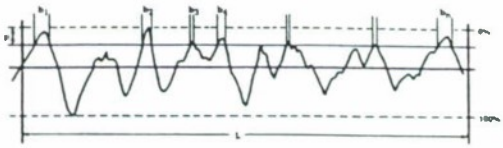

Bearing ratio t_p is the length of bearing surface (expressed as a percentage of the assessment length L), at a depth p below the highest peak.

t_p (%) is the ratio at the depth p.

$$t_p = \frac{b_1 + b_2 + b_3 + b_4 \ldots b_n}{L} \times 100 = \frac{100}{L} \sum_{i=1}^{i=n} b_i$$

The printout shows t_p% for each of the levels as for HSC.

The bearing ratio (or Abbott-Firestone) curve below, shows how the ratio varies with level.

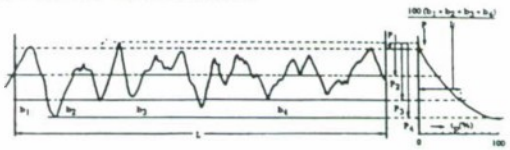

R_v, R_p, R_{pm}, R_t, W_v, W_p, W_t

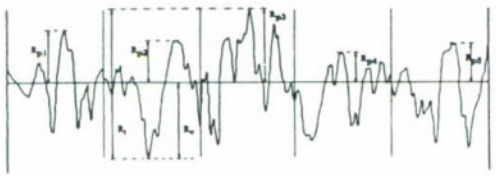

R_v R_v is the maximum depth of the profile below the mean line within the assessment length.

R_p R_p is the maximum height of the profile above the mean line within the assessment length.

R_{pm} R_{pm} is the mean of R_p values obtained for each sampling length of an assessment.

Where n = the number of cut-offs, then

$$R_{pm} = \frac{1}{n} \sum_{i=1}^{i=n} R_{pi}$$

R_t $R_t = R_p + R_v$ and is the maximum peak to valley height of the profile in the assessment length.

W_v, **W_p** and **W_t** are the corresponding parameters from the waviness profile.

R_{sk}, R_{ku}

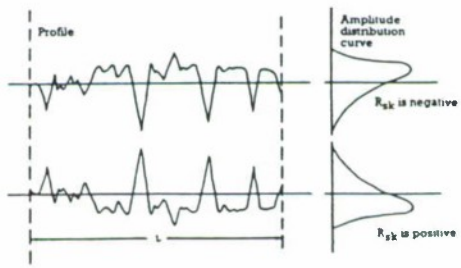

R_{sk} R_{sk} – Skewness – is the measure of the symmetry of the profile about the mean line. It will distinguish between asymmetrical profiles of the same R_a or R_q.

Where n = number of data points in the profile, then

$$R_{sk} = \frac{1}{nR_q^3} \sum_{i=1}^{i=n} (Y_i)^3$$

R_{ku} R_{ku} – Kurtosis – is a measure of the sharpness of the surface profile.

Where n = number of data points in the profile, then

$$R_{ku} = \frac{1}{nR_q^4} \sum_{i=1}^{i=n} (Y_i)^4$$

REFERENCES

[1] Barber, G.C., Ludema, K.C.,"The Break-In Stage of Cylinder-Ring Wear: A Correlation between Fired Engines and a Laboratory Simulator," Wear, 118, pp57-75(1987).

[2] Eilon,S., Saunders,O.A.," A study of piston-ring lubrication,"Proc. Inst. Mech. Eng., London, 171, p427(1957).

[3] de Faro Barros, A., Dyson,A.,J.Inst. Pet. London, 46, p433(1960).

[4] Tischbein,H.W.,"The friction of piston rings," NACA Tech. Memo. 1069(1939).

[5] El-Sherbiny,M.G.,"Cylinder liner wear," In D. Dowson and C.M. Taylor(eds.),9th Leeds-Lyon Symp. on Tribology, Leeds, 1982, IPC Science and Technology, Guildford, 1984.

[6] Willn,J.E., Brett,P.S.,"Piston ring scuffing during running-in -- the influence of lubricants and materials, Proc. Inst. Mech. Eng., Londeon, 191(22),p241(1977).

[7] Smith,C.A., Davis,F.A.,"Abrasive wear of piston ring and cylinder bore materials," Automot. Eng.,9(1),pp26-28(1984).

[8] Slone, R., Patterson, D.J., Morrison, K.M., Schwartz, G.B.,"Wear of Piston Rings and Liners by Laboratory Simulation," SAE paper 890146, pp55-64.

[9] Sreenath, A.V., Raman, N.,"Running-In Wear of A Compression Ignition Engine: Factors Influencing the Conformance between Cylinder Liner and Piston Rings," Wear, 38, pp271-289(1976).

[10] Balnaves,M., Czarkowski,D., Giannini, R., Shaver, B., Modetz, H.,"Fuel Property Effects on Ring and Liner Wear Rates in a DDC 6V-53T Using SLA Techniques," SAE paper 912326.

[11] Fritz, S.G., Cataldi, G.R.,"In Situ Piston Ring Wear Measurements in a Medium-Speed Diesel Engine," Lubrication Engineering, 46, 6, pp 365-370 (June 1990).

[12] Sudarshan, T.S., Bhaduri, S.B.,"Wear in Cylinder Liners," Wear, 91, pp269-279(1983).

[13] Sparrow,S.W., Scherger,T.A.,"Cylinder wear-where and why,"SAE Trans.,38(4),p117(1936).

[14] Nakayama,Y.,Endo,H.,"Effect of finishing grade on the wear of diesel engine cylinder wall," Bull.JSME,2(8),p584(1959).

[15] Dagnall,H.,"Exploring surface texture",Rank Taylor Hobson,1988.

[16] Wills,E.,"Surface finish in relation to cylinder liners",Wear,109,p351(1986).

[17] Stout,K.J.,Davis,E.J.,"Surface topography of cylinder bores - the relationship between manufacture, characterization and function," Wear,95,p111(1984).

[18] Stout,K.J.,Spedding,T.A.,"The characterization of internal combustion engine bores," Wear,83,p311(1982).

[19] Yahagi,Y.,"Corrosive wear of diesel engine cylinder bore," Tribology international, (6), pp365-373(1987).

[20] Jeng, Y.,"Impact of plateaued surfaces on tribological performance," Tribology Transactions, 39 (2), p354-361 (1996).

[21] Blau, P.J.," Friction and wear transitions of materials -- break-in, run-in, wear-in," Noyes Pubrications (1989).

[22] Wang,Y.S., Narasimhan,S.,Larson,J.M.,Barber,G.C.,"A review of ceramic tribology and application of Si-based ceramics to engine valves/seat inserts,"SAE paper 960304 (1996).

[23] Ludema, K.C.,"Friction, wear, lubrication -- a text book in Tribology,"CRC Press Inc (1996).

[24] Chung,Y.,Schock,H.J.,Brombolich,L.J.,"Fire ring wear analysis for a piston engine," SAE paper 930797, (1993).

[25] Henein, N.A., Marek, S.L., Fragoulis, A.N.,"Error analysis of time-dependent frictional torque in reciprocating internal combustion engine: effect of cylinder gas pressure," Tribology Transaction, Vol. 35, 3, pp. 516-522 (1992).

[26] Henein, N.A., Ma,Z., Huang, S., Bryzik, W., Glidewell, J.," In-situ wear measuring technique in engine cylinders," Presented at the 51st STLE Annual Meeting, Cincinnati, Ohio (1996).

[27] Raadnui,S.,Roylance,B.J.,"The Classification of Wear Particle Shape," Lubrication Engineering,51(5),pp432-437(1995).

[28] Jin,Y.,Yang,Q.,"Ferrographic Analysis of Wear Debris Generated in Locomotive Diesel Engines," Wear, 93, pp23-32(1984).

[29] Jin,Y.,Wang,C.,"Spherical Particles Generated During the Running-in Period of a Diesel Engine," Wear, 131,pp315-328(1989).

[30] Williams,C.G.,"Cylinder wear in gasoline engines,"SAE Trans., 38 (5), p191-196 (1936).

[31] Barber, G.C., Lee, J.C., Ludema, K.C., "Materials and surface finish effects in the breaking-in process of engines," Journal of Engineering for Gas Turbines and Power, 109, pp380-387(1987).

[32] Weiss, E.K.J., Bnthuer, B.B., Hardenberg, H.O.,"Diesel Fuel Sulphur and Cylinder Liner Wear of a Heavy-Duty Diesel Engine," SAE paper 872148.

[33] Ting,L.L., Mayler, J.E.,"Piston Ring Lubrication and Cylinder Bore Wear Analysis, Part I —— Theory," Journal of Lubrication Technology, pp305-314(July 1974).

[34] Wing, R.D., and Saunders, O., "Oil Film Temperature and Thickness Measurements on the Piston Rings of a Diesel Engine," Prec. Instn. Mech. Engrs., 184(3P), p119(1969-1970).